XLIIIrd RENCONTRES DE MORIOND

Electroweak Interactions and Unified Theories

I - Standard Model, precision Electroweak data at colliders, Search for the Brout-Englert-Higgs particle and theoretical variations

Standard Model Higgs Searches at the Tevatron (Low Mass)

Kohei Yorita
(On behalf of the CDF and DØ Collaborations)
Enrico Fermi Institute, University of Chicago
Chicago, IL 60637 USA

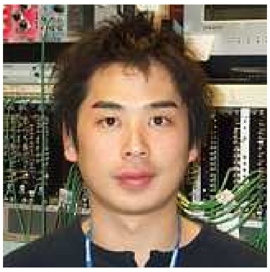

We present recent results of the Standard Model (SM) Higgs boson searches from the Collider Detector at Fermilab (CDF) and DØ experiments using 1.0-2.1 fb^{-1} data from proton-antiproton collisions with $\sqrt{s} = 1.96$ TeV at the Fermilab Tevatron. For Higgs mass (m_H) less than 135 GeV/c^2 (so-called low mass region), $W^{\pm}H \to l^{\pm}\nu b\bar{b}$, $ZH \to l^+l^-b\bar{b}$, and $ZH \to \nu\bar{\nu}b\bar{b}$ processes are the most sensitive channels and those results are summarized in this report. In addition, a new CDF search based on $H \to \tau^+\tau^- + 2jets$ mode is described. Both CDF and DØ have found no evidence for the Higgs boson, and therefore set upper limits on the Higgs production cross section. The latest Tevatron combined limits are also presented.

1 Introduction

The Higgs boson is an essential component in the Standard Model (SM), which provides masses to fundamental particles through electroweak symmetry breaking, but yet undiscovered as of now. Theory indicates that the Higgs should be a scalar and charge-neutral boson but no predictions on its mass. However, combining the results from the direct searches at LEP and the SM global fits based on electroweak data, the mass of the SM Higgs boson is bounded in the range of 114.4 to 144 GeV/c^2 at 95% confidence limit (CL) [1].

The CDF and DØ experiments at the Tevatron are currently the only places capable of searching for the Higgs boson. The dominant Higgs production mode at the Tevatron ($p\bar{p}$ collision with $\sqrt{s} = 1.96$ TeV) is via gluon fusion ($\sigma =\sim 1$ pb) which is about five to even ten times larger than the associated production of $W^{\pm}H$ and ZH. The fourth highest production is given by so-called Vector Boson Fusion (VBF) process with slightly lower production rate than ZH. In the low mass region ($m_H < 135$ GeV/c^2), the Higgs immediately decays to $b\bar{b}$ at 70∼80% or $\tau^+\tau^-$ at 7∼8% respectively. Although $gg \to H \to b\bar{b}$ mode is expected to provide the largest signal yield, it is overwhelmed by QCD multijet background. Therefore the most relevant channels at the Tevatron are $W^{\pm}H \to l^{\pm}\nu b\bar{b}$, $ZH \to l^{+}l^{-}b\bar{b}$, and $ZH \to \nu\bar{\nu}b\bar{b}$ as shown in figure 1.

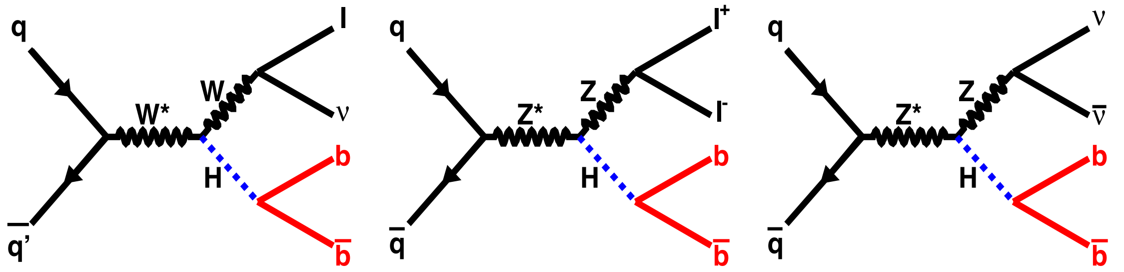

Figure 1: Tree level Feynman diagrams for signal processes used for low mass Higgs searches: From left to right, $W^{\pm}H \to l^{\pm}\nu b\bar{b}$, $ZH \to l^{+}l^{-}b\bar{b}$, and $ZH \to \nu\bar{\nu}b\bar{b}$ final states.

In addition to these channels, CDF newly performed the SM Higgs boson search using $H \to \tau^{+}\tau^{-} + 2jets$ from WH, ZH, VBF, and gluon fusion processes. In this report, all results and combined limits are briefly summarized.

2 Recent RunII Results

Both CDF and DØ have established the search for the SM Higgs as one of their highest priorities and already presented elsewhere and published (*e.g.* in [2]). This proceeding therefore mainly focuses on describing recent updates for analyzes with 1.0∼2.1 fb^{-1} of data, depending on channels.

For $H \to b\bar{b}$ associated with W/Z boson, b quark identification is one of the key elements in event selection. b quarks produce jets in detection and can be identified by either secondary vertex algorithm (SecVtx btagging) or jet probability algorithm (JetProb btagging) based on the large B hadron lifetime. The former algorithm looks for a displaced vertex from the primary vertex of an event [2,3] while the latter requires a low probability that all tracks contained in a jet originated from the primary vertex, based on the track impact parameters[3]. These btagging requirements are crucial to reduce large $W/Z + jets$ and QCD multijet backgrounds where non-$bjet$ (gluon jet and $u-, d-, c-, s-$ jets) contribution is dominated. However since the Higgs signal is still much smaller than the backgrounds even after btagging, all analyzes presented here employed multivariate techniques (Artificial Neural Net (ANN) or Boosted Decision Tree (BDT)) to further improve signal-to-background ratio.

Although significant improvements with enormous efforts have been achieved by both CDF and DØ, no single analysis by itself would reach the sensitivity needed for discovery or exclusion. Thus all channels studied must be combined.

2.1 Search for $W^{\pm}H \to l^{\pm}\nu b\bar{b}$

The event selection is imposed by having one high p_T isolated lepton (e or μ), missing transverse energy ($\not{E}_T$) from the neutrino (from W decay), and two or more jets (exact two jets in CDF) expected from Higgs decay. CDF and DØ results presented here are based on 1.9 fb^{-1} and 1.7 fb^{-1} data respectively. From previous results, CDF updated the analysis to include forward electron with η up to ∼2.0 and also added 1 *btag* category with neural net flavor separation (ANN$_{btag}$) in addition to double btagged events[3]. Candidate events are therefore classified into three categories: 2 SecVtx, 1 SecVtx + 1 JetProb, and 1 ANN$_{btag}$. Those three are exclusive to each other and have different signal purity. Thus they are analyzed separately but combined to obtain the final sensitivity in the likelihood calculation. DØ uses events with not only exact two jets but also three jets and performed sample splitting in a similar way of CDF (1 ANN *tight* bjet and 2 *loose* ANN bjets, depending on operation point with respect to fake rate and signal efficiency where they have been selected based on the optimal combined sensitivity to a WH signal)[4]. Dominant backgrounds are $W + b\bar{b}$ and $t\bar{t}$ events. Both CDF and DØ use ANN technique for the final fit to distinguish signal from such backgrounds. Figure 2 shows ANN output distribution (CDF) and dijet mass distribution (DØ) for 2 btagged events. No significant excess is observed, so upper cross section limits at 95% CL are set. For $m_H = 115$ GeV/c^2, DØ sets a limit of 1.4 pb (1.2 pb expected) and CDF sets a limit of 1.1 pb (1.0 pb expected) while SM prediction on $\sigma(p\bar{p} \to WH) \times BR(H \to b\bar{b})$ is 0.13 pb.

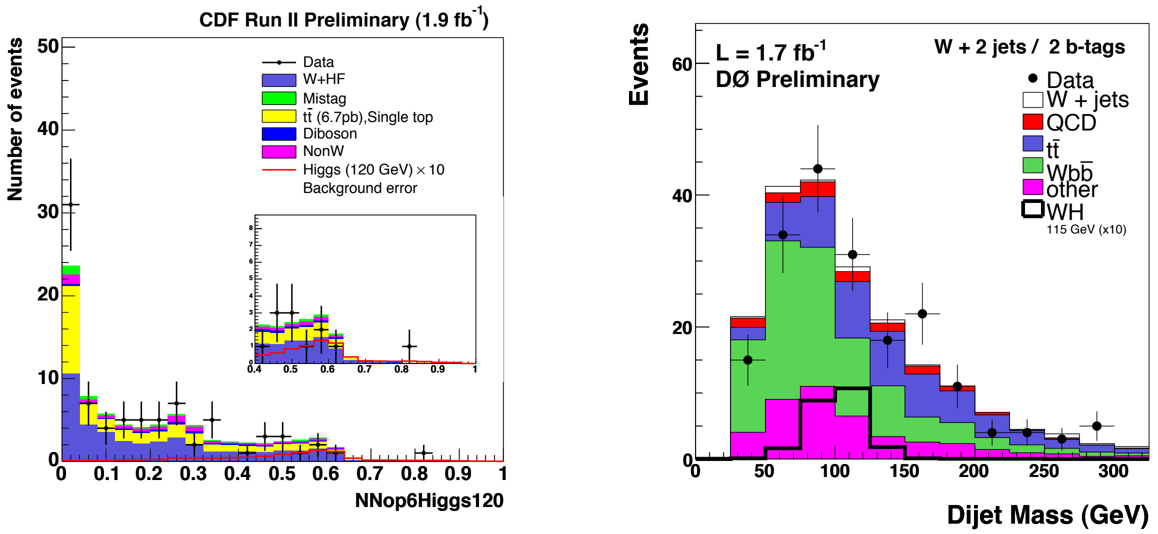

Figure 2: Left: ANN distribution from CDF. Right: Dijet mass distribution from DØ. Both are for events with 2 btagged jets. Higgs signal (times 10) is also shown for comparison.

2.2 Search for $ZH \to l^+l^-b\bar{b}$

Since this analysis was done in Summer 2007 based on relatively small data (1.0-1.1 fb^{-1}) compared to other analyzes summarized in this proceeding, only core parts of the analysis are briefly described here. More details can be found elsewhere[5,6]. The signature for this channel is two high p_T isolated leptons and two hight E_T jets that could be identified as b jets. The main backgrounds are $Z + jets$ with mis-btagging, $Z + b\bar{b}$ and $t\bar{t}$. DØ uses one dimensional ANN with ten kinematic variables while CDF's ANN analysis is two dimensions with eight variables to distinguish signal from $Z + jets$ and $t\bar{t}$ separately. CDF also employed ANN to improve the energy resolution of dijet invariant mass by correcting energies of two leading jets independently according to their projection onto the $\not\!\!E_T$ direction. This correction improves dijet mass resolution from 14% to 9% as shown in figure 3. No excess is found in signal region and so for $m_H = 115$ GeV/c^2, DØ sets a limit of 1.4 pb (1.6 pb expected) and CDF sets a limit of 1.3 pb (1.3 pb expected) while SM prediction on $\sigma(p\bar{p} \to ZH) \times BR(H \to b\bar{b})$ is 0.8 pb.

2.3 Search for $ZH \to \nu\bar{\nu}b\bar{b}$

In this channel, there is no leptons in the final state and so the signature is two high E_T jets which could be btagged and high $\not\!\!E_T$ due to the two neutrinos from Z decay. The main backgrounds arise from $Z + jets$, $Z + b\bar{b}$, $t\bar{t}$, and QCD. This analysis is challenging because except for $Z \to \nu\bar{\nu} + b\bar{b}$, all backgrounds are basically fakes originated from either mis-btagged

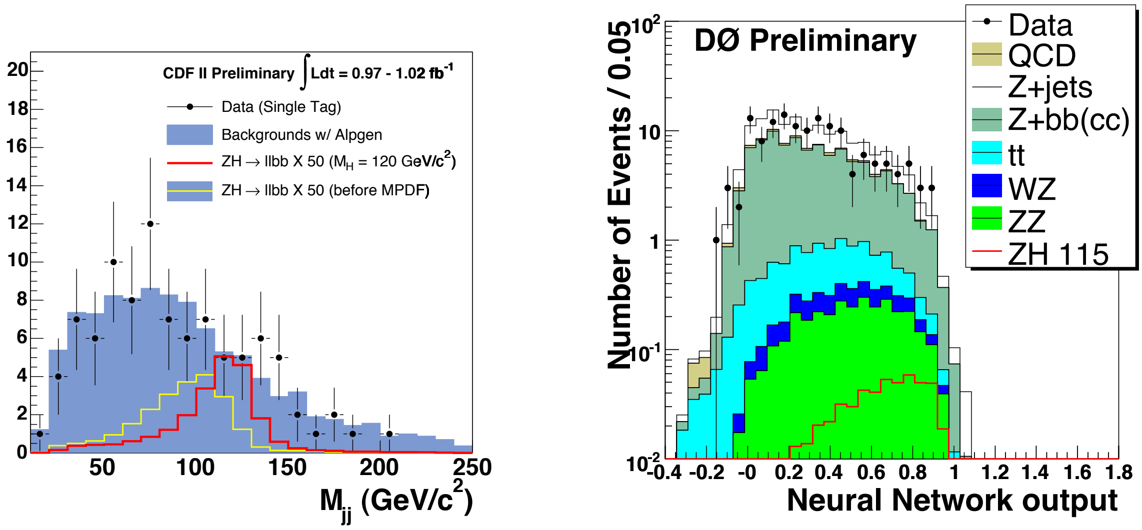

Figure 3: Left: Invariant mass distribution of two btagged jets (CDF). The red/yellow histograms is the invariant mass for the Higgs signal(times 50) after/before the ANN jet correction. Right: ANN output distribution (DØ).

jet or jet mis-reconstruction and/or jet energy mis-measurement that mimic bjet and large $\not\!\!E_T$, respectively. However there is a strong advantage that it gains some acceptance from WH when the lepton is lost in detection. DØ uses 2.1 fb^{-1} (the largest dataset in all analyzes presented in this report) and employs the Boosted Decision Tree (BDT) technique which is basically a machine learning technique to extend a simple cut-based analysis into a multivariate technique by continuing to analyze events that fail a particular criterion. The 95% CL limits are set with respect to the SM prediction as shown in figure 4. At 115 GeV/c^2, the limit is 7.5×SM (8.4×SM expected)[8]. In CDF, two separate ANN have been developed for this analysis. The first focuses on discerning real $\not\!\!E_T$ from fake $\not\!\!E_T$ generated by mis-measurement by using track information. The second ANN is trained to optimize the separation of both ZH and WH events from QCD and $t\bar{t}$ backgrounds as shown in figure 4. Using 1.7 fb^{-1} data, CDF found no excess. Therefore upper limits are set. The limit is 8.0 times over the SM prediction (8.3 expected) at $m_H = 115$ GeV/c^2 [7].

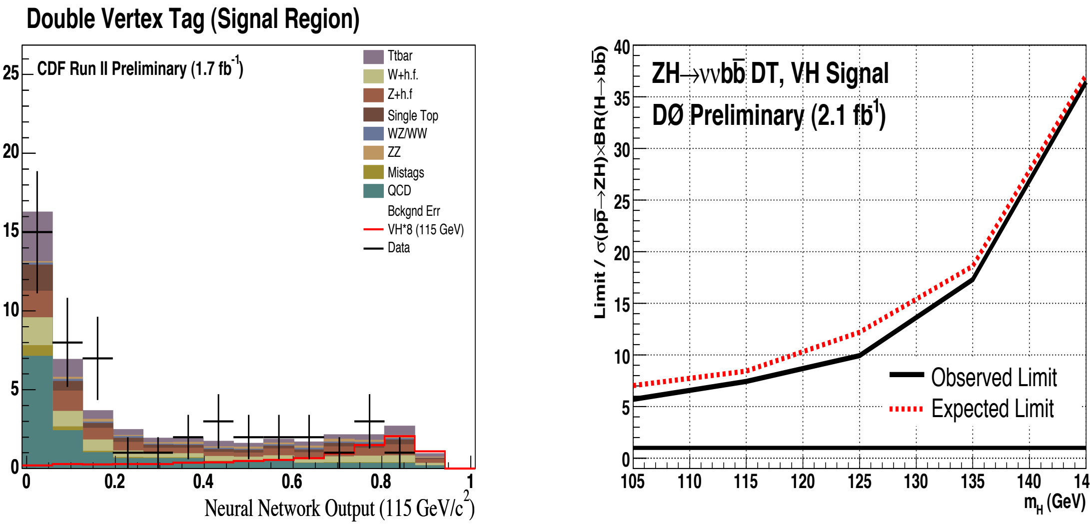

Figure 4: Left: ANN output distribution for 2 btagged events (CDF). Right: Upper limits (relative to the SM prediction) set by DØ $ZH \to \nu\bar{\nu}b\bar{b}$ analysis.

2.4 Search for $WH + ZH + VBF + ggH \to \tau^+\tau^- + 2jets$

All analyzes presented so far use $H \to b\bar{b}$ decay to take an advantage of the high branching ratio while it is smaller for $H \to \tau\tau$ (about 7~8%). CDF however performed the first dedicated search for the SM Higgs boson using τ decay. To recover disadvantage of Higgs decay rate, four signal processes are considered and simultaneously searched as shown in figure 5. The signature is one isolated lepton (τ_{lep}) from leptonic τ decay, one hadronic τ (τ_{had}) from another τ, and two or more jets. No other cuts are imposed in the event selection but instead ANN is trained in order to incorporate possible kinematic variables and their correlations to maximize discrimination power against backgrounds. Main backgrounds are $Z \to \tau\tau + jets$ and jet faking τ_{had} (mainly from $W + jets$ and QCD). After all jet $\to \tau_{had}$ backgrounds are estimated and modeled by data-driven way (using the same sign ($Q(\tau_{lep}) \times Q(\tau_{had}) > 0$) data), three ANN are trained: 1) Mixed signal vs $Z \to \tau\tau$, 2) Mixed signal vs QCD, 3) Mixed signal vs $t\bar{t}$, where mixed signal is a mixture of four signal events. Then given a event, those three ANN scores are calculated and the minimum of the three is selected for making the final ANN distribution. With 2 fb^{-1} CDF data, the simultaneous search was performed but there was no clear excess in signal region as shown in figure 5. Therefore 95% CL limits are set. The result at $m_H = 115$ GeV/c^2 is 30×SM (24 expected) [9].

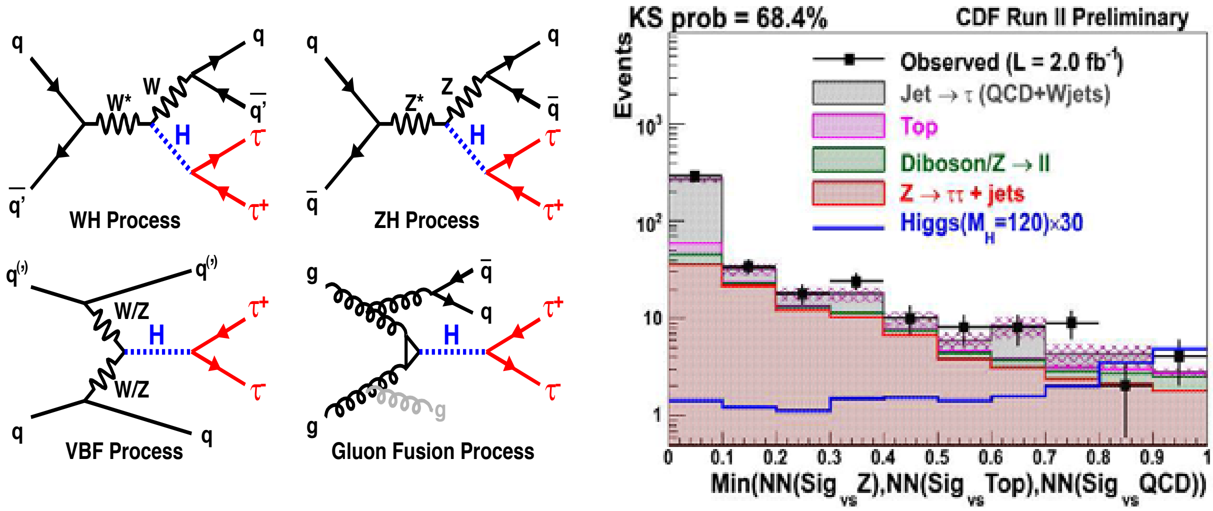

Figure 5: Left: Signal Feynman diagrams used in this analysis. Right: ANN distribution with 2.0 fb^{-1} CDF data. The Higgs signal (times 30) is shown in blue line.

3 Tevatron Combined Limits

Figure 6 shows the current Tevatron limits (at 95% CL) on the Higgs production cross section to the SM predictions. In this combination, all CDF and DØ results are included except for the new CDF's $H \to \tau^+\tau^- + 2jets$ result. Also for DØ $ZH \to \nu\bar{\nu}b\bar{b}$ analysis, only 0.9 fb^{-1} data is currently combined. At $m_H = 115$ GeV/c^2, the observed limit is 6.2×SM (4.3 expected) [10].

4 Conclusions

We have reviewed new preliminary results for the SM Higgs boson searches performed by the CDF and DØ collaborations with 1.0-2.1 fb^{-1} dataset accumulated from $p\bar{p}$ collisions at $\sqrt{s} =$ 1.96 TeV. No signal is found in both experiments and the 95% CL limits are set for a wide range of Higgs mass. At $m_H = 115$ GeV/c^2, combined result now is only about 5 times far from the SM

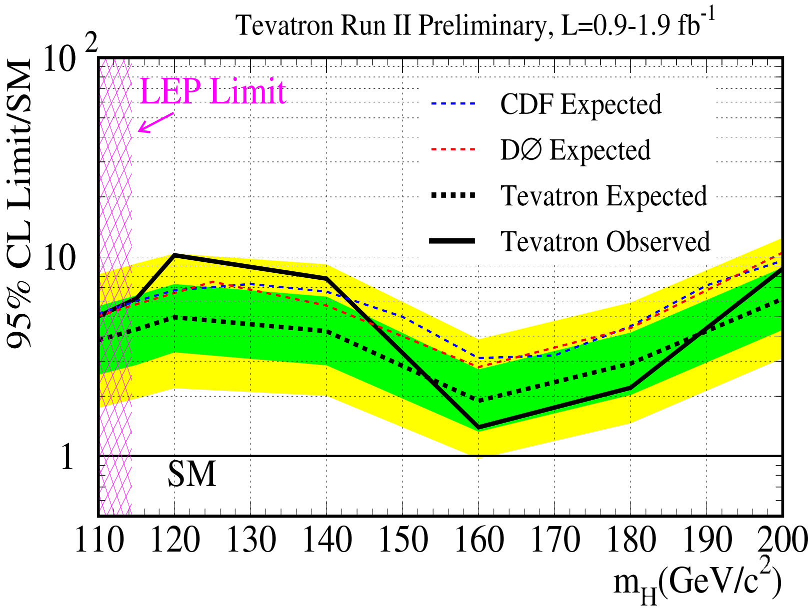

Figure 6: Tevatron combined limits: Ratio of the observed/expected 95% CL limits on Higgs production to the SM predictions as of December 2007. All channels described in this report are combined except for the CDF $H \to \tau\tau + 2jets$ result.

prediction for the exclusion. Furthermore, there are some results not yet combined and also more improvements can be expected and already planned by adding new decay channels, improving b-tagging quality and using advanced technique and so on. On the other hand, CDF and DØ expect to collect at least 6 fb^{-1} data by 2009. Therefore together with expected improvements, there might be a great chance to discover or exclude the SM Higgs even in this challenging low mass region by the end of Run II.

Acknowledgments

I would like to thank the members of the CDF and DØ collaborations for their work and effort in achieving the results presented in this report. Also I would like to thank the Moriond conference organizers for the invitation and great hospitality during the conference and the funding agencies for making this work possible.

References

1. LEP Electroweak Working Group, http://lepewwg.web.cern.ch/LEPEWWG/ (2008).
2. T. Aaltonen *et al.*, [CDF Collaboration], *Phys. Rev. Lett.* **100**, 041801 (2008).
3. CDF Collaboration, CDF Public Note 9219 and references therein (2008).
4. DØ Collaboration, Conference Note 5472-CONF (2007).
5. CDF Collaboration, CDF Public Note 8742 (2007).
6. DØ Collaboration, Conference Note 5482-CONF (2007).
7. DØ Collaboration, Conference Note 5586-CONF (2008).
8. CDF Collaboration, CDF Public Note 9166 (2008).
9. CDF Collaboration, CDF Public Note 9248 (2008).
10. TEVNPHWG Group, FERMILAB-PUB-07-656-E, arXiv:hep-ex:0712.2383v1

Searches for non-SM Higgs Bosons at the Tevatron

Andrew Haas *for the DZero and CDF collaborations*
Columbia University, New York, NY, USA

Extensions of the Standard Model (SM) predict Higgs phenomenology which can be quite different from that expected within the SM. This contribution discusses the latest results from searches for Higgs bosons by the DZero and CDF experiments at the Tevatron in several non-SM scenarios: supersymmetry, left-right symmetric (Higgs-triplet), and fermiophobic.

1 Introduction

The Tevatron accelerator at Fermilab has performed very well in recent years, delivering over 3.5 fb^{-1} of data. The DZero and CDF experiments are using this data to study many questions at the forefront of high-energy physics. A central goal is the understanding of electro-weak symmetry breaking, which gives the W and Z bosons mass while leaving the photon massless. In the SM, electro-weak symmetry breaking is delivered via the Higgs mechanism, which predicts a single neutral spin-0 boson - the Higgs boson. Extensions to the SM, such as supersymmetry, predict different productions and/or decays of the Higgs boson and often a richer spectrum of multiple Higgs bosons.

We will discuss first the most anticipated extension to the SM, supersymmetry. Both DZero and CDF have specifically tuned searches for the new neutral Higgs boson(s) of supersymmetry, in the $bh \rightarrow bbb$, $h \rightarrow \tau\tau$, and $bh \rightarrow b\tau\tau$ channels. Next we show the results for left-right symmetric or Higgs-triplet models, which predict a doubly-charged Higgs boson, H^{++}. Finally, DZero has considered the case where the Higgs prefers not to decay to fermions, the so-called fermiophobic scenario, leaving open the $h \rightarrow \gamma\gamma$ channel as the main decay mode for a low-mass Higgs boson.

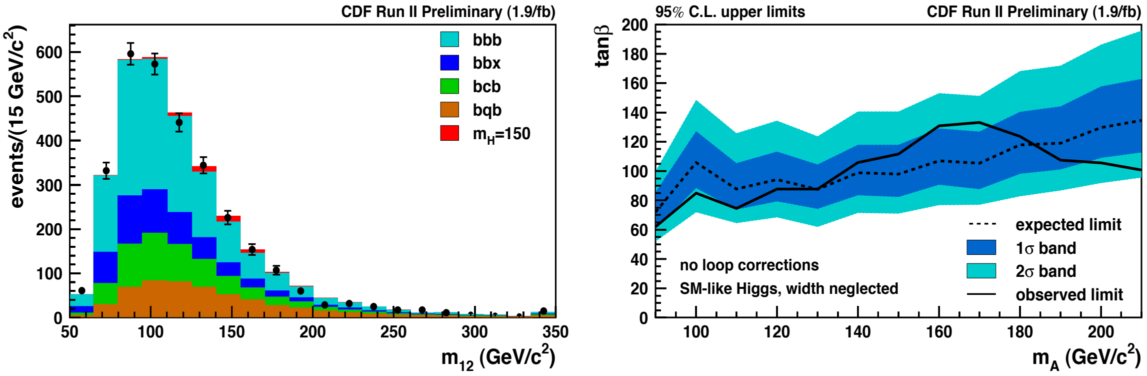

Figure 1: The di-jet invariant mass spectrum in bbb events and corresponding limits in the m_A - $tan\beta$ parameter space of the MSSM from the CDF $bh \rightarrow bbb$ analysis.

2 Searches in the MSSM at high $tan\beta$

In two-Higgs-doublet models of electro-weak symmetry breaking, such as the minimal supersymmetric extension of the standard model (MSSM) [1], there are five physical Higgs bosons: two neutral CP-even scalars, h and H, with H being the heavier state; a neutral CP-odd state, A; and two charged states, H$^{\pm}$. The ratio of the vacuum expectation values of the two Higgs fields is defined as $tan\beta = v_u/v_d$, where v_u and v_d refer to the fields that couple to the up-type and down-type fermions, respectively. At tree level, the coupling of the A boson to down-type quarks, such as the b-quark, is enhanced by a factor of $tan\beta$ relative to the SM, and the production cross section is therefore enhanced by $tan^2\beta$ [2]. At large $tan\beta$, this is also true either for the h or H boson depending on their mass. At high $tan\beta$, the h/H and A decay roughly 90% to bb and 10% to $\tau\tau$.

The dominant decay to bb is unfortunately drowned by QCD background, but due to the enhanced coupling to b-quarks the h/H and A are also produced in association with one or more b-quarks, opening the channel $bh \rightarrow bbb$. Both DZero and CDF have performed searches for an excess in the di-jet invariant mass spectrum of the bbb final state. CDF's latest results are shown in Figure 1, using 1.9 fb^{-1} of data. The dijet mass spectrum of the heavy flavor multi-jet background is derived from double-tagged data in a manner that accounts for tagging biases and kinematic differences introduced by the addition of the third tag. No excess is observed for any di-jet invariant mass window, so limits are placed in the Higgs mass vs. $tan\beta$ parameter space.

The subdominant decay of the h/H or A to $\tau\tau$ is much cleaner, so both DZero and CDF have searched for direct $h \rightarrow \tau\tau$ excesses, see Figures 2 and 3. The main background is from $Z \rightarrow \tau\tau$, which is essentially irreducible.

At DZero, a set of Neural Networks (NN) are trained to identify tau decays from jet backgrounds, for each of 3 tau types (charged pion-like, pion + EM shower-like, and 3-prong). One of the taus is required to decay to a muon, for triggering and to reduce QCD background. The QCD background is determined by comparing same-sign vs. opposite-sign candidates. Some loose selection cuts remove W backgrounds, such as requiring the visible W mass <20 GeV. Finally, a set of NN's (one for each tau type) is used to separate signal from backgrounds. Good agreement is seen between data and expected background at high NN output, so limits are placed on the signals' cross-sections and interpreted in the Higgs mass vs. $tan\beta$ parameter space. CDF has performed similar analyses, but using in addition the e+tau and e+mu decay channels, as well as more data. No NN separation is employed, however.

By adding the requirement that there be an associated b-quark in the production, followed by the clean di-tau decay, $bh \rightarrow b\tau\tau$ has the highest signal / background of any high $tan\beta$ MSSM

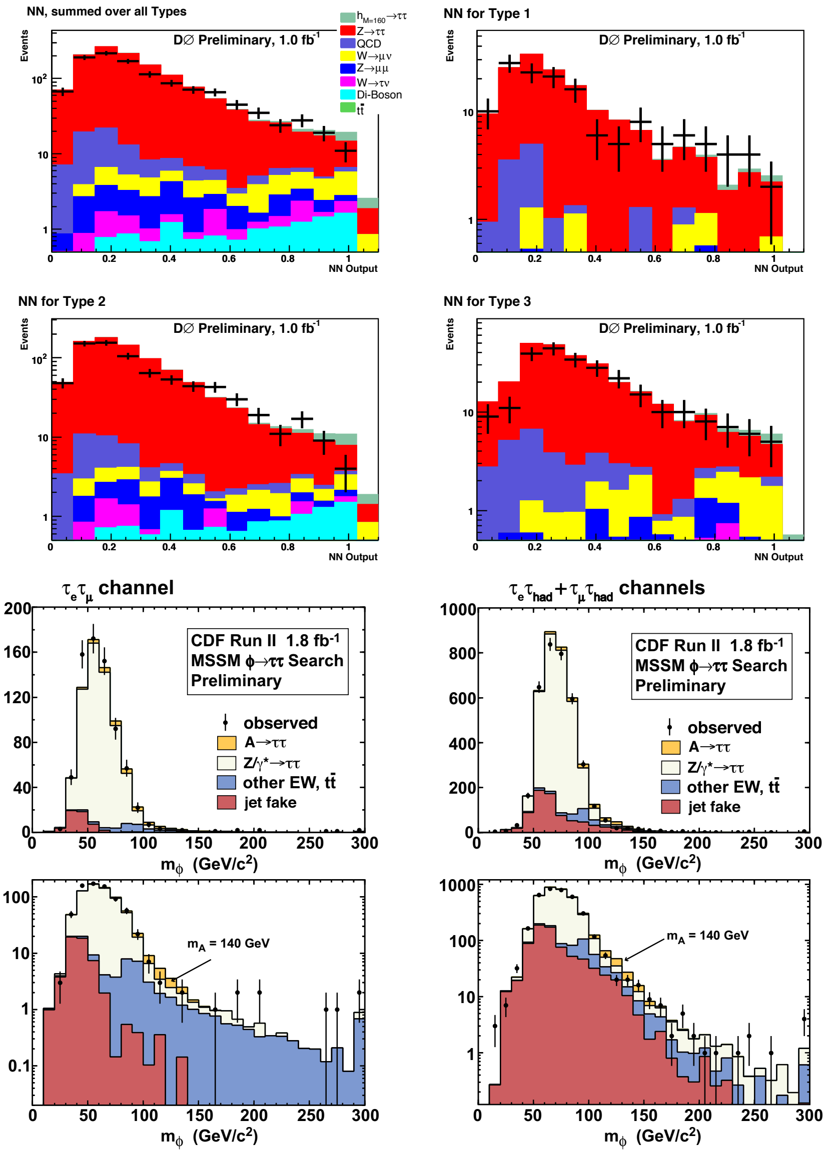

Figure 2: (top) NN outputs for all tau types (top left) and each tau type (see text) individually in the DZero $h \to \tau\tau$ analysis. (bottom) Visible mass distributions in the CDF $h \to \tau\tau$ analysis for the $e\mu$ and $lepton + \tau$ channels.

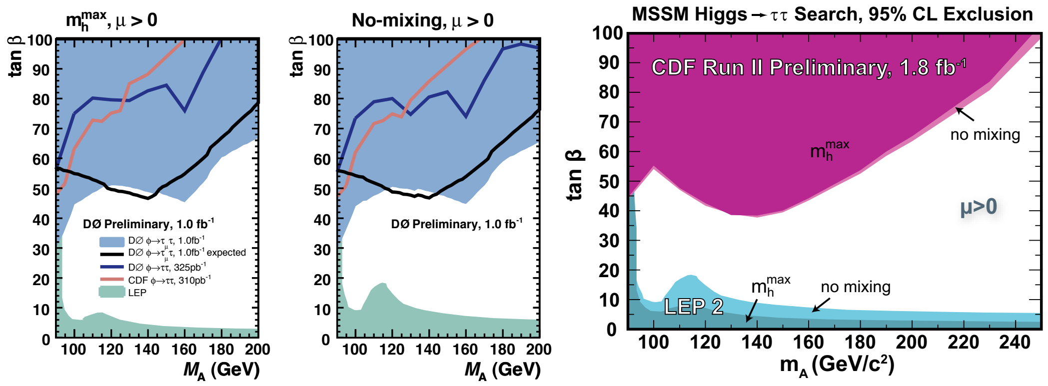

Figure 3: D0 (left) and CDF (right) limits in the m_A - $tan\beta$ parameter space of the MSSM from the $h \to \tau\tau$ analyses.

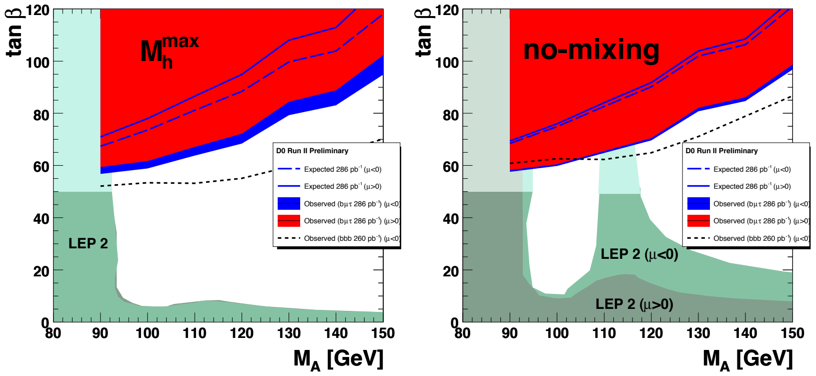

Figure 4: Limits in the m_A - $tan\beta$ parameter space of the MSSM from the DZero $bh \rightarrow b\tau\tau$ analysis.

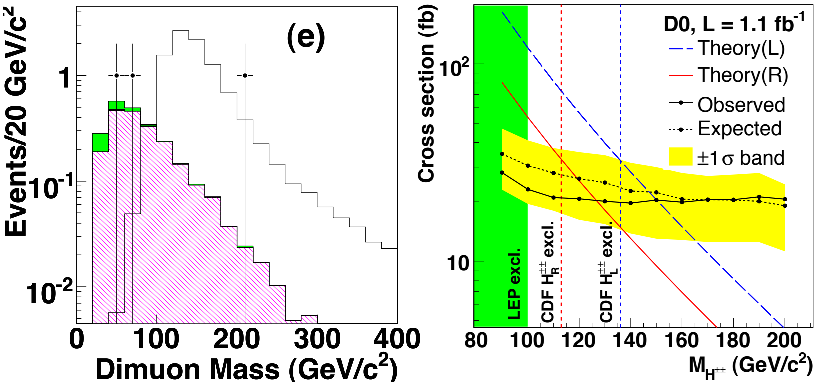

Figure 5: (left) Di-muon invariant mass spectrum in events with 3 muons. (right) Limits on the H^{++} mass for left- or right-handed Higgs bosons from the latest DZero search.

Higgs search. It also suffers from a low cross-section times branching ratio however. DZero has performed a search using just 344 pb^{-1} of data in this channel. Di-tau events are normalized to the $Z \rightarrow \tau\tau$ peak, and then an additional b-tagged jet is required with p_T >15 GeV. For a Higgs mass of 120 GeV and $tan\beta$=80, there are 5.3 signal events expected, with just 6.3 expected background events. Only 3 events are observed in data, and limits are placed in the Higgs mass vs. $tan\beta$ plane, as seen in Figure 4, competitive with the other channels.

3 Searches for $H^{++}H^{--}$

Many models of beyond-SM Higgs physics predict a doubly-charged Higgs boson, H^{++}, such as left-right symmetric models, Higgs-triplet models, and little-Higgs. DZero has recently updated its search for pair-produced $H^{++}H^{--}$, using 1.1 fb^{-1} of data. 3 muons are required, with p_T >15 GeV. At least one pair must have an invariant mass >30 GeV and $\Delta\phi$ <2.5 radians, to reduce backgrounds from QCD and Z decays. 3 events are observed in data, for an expectation of 3.1 events from backgrounds, and thus limits are set on the H^{++} mass as shown in Figure 5. Left-handed doubly-charged Higgs bosons, H_L^{++} have a larger production cross-section than right-handed, H_R^{++}, by about a factor of 2, due to their different coupling to the intermediate Z boson. Thus, the limit on the mass of H_L^{++} (>150 GeV) are higher than on H_R^{++} (>127 GeV).

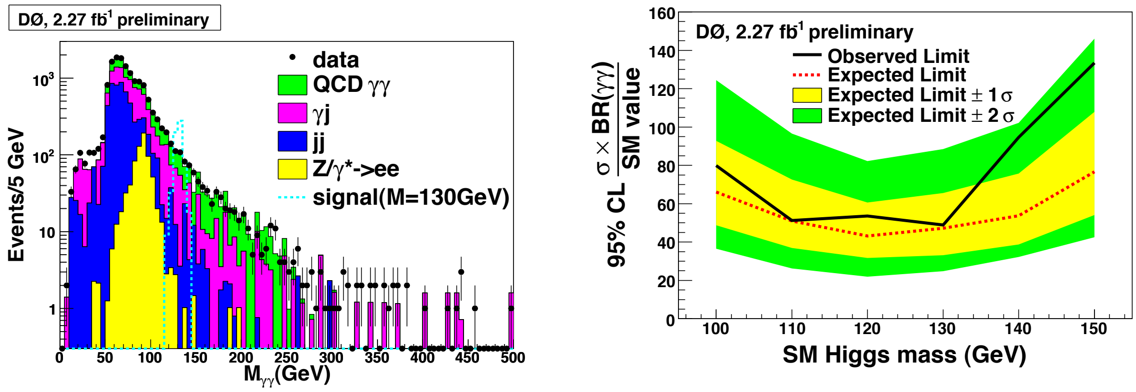

Figure 6: (left) Di-photon invariant mass spectrum and (right) limits on the $h \to \gamma\gamma$ cross-section in units of the SM cross-section from the latest DZero di-photon analysis.

4 Searches for $h \to \gamma\gamma$

Although the SM Higgs boson decays to the di-photon final state with a small branching ratio, this decay channel could be subject to a large enhancement in models where the Higgs does not couple strongly to fermions. In this case, fermion masses could arise from some other source. DZero has recently completed a search using 2.3 fb^{-1} of data for $h \to \gamma\gamma$. 2 isolated photons with p_T >25 GeV are required. QCD jets faking photons are estimated by looking at the calorimeter shower-shape correlations between the two photons in each event, and samples are divided into QCD di-jet, photon+jet, and di-photon backgrounds. $Z \to ee$ also contributes near the Z mass. Data agree very well with estimated backgrounds, and no significant excess is seen at any di-photon invariant mass range. Limits are therefore set on the cross-section times branching ratio for $h \to \gamma\gamma$ and are compared to the expected cross-section times branching ratio in the SM, as shown in Figure 6. The current analysis can exclude down to about 50 times the SM event rate at 120 GeV and in fact also contributes non-negligibly to the SM Higgs search.

5 Conclusions

CDF and DZero have searched for Higgs bosons in several models beyond the SM: the MSSM at high $tan\beta$ in b and τ channels, for doubly charged Higgs, and for fermiophobic Higgs. No significant excesses or deviations indicative of non-SM Higgs signatures have been seen so far. But the Tevatron experiments expect to more than double their data samples in the next two years, hone their search strategies, and enlarge the variety of models considered.

Acknowledgments

We would like to thank the Moriond organizers for a wonderful conference and the EU for their generous funding of young scientists attending.

References

1. H. P. Nilles, Phys. Rept. **110**, 1 (1984); H. E. Haber and G. L. Kane, Phys. Rept. **117**, 75 (1985).
2. J. F. Gunion, H. E. Haber, G. L. Kane, and S. Dawson, “The Higgs Hunter’s Guide,” Addison-Wesley, 1990.

W/Z Production : Asymmetry, Z(p_T), and W+charm at the Tevatron

Jiyeon Han for the CDF and D0 Collaborations
Department of Physics and Astronomy, University of Rochester,
Rochester NY 14627-0171, USA

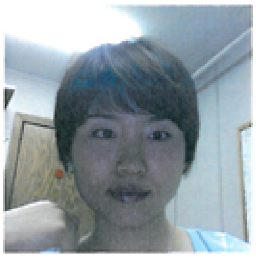

We report on W/Z production processes at the Tevatron, including the W charge asymmetry, the Z boson rapidity and p_T distributions, and the W+charm final state. The measurements test the Standard Model and yield constraints on parton distribution functions. The data samples used range from 0.3 to $2.1fb^{-1}$ of $p\bar{p}$ collisions at $\sqrt{s}$=1.96 TeV.

1 W/Z production at the Tevatron

1.1 Electroweak Physics at Tevatron

Investigations of electroweak processes at the Tevatron have focussed on three different areas: (a) the W mass and width, (b) diboson production, and (c) details of W/Z production processes. Precise measurements of the W mass constrain the mass of the Higgs boson, and measurements of the W width can be compared with Standard Model (SM) predictions. Diboson production provides information on gauge boson self-interactions and is sensitive to physics beyond the SM. Understanding diboson production is also relevant to new particle searches because it is the background to Higgs and SUSY particle production. Measurement of details of W/Z production processes, such Z boson rapidity and p_T distributions and the W charge asymmetry provide information on the up and down parton distribution functions (PDFs) in the proton, while the W+charm cross section is sensitive to the PDF of strange quarks.

1.2 Detectors

We report on results from CDF and D0 Tevatron experiments at Fermilab. The CDF detector has a larger tracking volume which yields better momentum resolution for charged tracks than the D0 detector in the central region. The D0 detector has a larger muon acceptance and more coverage in the forward rapidity region.[1,2]

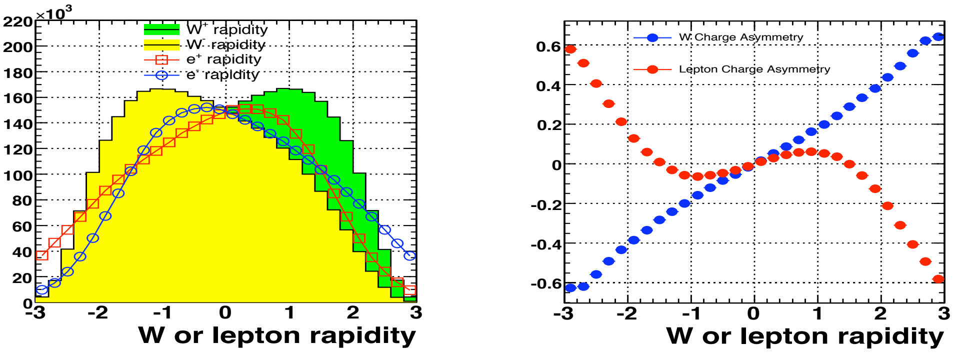

Figure 1: The left figure shows the W boson and lepton rapidity distribution. The right figure replaces the plot with the predicted W and lepton charge asymmetries.

1.3 W Boson and Lepton Charge Asymmetry

$W^+(W^-)$ events are produced in the collisions of $u(\bar{u})$ and $\bar{d}(d)$ quarks. Since, on average, the $u(\bar{u})$ quark carries a higher momentum fraction than the $\bar{d}(d)$ quark, the $W^+(W^-)$ is boosted along the proton (anti-proton) direction. This results in a W charge asymmetry. The W charge asymmetry $(A(y_W))$ is defined as :

$$A(y_W) \quad = \quad \frac{d\sigma(W^+)/dy_W - d\sigma(W^-)/dy_W}{d\sigma(W^+)/dy_W + d\sigma(W^-)/dy_W} \tag{1}$$

At LO, it can be described in terms of the momentum fractions of the u and d quarks :

$$A(y_W) \quad \approx \quad \frac{d(x_2)/u(x_2) - d(x_1)/u(x_1)}{d(x_2)/u(x_2) + d(x_1)/u(x_1)} \tag{2}$$

where $x_{1,2} = \frac{M_W}{\sqrt{s}} e^{\pm y_W}$. The $A(y_W)$ is sensitive to slope of $d(x)/u(x)$.

Experimentaly, the lepton charge asymmetry is measured:

$$A(\eta_\ell) \quad = \quad \frac{d\sigma(\ell^+)/d\eta_\ell - d\sigma(\ell^-)/d\eta_\ell}{d\sigma(\ell^+)/d\eta_\ell + d\sigma(\ell^-)/d\eta_\ell} \tag{3}$$

The measured lepton charge asymmetry is a convolution of the W charge asymmetry, and the asymmetry from the V-A interaction. Figure 1 shows the W boson and the lepton rapidity distributions and the resulting W and lepton charge asymmetries.
At large lepton pseudorapidities, the V-A interaction distorts the boson production asymmetry.

DØ and CDF collaboration use different approaches in the measurement of the W asymmetry. The DØ collaboration uses the traditional method of measuring the charge asymmetry in the muon decay channel. The data sample consists of 0.3 fb^{-1}. Figure 2 shows the lepton charge asymmetry versus muon pseudorapidity. The central region measurements by both CDF and DØ $(|\eta_\mu| < 1.3)$ have been used to constrain PDFs in previous fits. The high rapidity region $(|\eta_\mu| > 1.3)$ probes the PDFs at higher x. The high rapidty region is still statistics limited.

A new measurement by the CDF collaboration extracts the W charge asymmetry from the lepton charge asymmetry. The W boson rapidity (y_W) can be determined from the 4-momentum of the final state neutrino. However, the momentum of the neutrino in z-direction (P_z^ν) is not measured and only its transverse momentum is known (the missing transverse energy of the event). The P_z^ν is calculated as follows:

$$M_W^2 = (E_\ell + E_\nu)^2 - (P_\ell + P_\nu)^2 \tag{4}$$

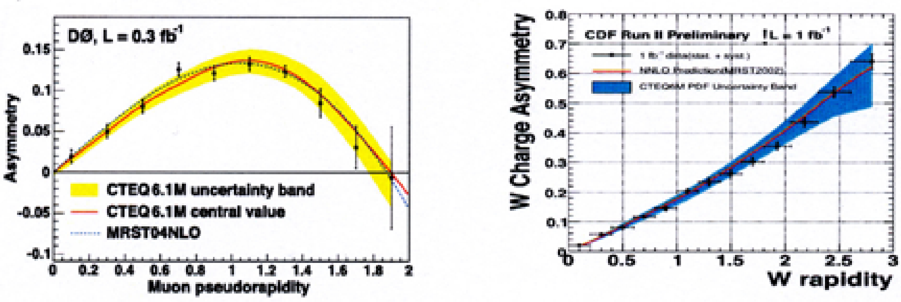

Figure 2: The left plot shows the lepton charge asymmetry in muon pseudorapidity measured in DØ, and the right plot shows the W boson charge asymmetry in boson rapidity measured in CDF.

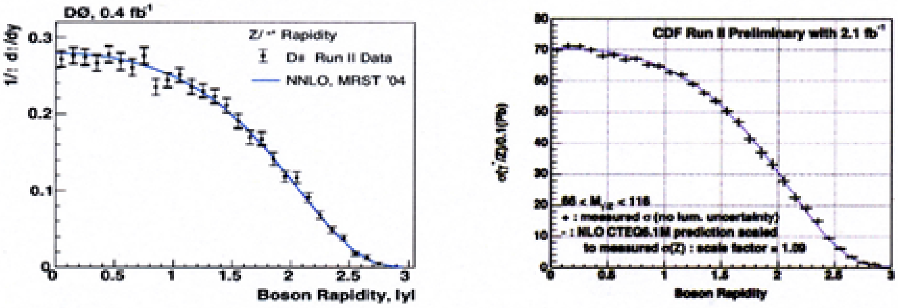

Figure 3: Z boson rapidity distributions. The left plot is the normalized of Z boson rapidity distribution measured at DØ, and the right plot is the Z boson rapidity measured at CDF. The theory prediction is normalized to the measured total σ.

where M_W is constrained to the W boson mass. There are two solutions for P_z^{ν}. Each P_z^{ν} solution is weighted by a factor which includes the $W^{\pm}$ production cross section ($d\sigma/dy_W$), the V-A angular distribution function in the center-of-mass frame ($1 \pm cos^2\theta^*$), and a $W^{\pm}$ transverse momentum (P_T^W) factor to account for higher order QCD corrections to the V-A $cos\theta^*$ term. The dependence on input $d\sigma/dy_W$ is removed by iterating the measurement. Each iteration is used further to constrain $d\sigma/dy_W$. Here, the larger acceptance electron sample with 1 fb^{-1} is used.

The W charge asymmetry for 1 fb^{-1} data is shown in Figure 2. There is good agreement with the NNLO prediction using MRST2002 PDFs.[5,6] The experimental error is smaller than the current uncertainty in the PDFs, and the new data can be used further constrain PDFs in future fits.

1.4 The Z Boson Rapidity Distribution: $d\sigma/dy$

In the Drell-Yan process, the quark and anti-quark carry parton momentum fractions, x_1 and x_2. The difference in the parton momentum fractions ($x_{1,2}$) determine the rapidity of the final state Z boson (y_Z). Since high y_Z corresponds to high x_1 and low x_2, this region probes PDFs at high x. In addition, the $d\sigma/dy$ distribution tests QCD theory predictions at higher orders. In higher order (NLO or NNLO), gluons splitting in the initial state also contribute to the rapidity distribution. Both DØ and CDF measure $d\sigma/dy$ using the dielectron final state. In both measurements, y_Z measurements extend up to 2.9. The DØ measurement, shown in Figure 3, with 0.4 fb^{-1} shows good agreement with the NNLO MRST[7] prediction. The CDF measurement, also shown in Figure 3, uses 2.1 fb^{-1}. Figure 4 shows the ratio of the CDF data to the NLO calculation with NLO CTEQ6.1M PDFs.[8]

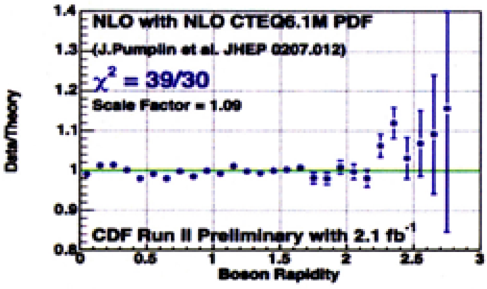

Figure 4: Ratio of data and theory prediction for the Z boson rapidity distribution in CDF. Here, the NLO calculation with NLO CTEQ6.1M PDFs is used. The theory prediction is normalized to the measured σ.

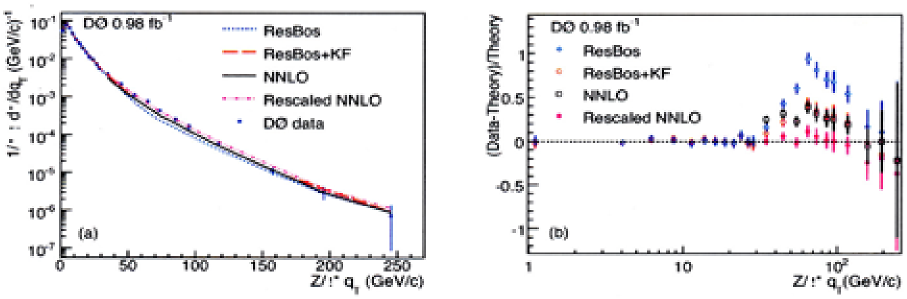

Figure 5: The left plot shows the normalized differential cross section of Z boson p_T up to $p_T < 260GeV/c$. The right plot shows the fractional difference between data and the theory predictions. "KF" is the scale factor(K-factor) of NLO to NNLO theory calculation.

1.5 Z(p_T) Distribution

The Z boson p_T which can be measured over a wide range of values provide a test of QCD. In the $p_T > 30GeV/c$ region, where the p_T originates from the radiation of energetic gluons, the perturbative QCD calculation[9](NNLO[10]) gives reliable predictions. In the $p_T < 30GeV/c$ region, where multiple soft gluon emission is dominant, the soft gluon resummation technique is used (ResBos).[11,12] The DØ measurement in the Z with 0.98 fb^{-1} of data in the ee channel is shown in Figure 5. The ResBos curve is the gluon resummation calculation including PHOTOS[15], which accounts for radiated photons in the final state. The "Rescaled NNLO" is the NNLO calculation rescaled to match the data at $p_T = 30GeV/c$. The right hand side of Figure 5 shows the fractional differences between the data and theory on a linear scale. In the $p_T < 30GeV/c$ region, the ResBos calculation describes the data well. For $p_T > 30GeV/c$, the data is higher than all predictions. The NNLO theory prediction agrees with the data only in shape.

DØ also investigated the "Small-x broadening effect"[13,14] that predicts a wider p_T distribution in the large rapidity region. This effect modifies the resummation form factor in the small-x parton region. At the Tevatron, Z bosons with $2 < |y| < 3$ probe the Bjorken x region, $0.002 < |x| < 0.006$. Therefore, a measurement of the Z boson p_T in the high rapidity region is sensitive to the modified form factor. Figure 6 shows the $p_T < 30GeV/c$ region for all y_Z and for $|y_Z| > 2$. The standard ResBos calculation agrees well with the data in all y_Z. The $|y_Z| > 2$ region data does not favor an additional small-x form factor. This is the first test of the "small-x broadening effect" using the high y region at the Tevatron.

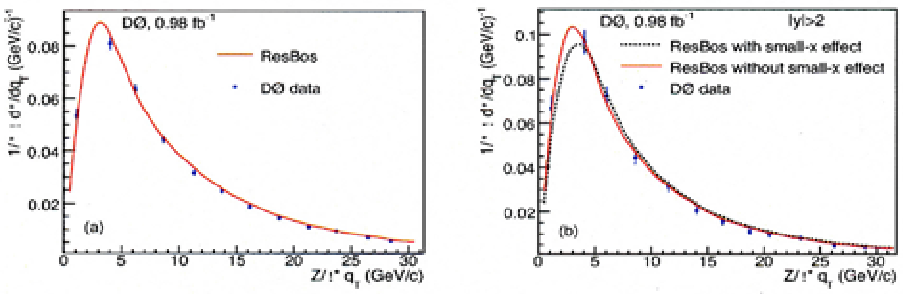

Figure 6: The plots show the normalized differential cross section of Z boson p_T measured at DØ. The left plot shows the result for all boson rapidity, and the right plot shows the result in the high rapidity region ($|y_Z| > 2$), which is sensitive to the "small-x broadening effect".

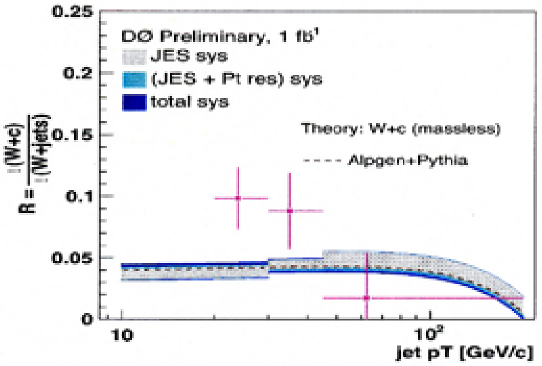

Figure 7: The cross section ratio W+c-jet to W+jets measured at DØ.

1.6 W+Charm Cross Section

The W+charm process, $g + s \rightarrow W^- + c$, is a background to top, SUSY particle, and SM Higgs production. Since CKM matrix element, $|V_{cd}|^2$ suppresses the d-quark-gluon fusion production, the W+charm production probes the s-quark PDF. Strange quarks contributes to the processes, $p\bar{p}/pp \rightarrow sg \rightarrow W^- + c$ and $p\bar{p}/pp \rightarrow s\bar{c} \rightarrow H^-$, at the Tevatron and LHC. At hadron colliders, the s-quark distribution is probed at large $Q^2 \approx M_W^2$.

The DØ and CDF collaborations tag the c-jet by looking for the muon from the decay of the charm particle in the c-jet. The muon from the decay of the charm particle and the lepton from the W boson decay have the opposite electric charge. The opposite charge requirement is used in the event selection. All leptonic channels are allowed for the W boson decay. $Z \rightarrow \mu\mu$ events are rejected by requiring $M_{\mu\mu} < 70GeV/c^2$ for the muon decay channel. DØ measures the cross section ratio of the W+c-jet to W+jets processes, $\frac{\sigma(p\bar{p} \rightarrow W+c-jet)}{\sigma(p\bar{p} \rightarrow W+jets)}$, using $1\ fb^{-1}$ data. The fraction of $\sigma(W + c - jet)$ compared with the theory versus jet p_T is shown in Figure 7. The fraction of $\sigma(W + c - jet)$ for $p_T > 20GeV/c$ is 0.071 ± 0.017. The measured fraction in the electron channel is $0.060 \pm 0.021(stat.)^{+0.005}_{-0.007}(sys.)$ and the fraction in the muon channel is $0.093 \pm 0.029(stat.) \pm 0.005(sys.)$.

CDF measures the total cross section of W+c-jet with $1.8\ fb^{-1}$ data. Both electron and muon channels are used for the W boson selection. The c-jets with $p_T(c) > 20GeV/c$ and $|\eta(c)| < 1.5$ are identified using the semi-muonic decay of the charm particle in the jet. The measured cross section for the leptonic channel, $\sigma_{Wc} \times BR(W \rightarrow \ell\nu)$, is $9.8 \pm 2.8(stat.)^{+1.4}_{-1.6}(sys.) \pm 0.6(lum)pb$, which agrees with the NLO calculation, $11.0^{+1.4}_{-3.0} pb$.

1.7 Conclusion

New high statistics measurements of W and Z production processes at the Tevatron are used to provide new constraints on nucleon PDFs. The W charge asymmetry and Z boson $d\sigma/dy$ measurement have been extended up to $y \approx 2.9$. The Z boson $d\sigma/dy$ measurement is with 2.1 fb^{-1} of data, and 8 fb^{-1} is expected by end of 2009.

Acknowledgments

We thank the CDF and DØ collaborations, the Fermilab staff, and the members of the University of Rochester CDF group.

References

1. D. Acosta et al. (CDF Collaboration) , *Phys. Rev.* D **71**, 052003 (2005).
2. B. Abbott et al. (D0 Collaboration) , *Phys. Rev.* D **61**, 032004 (2000).
3. J. Pumpkin et al. , JHEP **0207**, 012 (2002) and D. Stump et al. , JHEP **0310**, 046 (2003).
4. A.D. Martin et al. (MRST Collaboration), *Phys. Lett.* B **604**, 61 (2004).
5. C. Anastasiou et al. , *Phys. Rev.* D **D69**, 094008 (2004).
6. A.D. Martin, R.G. Roberts, W.J. Stirling and R.S. Thorne (MRST Collaboration), EPJ **C28**, 455 (2003).
7. L. Dixon et al. (MRST Collaboration) , *Phys. Rev.* D **69**, 09408 (2004).
8. J. Pumplin et al. (CTEQ Collaboration), hep-ph/ **0201195**, 455 (2002).
9. P.B. Arnold and M.H. Reno , Nucl. Phys. **B319**, 37 (1989); R.J. Gonsalves, J. Pawlowski and C-F. Wai , *Phys. Rev.* D **40**, 2245 (1989);.
10. K. Melnikov and F. Petriello , *Phys. Rev.* D **74**, 114017 (2006).
11. C. Balazs and C.P Yuan , *Phys. Rev.* D **56**, 5558 (1997)
12. P.B. Arnold and R. Kauffman , Nucl. Phys. **B349**, 381 (1991).
13. P. Nadolsky, D.R. Stump, and C.P. Yuan , *Phys. Rev.* D **61**, 014003 (2000).
14. P. Nadolsky, D.R. Stump, and C.P. Yuan , *Phys. Rev.* D **64**, 114011 (2001).
15. E. Barberio and Z. Was , Comput. Phys. Commun. **79**, 291 (1994).

ELECTROWEAK MEASUREMENTS FROM HERA

Y. R. de Boer

On behalf of the H1 and ZEUS collaborations

DESY
Notkestrasse 85
22607 Hamburg, Germany

New preliminary electroweak results from the HERA lepton-proton collider experiments H1 and ZEUS are presented. These include new high Q^2 neutral current cross section measurements, limits on a possible quark radius in the search for contact interactions as well as on quark-Z coupling parameters, extracted in combined electroweak and QCD fits. Furthermore, new charged current cross section measurements as a function of the lepton-beam polarisation are presented, as well as charged current measurement results, using the combined HERA I data from H1 and ZEUS. Finally, measurements of the single W boson production cross section and the W boson polarisation fractions are presented.

1 Introduction

The lepton-proton collider HERA [1] has facilitated measurements of electroweak (EW) interactions between quarks and leptons in deep inelastic scattering (DIS) at a centre of mass energie up to 320 GeV and four momentum of the exchanged boson squared (Q^2) up to 40000 GeV^2. The data taking took place in the years 1994-2000 (HERA I) and 2003-2007 (HERA II). Two collider-mode detectors, H1 [2] and ZEUS [3], have each collected approximately 0.5 fb^{-1} of data, divided in electron-proton (e^-p) and positron-proton (e^+p) data. Previously obtained HERA results have led to a significantly improved understanding of the proton substructure[4,5] allowing for measurements of important EW parameters [6,7,8,9] as well as searches [10,11] for contact interactions. In these proceedings, updates are presented to these analyses along with new results from H1 regarding the single production of W bosons at HERA.

2 Neutral Current Cross Section Measurement

New H1 Neutral Current (NC) single differential cross section measurements [12] as a function of Q^2, are presented in Figure 1. The analysis includes previously published [7,13,14] HERA I and preliminary [15] HERA II data, corresponding to an integrated luminosity of 270 pb^{-1} of e^+p data and 165 pb^{-1} of e^-p data. The measurement precision is better than 10% for Q^2 up to 20000 GeV^2. The data agree well with SM QCD expectations, which are based on parton distribution functions obtained using high energy HERA I data. [4]

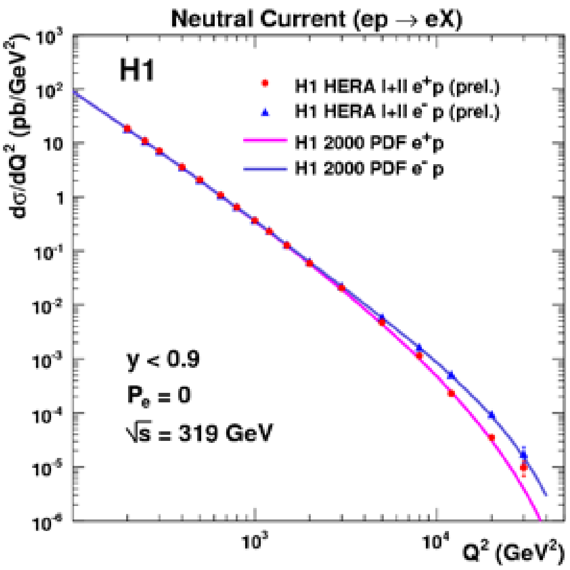

Figure 1: NC single differential cross sections as a function of Q^2, measured by H1 using e^+p (points) and e^-p (triangles) DIS data from the full HERA I+II data set, compared to the SM QCD expectations (solid lines). The interference between the photon and Z boson, which is different in e^+p and e^-p collisions, becomes visible at Q^2 of the order 10^4 GeV^2.

3 Derivation of Limits on the Quark Radius in Contact Interactions

In the search for contact interactions, both H1 and ZEUS derive limits on a possible quark radius using high Q^2 NC events.[12,16] A form factor f_q, as a function of Q^2 and a hypothetical quark radius R_q, is defined as $f_q\left(Q^2, R_q\right) \equiv 1 - \frac{1}{6}\left\langle R_q^2\right\rangle Q^2$. This leads to an altered single differential cross section $\mathrm{d}\sigma/\mathrm{d}Q^2 = f_q\left(Q^2, R_q\right)\mathrm{d}\sigma_{SM}/\mathrm{d}Q^2$ for contact interactions, which can be fit to the data, as is shown in Figure 2. The 95% Confidence Level (CL) limits on the quark radius are determined from the fit to be $0.74 \cdot 10^{-18}$ m and $0.62 \cdot 10^{-18}$ m, by H1 and ZEUS, respectively. These limits confine a hypothetical quark radius to be less than or equal to the resolution power of HERA.

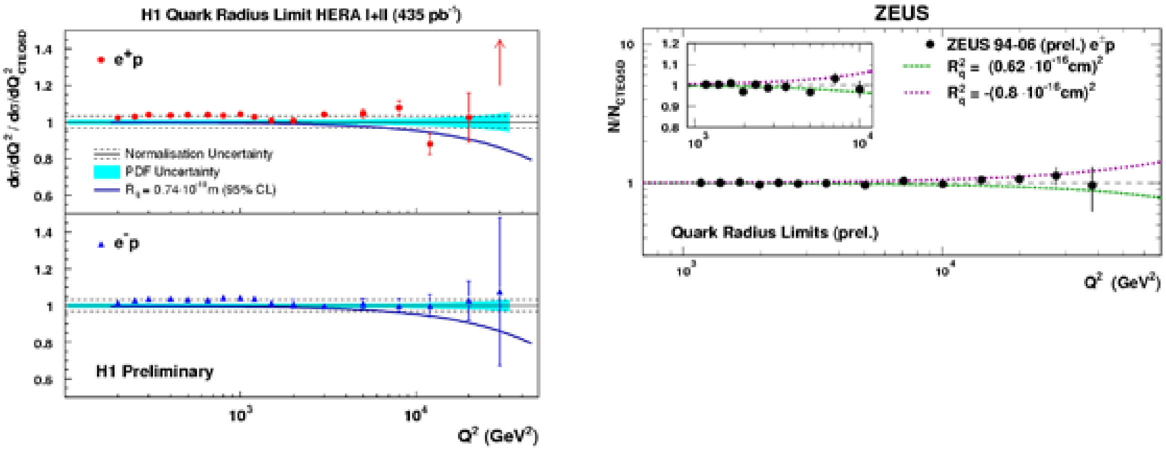

Figure 2: NC single differential cross sections as a function of Q^2 normalised to the SM expectation $\mathrm{d}\sigma_{SM}/\mathrm{d}Q^2$. The lines represent corrections due to the hypothetical quark radius R_q at its 95% CL limit for H1 e^+p data (top left), H1 e^-p data (bottom left), and for ZEUS $e^{\pm}p$ (right).

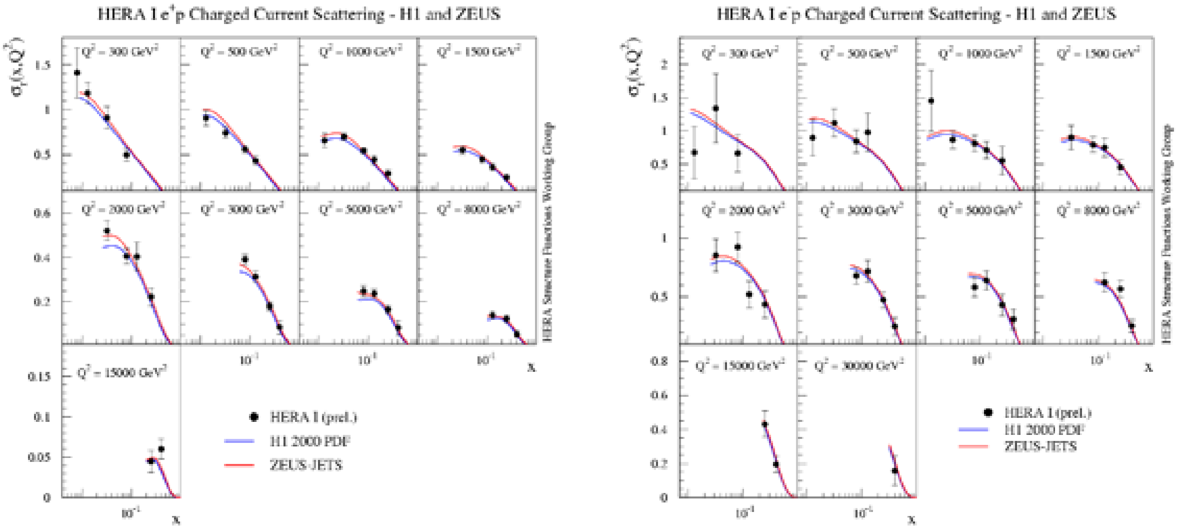

Figure 3: Reduced CC cross sections (points), using the combined HERA I data of H1 and ZEUS, in bins of Q^2 for e^-p (left) and e^+p (right) data. The curves are NLO QCD fits, performed by H1 and ZEUS to their own data.

4 Combination of H1 and ZEUS Charged Current HERA I Data

The H1 and ZEUS collaborations are combining their data to improve the precision of DIS measurements.[17] New preliminary results, using combined HERA I data of H1 and ZEUS, are shown in Figure 3, depicting CC reduced cross sections in bins of Q^2. A good agreement is observed between the combined data[18] and the QCD fits of each experiment[4,19] to their own data. The e^+p data correspond to a total integrated luminosity of approximately $200\,\mathrm{pb}^{-1}$ and have a typical precision of 8%. The statistical gain in precision is most significant in the statistically limited e^-p data set, where the combined data ($30\,\mathrm{pb}^{-1}$) leads to an increase of the precision to about 20%. The precision is expected to increase further with the future inclusion of the HERA II data.

5 Charged Current Cross Section Measurement using Polarised Lepton-Beams

During the HERA II running period, longitudinally polarised lepton-beams were used. The polarisation is defined as $P_e \equiv (N_R - N_L)\,/\,(N_R + N_L)$, with N_R (N_L) the number of right (left) handed leptons in the beam. The SM predicts a linear scaling of the CC cross section with the beam polarisation, due to the absence of a right handed neutrino. New ZEUS results,[20] using data from the years 2006-2007, are shown in Figure 4, together with previously obtained HERA measurements.[21,9] A good agreement between the measurements in the different data sets and the SM expectations is observed.

6 Measurement of the quark-Z coupling

The cross section of NC DIS events composes of photon (γ) and Z exchange diagrams. Due to the heavy Z boson propagator, the contribution from pure Z exchange is suppressed. The contribution from γZ interference, however, is still sensitive to the vector and axial-vector couplings of the Z boson to the quark. Limits at 68% CL on these couplings are extracted, using combined EW and QCD fits where the coupling parameters pertaining to both the up and down quark are left free in the fit.[22,23] In particular, the limits concerning the couplings to the up quark (v_u and a_u) profit from including the polarised HERA II data. The results are shown in

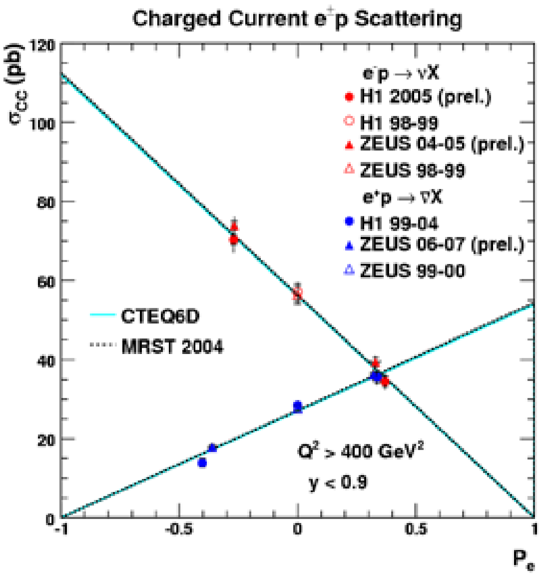

Figure 4: The polarisation dependence of the charged current cross section on the lepton-beam polarisation P_e. The curves are the SM QCD predictions using two different PDF fits.

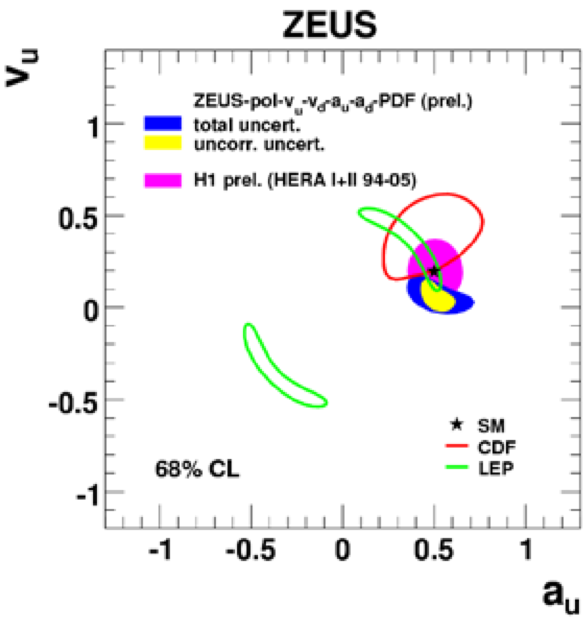

Figure 5: Limits at 68% CL on the vector and axial-vector couplings of the Z boson to the up quark, a_u and v_u respectively, shown for H1 and ZEUS in comparision with other experiments and the SM prediction.

Figure 5, in comparison with results obtained by CDF and LEP.[24,25] The HERA experiments provide a better measurement than the Tevatron and resolve the ambiguity in the LEP results.

7 Measurement of Single W Boson Production

Single W boson production in the SM is a rare process at HERA with a cross section of order 1 pb.[26] In the case of leptonic W boson decay, for which the branching ratio is about 30%, the event gives rise to a characteristic '$\ell + \not{P}_T$' detector signature, consisting of an energetic isolated electron or muon (ℓ) and large missing transverse momentum ($\not{P}_T$). The full HERA I+II high energy data sample, collected with the H1 detector in the years 1994-2007 and corresponding to an integrated luminosity of 478 pb^{-1}, is analysed and 59 $\ell + \not{P}_T$ events are selected[27] compared to a SM expectation of 58.9 ± 8.2. This yield is presented in Figure 6 (left) as a function of the tranverse momentum of the hadronic system (P_T^X). Notwithstanding an excess of the data over the MC prediction in the small region of phase space where $P_T^X > 25$ GeV, a good over-all agreement with the SM is observed. The single W boson production cross section is determined[28] to be $\sigma_W = 1.2 \pm 0.3$ (stat) ± 0.2 (sys) pb, which is in good agreement with the (NLO) SM expectation of 1.3 ± 0.2 pb. The quoted errors on the measured cross section include theoretical and experimental uncertainties.

8 Measurement of the W Boson Polarisation Fractions

The measurement of the W boson polarisation fractions is based on the $\ell + \not{P}_T$ data sample discussed in Section 7 and makes use of the $\cos\theta^*$ distributions in the decay $W \rightarrow e/\mu + \nu$. θ^* is defined as the angle between the W boson momentum in the lab frame and that of the charged decay lepton in the W boson rest frame. For the left handed polarisation fraction F_-, the longitudinal fraction F_0 and the right handed fraction $F_+ \equiv 1 - F_- - F_0$, the $\cos\theta^*$

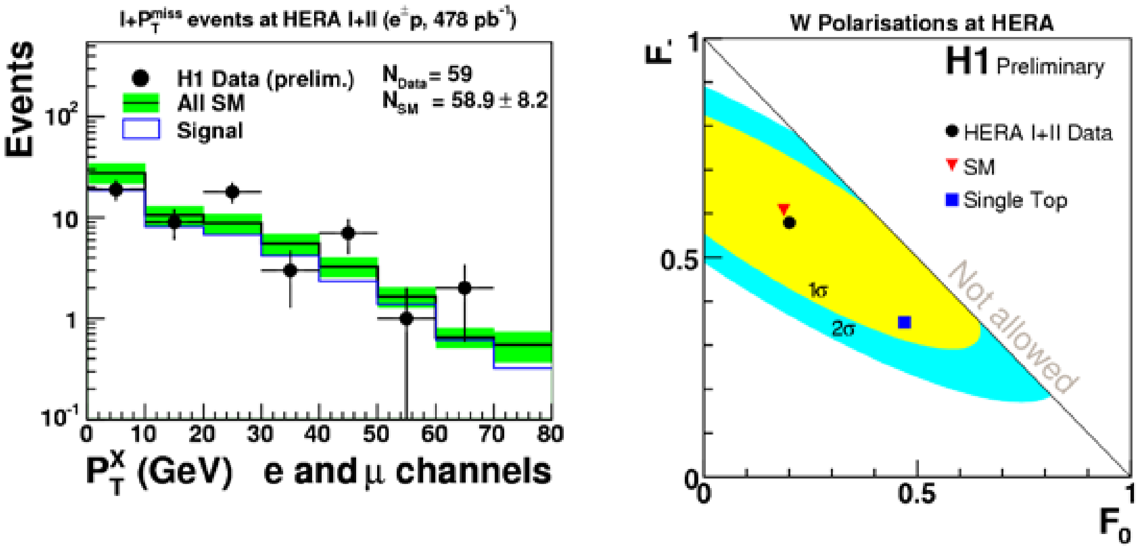

Figure 6: Left: The hadronic transverse momentum (P_T^X) distribution in the electron and muon channels combined. The data (points) are compared to the SM expectation (open histogram). The main contribution from single W production is also shown (hatched histogram). Right: Measured values for the polarisation fractions F_- and F_0 with the 1 and 2σ CL contours.

distributions for W^+ bosons are given [29] by

$$\frac{d\sigma_W}{d\cos\theta^*} \propto (1-F_- - F_0)\cdot\frac{3}{8}(1+\cos\theta^*)^2 + F_0\cdot\frac{3}{4}\left(1-\cos^2\theta^*\right) + F_-\cdot\frac{3}{8}(1-\cos\theta^*)^2 . \qquad (1)$$

For W^- bosons, the $\cos\,\theta^*$ distributions have opposite values. To allow the combination of both channels, $\cos\,\theta^*$ is multiplied with the sign of the lepton charge $q_\ell = \pm 1$. Therefore, from the $\ell + \not{P}_T$ data sample, only events for which a reliable measurement of the charge of the isolated lepton exists are used. The reconstruction of the W boson rest frame is performed and the W boson differential cross section as a function of the decay angle θ^* is derived and fit to the model defined in Equation 1. In the fit, the optimal values for F_- and F_0 are simultaneously extracted using a χ^2 minimisation method. The result is shown in Figure 6 (right) and found to be in good agreement with the SM. F_- and F_0 are also extracted in fits where one parameter is fixed to its SM value. No deviations from the SM are observed and the values are determined to be:

$$\begin{aligned} F_- &= 0.58 \pm 0.15\,(\text{stat}) \pm 0.12\,(\text{sys}) \quad \text{SM:} \quad 0.61 \pm 0.01\,(\text{stat}), \\ F_0 &= 0.15 \pm 0.21\,(\text{stat}) \pm 0.09\,(\text{sys}) \quad \text{SM:} \quad 0.19 \pm 0.01\,(\text{stat}). \end{aligned}$$

9 Summary

Preliminary H1 results of NC cross section measurements at high Q^2 have been presented, using the complete HERA I+II high energy data set. A good agreement with the QCD SM expectations is observed. In the search for contact interactions, H1 and ZEUS derive strong upper limits on a possible quark radius of respectively $0.74 \cdot 10^{-18}$ m and $0.62 \cdot 10^{-18}$ m at 95% CL. In addition, two dimensional limits at 68% CL on the vector and axial vector couplings of the Z boson to the up quark were shown, using combined EW and QCD fits. New measurements of the charged current cross section as a function of the lepton-beam polarisation, using data taken in the years 2006-2007, have been presented. A good agreement is observed with previous measurements and with the SM, which forbids right handed charged currents. Recently derived CC cross section measurements are presented, using the combined HERA I data of both experiments. The combination of the data has led to significant improvements in the statistical precision. The cross section measurements using the combined data are in good agreement with the previously established QCD fits of H1 and ZEUS to their own data. A single W boson production cross section measurement is performed by H1 using the full HERA I+II data and found to be $\sigma_W = 1.2 \pm 0.3$ (stat) ± 0.2 (sys) pb, which is in good agreement with the (NLO) SM expectation of 1.3 ± 0.2 pb. Finally, the W boson polarisation fractions are measured and found to be in good agreement with the SM.

References

1. P. Schmueser, Nucl. Instrum. Meth. A **235**, 201 (1985).
2. I. Abt *et al.* [H1 Collaboration], Nucl. Instrum. Meth. A **386**, 310 (1997).
3. ZEUS Coll., U. Holm (ed.) Status Report (unpublished), DESY (1993), available on `http://www-zeus.desy.de/bluebook/bluebook.html`
4. C. Adloff *et al.* [H1 Collaboration], Eur. Phys. J. C **21**, 33 (2001).
5. S. Chekanov *et al.* [ZEUS Collaboration], Phys. Rev. D **67**, 012007 (2003).
6. A. Aktas *et al.* [H1 Collaboration], Phys. Lett. B **632**, 35 (2006).
7. C. Adloff *et al.* [H1 Collaboration], Eur. Phys. J. C **13**, 609 (2000).
8. J. Breitweg *et al.* [ZEUS Collaboration], Eur. Phys. J. C **12**, 411 (2000) [Erratum-ibid. C **27**, 305 (2003)].
9. S. Chekanov *et al.* [ZEUS Collaboration], Phys. Lett. B **637**, 210 (2006).
10. C. Adloff *et al.* [H1 Collaboration], Phys. Lett. B **568**, 35 (2003).
11. J. Breitweg *et al.* [ZEUS Collaboration], Eur. Phys. J. C **14**, 239 (2000).
12. [H1 Collaboration] H1 prelim-07-141.
13. C. Adloff *et al.* [H1 Collaboration], Eur. Phys. J. C **19**, 269 (2001).
14. C. Adloff *et al.* [H1 Collaboration], Eur. Phys. J. C **30**, 1 (2003).
15. A.Aktas *et.al.* [H1 Collaboration], Contributed paper to the 33rd International Conference on High Energy Physics, ICHEP06, July 26 - August 2, 2006 Moscow.
16. [ZEUS Collaboration] ZEUS prelim-07-028.
17. [H1 and ZEUS Collaborations] H1 prelim-08-045, ZEUS prelim-08-003.
18. [H1 and ZEUS Collaborations] H1 prelim-07-007, ZEUS prelim-07-026.
19. S. Chekanov *et al.* [ZEUS Collaboration], Eur. Phys. J. C **42**, 1 (2005).
20. [ZEUS Collaboration] ZEUS prelim-07-023.
21. A. Aktas *et al.* [H1 Collaboration], Phys. Lett. B **634**, 173 (2006).
22. [H1 Collaboration] H1 prelim-07-041.
23. [ZEUS Collaboration] ZEUS prelim-07-027.
24. [LEP Collaborations] hep-ex/0412015.
25. D. E. Acosta *et al.* [CDF Collaboration], Phys. Rev. D **71**, 052002 (2005).
26. U. Baur, J. A. M. Vermaseren and D. Zeppenfeld, Nucl. Phys. B **375**, 3 (1992).
27. [H1 Collaboration] H1 prelim-07-063.
28. [H1 Collaboration] H1 prelim-07-161.
29. K. Hagiwara, R. D. Peccei, D. Zeppenfeld and K. Hikasa, Nucl. Phys. B **282**, 253 (1987).

ON THE POSSIBLE LINKS BETWEEN ELECTROWEAK SYMMETRY BREAKING AND DARK MATTER

T. HAMBYE AND M.H.G. TYTGAT[a]

Service de Physique Théorique, Université Libre de Bruxelles, 1050 Brussels, Belgium

The mechanism behind electroweak symmetry breaking (EWSB) and the nature of dark matter (DM) are currently very important issues in particle physics. Usually, in most models, these two issues are not or poorly connected. However, since a natural dark matter candidate is a weakly interacting massive particle or WIMP, with mass around the electroweak scale, it is clearly of interest to investigate the possibility that DM and EWSB are closely related. In the context of a very simple extension of the Standard Model, the Inert Doublet Model, we show that dark matter could play a crucial role in the breaking of the electroweak symmetry. In this model, dark matter is the lightest component of an inert scalar doublet which can induce dynamically electroweak symmetry breaking at one loop level. Moreover, in a large fraction of the parameter space of this model, the mass of the dark matter particle is essentially determined by the electroweak scale, so that the fact that the WIMP DM mass is around the electroweak scale is not a coincidence.

1 Introduction

If one think about what kind of new physics the Large Hadron Collider could observe, beside elucidating the origin of electroweak symmetry breaking, which is the first goal of this accelerator, there are at least 2 issues which come directly to mind. The first one is the physics which would cure the hierarchy problem(s) related to the scalar sector of the theory. The second one is the particle at the origin of the dark matter in the universe. The reason why one might observe the DM particle at LHC is not as clear at all as for the physics at the origin of EWSB, but it is at least what we expect in the most straightforward explanation for the relic DM density of the universe, which is the WIMP mechanism. If the DM relic density of the universe is due to the

---

[a] Talks given by M.T. at this Moriond Conference and by T.H. at the 4th Dark Side of the Universe Conference, June 2008, Cairo, Egypt, based on Ref. [1].

simple freeze out of the pair annihilation of a stable thermal particle, and if the annihilation cross section is driven by gauge couplings (or more generally couplings of order unity), the DM mass which is e.g. necessary to have the right relic density as observed in the universe ($\Omega_{DM} \simeq 0.22$ [2,3]) turns out to be around the electroweak scale. This leads to a coincidence problem since what sets the DM mass is the observed DM relic density which a priori has nothing to do with the electroweak scale. In most models it is a coincidence.[b] In this talk we consider the following two questions curiously not often considered. First could it be not a coincidence due to some deep reason? Second, if the DM particle is around the electroweak scale, could it play a direct role in the dynamic of EWSB? In the following, focusing on these phenomenological issues of DM and EWSB, we consider an extremely simple model, the inert Higgs doublet model, which shows that DM could have indeed a crucial role in EWSB and that the WIMP scale coincidence above might not be accidental.

2 The inert Higgs doublet model

The model we consider is extremely simple.[4–9] It is based on only 2 assumptions. First it assumes the existence of a second Brout-Englert-Higgs (Higgs for short) doublet, H_2. Second it assumes a discrete symmetry, the simplest one is a Z_2 symmetry, such that all SM particles are even under it, except the second Higgs doublet. To assume such a discrete symmetry has several virtues. It automatically leads to no flavor changing neutral current problems which in more general 2 Higgs doublet model are generic. Moreover if the Z_2 symmetry is not spontaneously broken, which is the case for large fractions of the scalar potential parameters, it leads to a stable DM candidate in the form of the lightest H_2 component. The doublet $H_2 \equiv (H^+\, (H_0 + iA_0)/\sqrt{2})^T$, since it is complex, has four components, 2 charged, $H^\pm$, one neutral scalar, H_0, and one neutral pseudoscalar, A_0.

The most general scalar potential one can write contains 2 mass and five quartic terms:

$$\begin{aligned} V &= \mu_1^2|H_1|^2 + \mu_2^2|H_2|^2 + \lambda_1|H_1|^4 + \lambda_2|H_2|^4 \qquad (1) \\ &+\lambda_3|H_1|^2|H_2|^2 + \lambda_4|H_1^\dagger H_2|^2 + \frac{\lambda_5}{2}\left[(H_1^\dagger H_2)^2 + h.c.\right] \end{aligned}$$

with real quartic couplings. After $SU(2)\times U(1)$ symmetry breaking, from the vacuum expectation value of H_1, $\langle H_1\rangle = v/\sqrt{2}$ with $v = -\mu_1^2/\lambda_1 = 246$ GeV, we get the following mass spectrum

$$\begin{aligned} m_h^2 &= \mu_1^2 + 3\lambda_1 v^2 \equiv -2\mu_1^2 = 2\lambda_1 v^2 \\ m_{H^+}^2 &= \mu_2^2 + \lambda_3 v^2/2 \\ m_{H_0}^2 &= \mu_2^2 + (\lambda_3+\lambda_4+\lambda_5)v^2/2 \\ m_{A_0}^2 &= \mu_2^2 + (\lambda_3+\lambda_4-\lambda_5)v^2/2. \qquad (2) \end{aligned}$$

with h the Higgs boson from H_1. To have a dark stable particle, i.e. neutral, H_0 or A_0, we therefore need $\lambda_L \equiv \lambda_3+\lambda_4+\lambda_5 < \lambda_3$ and/or $\lambda_S \equiv \lambda_3+\lambda_4-\lambda_5 < \lambda_3$.

The DM properties of this model have been studied in a series of papers which show that this model is perfectly viable and moreover testable. There are 4 types of processes which drive the relic density:[8] annihilation to a pair of gauge bosons, to a pair of Higgs boson, to a pair of fermion via a Higgs boson, and coannihilation to a fermion pair of the DM particle with the other neutral H_2 component via a Z boson or with $H^\pm$ via a $W^\pm$. The cross sections are exactly the same for H_0 and A_0 so that both DM candidates are equally good. Annihilations

---

[b] For example in the MSSM neutralino scenario there is no direct link between these 2 scales, due to the μ problem. There exists however models where such link exists as in the NMSSM.

to a pair of gauge bosons tend to be too fast to give the right relic density, except in 2 mass regimes. A low mass regime where the DM mass is below the W and Z mass thresholds; it requires [8,6] $40\,\mathrm{GeV} < m_{DM} < 75$ GeV (in this case the relic density is determined by the 2 processes with light fermions in the final state). And a high mass regime [8] (also possible because asymptotically, for large DM mass, the annihilation to a pair of gauge bosons drops as $1/m_{DM}^2$); it requires $600\,\mathrm{GeV} \lesssim m_{DM} \lesssim 100$ TeV.

For direct detection the main process is elastic scattering of DM with a nucleon via a Higgs boson. For the low mass regime most of the parameter space cannot be probed by present experiments but will be by the future ones, see [8,6]. Similarly in this regime, and for usual Navarro-Frank-White DM galactic density profile, most of the parameter space will be covered by the GLAST satellite experiment, see [8,9]. This model is therefore testable. The high mass regime, on the other hand, leads to more suppressed rates.

3 Electroweak Symmetry Breaking induced by Dark Matter

Although EWSB can be perfectly induced in the SM by the scalar potential of the Higgs boson without the need of any additional particle, the inert Higgs doublet model offers the possibility to have a dynamical origin for the EWSB. It provides an example of DM model where due to the fact that DM is around the electroweak scale, it can easily have an important role for EWSB, by driving it at one loop through the Coleman-Weinberg mechanism.[10,11] Consider a regime where μ_1^2 would be positive, vanishing or more generally much less negative than its ordinary value in the SM $-\lambda v^2$. In this case there is no or very little EWSB at tree level. There is not either EWSB at one loop in the SM. This is due to the well-known fact that the one loop effective potential is dominated in the SM by the top loops which have the wrong sign for EWSB. These loops can lead to a potential with an extremum in v but only to a maximum, i.e. they destabilize the Higgs vacuum. However in the inert Higgs doublet model the situation is totally different. There are additional scalar loops involving H_2. Neglecting gauge bosons loops as well as fermion loops other than top ones, using the $\overline{MS}$ prescription, we get the following effective Higgs potential

$$V_{\text{eff}}(h) = \mu_1^2 \frac{h^2}{2} + \lambda_1 \frac{h^4}{4} + \frac{1}{64\pi^2} \sum_i n_i m_i^4 \big(ln \frac{m_i^2}{\mu^2} - 3/2\big) \tag{3}$$

where $n_i = \{1,1,1,1,2,2,-12\}$ is the number of degrees of freedom for each species $i = \{h, H_0, G_0, A_0, h^\pm, H^\pm, t\}$ which couples to the Higgs boson with tree level masses given in Eq. (2), $m_{G_0}^2 = m_{h^\pm}^2 = \mu_1^2 + \lambda_1 v^2$, $m_t^2 = g_t^2 v^2/2$ (with G_0, $G^\pm$, the 3 would-be Goldstone bosons in H_1 and g_t the top Yukawa coupling). Since they are scalar loops, the H_2 loops have the right sign, i.e. they restabilize the potential and can lead to a minimum in v, so that EWSB is driven by the DM inert Higgs doublet. Imposing that the effective potential has an extremum in $v = 246$ GeV, the Higgs mass at one-loop is given by

$$\begin{aligned} M_h^2 \;&=\; \frac{d^2 V_{\text{eff}}}{dh^2} = m_h^2 + \frac{1}{32\pi^2}\Big[6\lambda_1 f(m_h^2) + \lambda_L f(m_{H_0}^2) + 2\lambda_1 f(m_{G_0}^2) + \lambda_S f(m_{A_0}^2) \\ &+\; 4\lambda_1 f(m_{h^+}^2) + 2\lambda_3 f(m_{H^+}^2) + 36\lambda_1^2 h^2 \log\frac{m_h^2}{\mu^2} + \lambda_L^2 h^2 \log\frac{m_{H_0}^2}{\mu^2} \\ &+\; 4\lambda_1^2 h^2 \log\frac{m_{G_0}^2}{\mu^2} + \lambda_S^2 h^2 \log\frac{m_{A_0}^2}{\mu^2} + 8\lambda_1^2 h^2 \log\frac{m_{h^+}^2}{\mu^2} + 2\lambda_3^2 h^2 \log\frac{m_{H^+}^2}{\mu^2} \\ &-\; 36 g_t^2 h^2 f(m_t^2) - 12 g_t^4 h^2\Big]\Big|_{\langle h\rangle = v} \end{aligned} \tag{4}$$

with $f(m^2) = m^2(\log(m^2/\mu^2) - 1)$.

Since H_2 has no vacuum expectation value, there is no mixing between the scalars and it is straightforward to compute the contribution of one-loop corrections to the mass of the other scalars from the second derivative of the effective potential around the Higgs *vev*. This still requires to keep track of the dependence of the propagators on h, H_0, A_0 and $H^\pm$ though. The fact that there is no mixing also means that the extremum is necessarily a minimum if all masses are positive. The result is

$$\begin{aligned}
M_{H_0}^2 &\equiv \frac{\partial^2 V_{\rm eff}}{\partial H_0^2} = m_{H_0}^2 + \frac{1}{32\pi^2}\Big[\lambda_L f(m_h^2) + 6\lambda_2 f(m_{H_0}^2) \\
&+ \lambda_S f(m_{G_0}^2) + 2\lambda_2 f(m_{A_0}^2) + 2\lambda_3 f(m_{h^+}^2) + 4\lambda_2 f(m_{H^+}^2) \\
&- 2\lambda_L^2 v^2 g(m_h^2, m_{H_0}^2) - 2\lambda_5^2 v^2 g(m_{G_0}^2, m_{A_0}^2) - (\lambda_4+\lambda_5)^2 v^2 g(m_{h^+}^2, m_{H^+}^2)\Big]\Big|_{\langle h\rangle = v} \\
M_{A_0}^2 &\equiv \frac{\partial^2 V_{\rm eff}}{\partial A_0^2} = m_{A_0}^2 + \frac{1}{32\pi^2}\Big[\lambda_S f(m_h^2) + 2\lambda_2 f(m_{H_0}^2) \\
&+ \lambda_L f(m_{G_0}^2) + 6\lambda_2 f(m_{A_0}^2) + 2\lambda_3 f(m_{h^+}^2) + 4\lambda_2 f(m_{H^+}^2) \\
&- 2\lambda_S^2 v^2 g(m_h^2, m_{A_0}^2) - 2\lambda_5^2 v^2 g(m_{G_0}^2, m_{H_0}^2) - (\lambda_4-\lambda_5)^2 v^2 g(m_{h^+}^2, m_{H^+}^2)\Big]\Big|_{\langle h\rangle = v} \\
M_{H^\pm}^2 &\equiv \frac{\partial^2 V_{\rm eff}}{\partial H^+ \partial H^-} = m_{H^\pm}^2 + \frac{1}{32\pi^2}\Big[\lambda_3 f(m_h^2) + 2\lambda_2 f(m_{H_0}^2) + \lambda_3 f(m_{G_0}^2) \\
&+ 2\lambda_2 f(m_{A_0}^2) + 2(\lambda_3+\lambda_4) f(m_{h^+}^2) + 8\lambda_2 f(m_{H^+}^2) - \frac{1}{2}(\lambda_4+\lambda_5)^2 v^2 g(m_{h^+}^2, m_{H_0}^2) \\
&- 2\lambda_3^2 v^2 g(m_h^2, m_{H^+}^2) - \frac{1}{2}(\lambda_4-\lambda_5)^2 v^2 g(m_{h^+}^2, m_{A_0}^2)\Big]\Big|_{\langle h\rangle = v}.
\end{aligned}$$

with $g(m_1^2, m_2^2) = [f(m_1^2) - f(m_2^2)]/(m_2^2 - m_1^2)$.

4 Constraints

In order that this dynamical mechanism of EWSB, driven by the DM doublet, does work, there are essentially 3 constraints:

1) EWSB. The general strategy is simple. The contribution of at least some of the loops with H_2 particles must be large enough to compensate the large, negative, contribution of the top quark. This requires that at least one of the λ_{3-5} couplings must be large and positive. This will inevitably drive some of the scalar particle masses in the few hundred GeV range. Imagine that EWSB is driven by loop corrections of $H^\pm$ and A_0, with $\lambda_3 \simeq \lambda_S$. In this case the $\lambda_{3,S}$ contribution is relevant with respect to the top loop one provided $\lambda_{3,S} \gtrsim 2g_t^2$. Asking that their contribution is large enough for the Higgs mass to be above $\sim$ 115 GeV requires $\lambda_{3,S} \gtrsim 5g_t^2$, approximately, i.e. fairly large but still perturbative quartic couplings. This gives $M_{H^\pm,A_0} \gtrsim 380$ GeV.

2) DM mass. Calculating the H_0 relic density using the one loop induced coupling $\lambda_L^{eff} = \frac{1}{v}\partial^3 V_{eff}/\partial h \partial^2 H_0 \equiv \frac{1}{v}\partial M_{H_0}^2/\partial v$, the low mass regime turns out to be still perfectly viable. Since at least one of the components of the inert Higgs doublet must be very heavy to break the electroweak symmetry while, in this case, the DM candidate must be lighter than M_W, this leads to large mass splittings between at least 2 of the inert Higgs components.

As for the large DM mass regime, it can be shown that it can work only for less phenomenologically interesting special cases. In the following we will consider only the low mass regime.

3) Electroweak precision measurements. The most important constraints on the model from electroweak precision measurements comes from the ρ parameter or equivalently the Peskin-Takeuchi T parameter.[3] A doublet with large mass splitting gives a contribution

$$\Delta T = \frac{1}{32\pi^2 \alpha v^2}\left[f(M_{H^\pm}, M_{H_0}) + f(M_{H^\pm}, M_{A_0}) - f(M_{A_0}, M_{H_0})\right] \qquad (5)$$

	λ_1	λ_2	λ_3	λ_4	λ_5	M_h	M_{H_0}	M_{A_0}	$M_{H^\pm}$	h_{BR}	W_{BR}
I	-0.11	0	5.4	-2.8	-2.8	120	12	405	405	100%	0%
I	-0.11	-2	5.4	-2.7	-2.7	120	43	395	395	100%	0%
I	-0.11	-3	5.4	-2.6	-2.6	120	72	390	390	94%	6 %
I	-0.30	0	7.6	-4.1	-4.1	180	12	495	495	100%	0 %
I	-0.30	-2.5	7.6	-3.8	-3.8	180	64	470	470	100%	0 %
II	-0.29	-5	-0.07	5.5	-5.53	150	54	535	63	0%	100 %

Table 1: Instances of parameters with WMAP DM abundance. Also given are the relative contribution of Higgs mediated annihilation (h_{BR}) and gauge processes (W_{BR}).

with $f(m_1, m_2) = (m_1^2 + m_2^2)/2 - m_1^2 m_2^2/(m_1^2 - m_2^2)\ln(m_1^2/m_2^2)$.[6] To give an idea of what is going on, the contribution from $M_{H^\pm} \sim 450$ GeV and $M_{DM} \sim 75$ GeV tree level masses gives $\Delta T \sim 1$, while electroweak precision measurements impose $|\Delta T| \lesssim 0.2$. There is however a nice and painless cure to this problem: as a quick inspection of Eq. (5) reveals, if either H_0 or A_0 is degenerate with $H^\pm$, the contribution of the inert doublet to the ΔT parameter vanishes identically. Physically, this is due to the existence of a custodial symmetry in the limit $M_{H^\pm} = M_{A_0}$ or $M_{H^\pm} = M_{H_0}$ (i.e. $\lambda_4 = \pm\lambda_5$). Technically, an exact or approximate custodial symmetry does not only avoid large corrections to the T parameter. It also implies that it is no fine tuning to take, for instance, the DM particle to be much lighter than the other components of the inert doublet (i.e. λ_L or λ_S much different from the other quartic couplings) as required by the EWSB and DM constraints.

From the three constraints above, we can now consider four cases, see the numerical examples of Table 1. Case I corresponds to a light H_0 and to two heavy, nearly degenerate A_0 and $H^\pm$ (*i.e.* $m_{H_0} << m_{A_0} \simeq m_{H^+}$ or $\lambda_L << \lambda_S \simeq \lambda_3$). Case II has a reversed hierarchy, *i.e.* $m_{H_0} \lesssim m_{H^+} << m_{A_0}$ or $\lambda_L \lesssim \lambda_3 << \lambda_S$). The two last corresponds to A_0 as the DM candidate, with $m_{A_0} << m_{H_0} \simeq m_{H^+}$ (case III) and $m_{A_0} \lesssim m_{H^+} << m_{H_0}$ (case IV). Cases III and IV can be obtained from cases I and II simply by switching H_0 with A_0. This leaves the relic density unchanged, so that Table 1 is relevant for these cases too.

All the examples of Table 1 have a DM abundance in agreement with WMAP data. As announced, we observe that some of the quartic couplings must be large. Also, in all the working cases the DM mass is below M_W. In Case I (similarly case III), the DM abundance is determined by its annihilation through the Higgs particle only and thus depends on M_h and the effective trilinear hH_0H_0 coupling, *i.e.* λ_L^{eff} above. For various, albeit large, couplings we found the correct abundance for DM masses in the range $M_{H_0} \sim (10-72)$ GeV. Below this range, the Higgs mediated annihilation is too suppressed. For this calculation the one-loop contribution to λ_L^{eff} is important in some cases. In case II (resp. case IV) coannihilation through the W^+ can play a role if the $H^+ - H_0$ (resp. $H^+ - A_0$) splitting is not too large. Notice that the masses of $H^\pm$ quoted in Table 1 are consistent with collider data because the H^+ does not couple to fermions, is short lived and, if $M_{H^\pm} > M_Z/2$, does not contribute to the width of the Z boson.

Imposing the perturbativity condition that the quartic couplings $\lambda_{3,L,S}$ are smaller than *e.g.* 2π or 4π gives $M_h \lesssim 80$ GeV or $M_h \lesssim 175$ GeV in Cases II and IV while for Cases I and III we have $M_h \lesssim 150$ GeV or $M_h \lesssim 350$ GeV. We have checked that these M_h bounds can be saturated, keeping $\Omega_{DM} \sim 0.22$.

In the Table we considered only the case $\mu_1 = \mu_2 = 0$ because it is a particularly clear and intriguing case. It shows an example of model where starting from no scale at all, through dimensional transmutation, one can generate all scales of the SM. This cannot be realized in the SM but can work adding to the SM the DM particle, which anyway has to be added to the SM, as in the inert Higgs doublet model. Moreover it shows clearly that it is possible to work in a regime where both DM mass scale and electroweak scale are directly related to a small unique scale. The later feature holds more generally as long as $\mu_{1,2}$ are small with respect to the electroweak scale. In view of the hierarchy problem it is however difficult to justify the strict $\mu_1 = \mu_2 = 0$ conformal case. Note also that this scenario of EWSB driven by DM can be realized over a large parameter range beyond the case μ_1, $\mu_2 = 0$. In particular in the case $\mu_1^2 > 0$.

The existence of a second Higgs doublet has several consequences for colliders.[12] The main ones is that if $m_{DM} < m_h/2$, the Higgs can decay invisibly to a pair of DM particles. This leads to a smaller branching ratio of $h \to b\bar{b}$, and thus to a slightly lower bound on the Higgs mass from LEP data: $M_h > 105$ GeV instead of 114.4 GeV.[3] Similarly the suppression of the visible branching ratios render more difficult but not impossible the search for the Higgs boson at LHC. Possibility of tests at LHC, by producing the inert Higgs doublet components, do exist.[12]

5 Summary

We have shown that Dark Matter in the form of the lightest neutral component of a single inert scalar doublet could be responsible for EWSB. As a result of all constraints we get the bound on the mass of the Higgs $M_h \lesssim 350$ GeV while the mass of dark matter is in the range $M_{DM} \sim (10 - 72)$ GeV. Such a DM candidate is in a range of couplings that makes it accessible to both direct (ZEPLIN, Xenon,...) and indirect (GLAST) future searches (cf Figure 5 of [8]). Another interesting feature of our framework is that it provides a hint for why the DM mass would be around the electroweak scale, as required by the WIMP paradigm, *i.e.* $M_{DM} \propto v$ in our scenario in a large part of the parameter space.

Acknowledgments

We thank the FNRS-FRS for support.

References

1. T. Hambye and M. Tytgat, Phys. Lett. **B659** (2008) 651.
2. D. N. Spergel *et al.*, arXiv:astro-ph/0603449.
3. W.M. Yao *et al.* [Particle Data Group], J. Phys. G **33** (2006) 1.
4. N.G. Deshpande and E. Ma, Phys. Rev. **D18** (1978) 2574.
5. E. Ma, Phys. Rev. **D73** (2006) 077301.
6. R. Barbieri, L.J. Hall and V.S. Rychkov, Phys. Rev. **D74** (2006) 015007.
7. D. Majumdar and A. Ghosal, arXiv:hep-ph/0607067.
8. L. Lopez Honorez, E. Nezri, J.F. Oliver and M.H.G. Tytgat, JCAP **0702** (2007) 028.
9. M. Gustafsson, E. Lundstrom, L. Bergstrom and J. Edsjo, Phys. Rev. Lett. **99** (2007) 041301.
10. S. R. Coleman and E. Weinberg, Phys. Rev. **D7** (1973) 1888.
11. E. Gildener and S. Weinberg, Phys. Rev. **D13**, 3333 (1976); M. Sher, Phys. Rept. **179**, 273 (1989); J.P. Fatelo, J.-M. Gérard, T. Hambye and J. Weyers, Phys. Rev. Lett. **74** (1995) 492; "T. Hambye, Phys. Lett. **B371**, 87 (1996); R. Hempfling, Phys. Lett. **B379** (1996) 153; W.F.S. Chang, J.N. Ng and J.M.S. Wu, Phys. Rev. **D75** (2007) 115016; K.A. Meissner and H. Nicolai, Phys. Lett. **B648**, 312 (2007); J.R. Espinosa and M. Quiros, Phys. Rev **D76** (2007) 076004; R. Foot, A. Kobakhidze and R.R. Volkas, Phys. Lett. **B655** (2007) 75; R. Foot, A. Kobakhidze, K.L. McDonald, R.R. Volkas, Phys.Rev. **D77** (2008) 035006.
12. Q. H. Cao, E. Ma and G. Rajasekaran, Phys. Rev. **D76** (2007) 095011.

HOLOGRAPHIC MODELS OF ELECTROWEAK SYMMETRY BREAKING

GUSTAVO BURDMAN
Physics Institute, University of Sao Paulo, R. do Matao 187, Travessa R,
Cidade Universitaria, Sao Paulo, Brazil

We review the status of models of electroweak symmetry breaking in a slice of anti–de Sitter space. These models can be thought of as dual to strongly interacting theories of the electroweak scale. After an introduction to some generic issues in bulk theories in AdS$_5$, we concentrate on the model-building of the Higgs sector.

1 The Hierarchy Problem and Strong Dynamics

As the Large Hadron Collider (LHC) gets close to start taking data, we continue to ponder what new physics could appear at the TeV scale. In the standard model (SM) the electroweak symmetry is broken by a scalar doublet. This implies the existence of an elementary Higgs boson that must be relatively light (< 1 TeV) to unitarize electroweak scattering amplitudes, even lighter to satisfy electroweak precision constraints. However, its mass, and with it the electroweak scale, is unstable under radiative corrections. In order to keep it below the TeV scale and close to $v \simeq 246$ GeV, the bare mass parameter (presumably controlled by ultraviolet physics) must be finely adjusted to cancel against quadratically divergent loop corrections driven by the SM states. The need for this cancellation is highly unnatural and is called the hierarchy problem. In order for naturalness to be restored, new physics must cancel the quadratic divergences at a scale not far above the TeV scale.

The solution of the hierarchy problem is likely to shed light on the origin of electroweak symmetry breaking (EWSB). We can classify scenarios of new physics beyond the SM by how they solve the hierarchy problem. For instance, in supersymmetric theories at the weak scale [1], the quadratic divergences in the Higgs mass squared are canceled by the contributions of superpartners of the SM particles. Soft SUSY breaking allows for enough contributions to m_h^2 to trigger EWSB radiatively.

An alternative to solve the hierarchy problem is the possibility that some sort of new strong dynamics is present at or just above the TeV scale[2]. For instance, in Technicolor theories[3,4] the new strong interaction becomes strong enough at the TeV scale to trigger the condensation of Techni-fermions. If some of these are $SU(2)_L$ doublets, this triggers EWSB. There is no Higgs in this type of QCD-like scenario. The hierarchy problem is solved by dimensional transmutation, i.e. just as in the strong interactions the coupling becomes strong at low energies triggering EWSB naturally. The TeV scale is encoded in the running of this new strong coupling in the same way that the typical scale of hadronic physics (~ 1 GeV) is encoded in the running of α_s.

The trouble starts when one tries to construct the operators responsible for fermion masses. For this purpose one needs to extend the gauge group in Extended Technicolor (ETC) models. If at some energy scale $\Lambda_{\rm ETC}$ the ETC gauge bosons acquire masses, they generate four-fermion operators involving both fermions and Techni-fermions:

$$\frac{g^2_{\rm ETC}}{M^2_{\rm ETC}}\,\bar{f}_L f_R \bar{T}_R T_L \qquad (1)$$

At the lower TC scale $\Lambda_{\rm TC}$, the formation of the Techni-condensate $\langle \bar{T}_L T_R\rangle \sim \Lambda^3_{\rm TC}$ results in a fermion mass of the order of

$$m_f \simeq \frac{g^2_{\rm ETC}}{M^2_{\rm ETC}}\,\Lambda^3_{\rm TC} \qquad (2)$$

Clearly, if one wants to explain the fermion mass hierarchy one needs either several very different ETC scales, or some non-standard type of dynamics, most probably both. Particularly troublesome for ETC models are heavier masses, say above the charm mass. To obtain the top mass the ETC mechanism fails given than the ETC scale should be right on top of the TC scale.

Several complications of the ETC/TC idea allow for the fermion mass hierarchy (tumbling[5], walking TC [6]) and even for the top quark mass (top-color assisted TC [7]). In any case, it is clear that the dynamics associated with TC/ETC models must be quite different from that of a simple scaled up QCD-type theory. In addition to their problems with the generation of fermion masses, scaled up QCD TC models tend to predict a rather large S parameter

$$S \simeq \frac{N}{6\pi} \qquad (3)$$

where $N = N_{\rm tc}N_{\rm D}$ is the product of the number of Techni-colors and the number of weak doublets.

Despite all these problems, the idea that a new strong interaction at or just above the TeV scale is responsible for EWSB (and solves the hierarchy problem) remains attractive. Perhaps the new strong interaction is quite different from QCD and we do not have yet neither the theoretical tools nor the experimental guidance needed to build it.

2 Building Strongly Coupled Theories in AdS$_5$

Fortunately, there is a way to build a large array of strongly coupled theories of EWSB by using the AdS/CFT correspondence[8]. The conjecture relates a Type IIB string theory on AdS$_5 \times S^5$ with a four-dimensional $\mathcal{N} = 4$ SU(N) gauge theory, which is a conformal field theory. By extension, we can assume that at low energies we can describe the string theory by a higher dimensional field theory. As long as the AdS radius $R_{\rm AdS}$ is much larger than the string scale ℓ_s the description in the higher-dimensional theory is weakly coupled. On the other hand, this leads to $\tilde{g}N \gg 1$, where $\tilde{g}$ is the gauge coupling of the Yang-Mills theory. Then, the description of a weakly coupled theory in AdS$_5$ corresponds to a strongly coupled four-dimensional theory. We can think of the large N limit of the 4D gauge theory in terms of planar diagrams, which in turn are reminiscent of a loop expansion in the topology of the world-sheet in string theory.

In the original AdS/CFT correspondence, the boundary of AdS space is set at infinity, and is just a Minkowski 4D boundary. The corresponding 4D theory is exactly conformal, and therefore is not suitable for building models of EWSB. For our purposes, we want to consider an ultra-violet (UV) cutoff of the 4D theory, corresponding to a UV boundary at a finite coordinate in the extra dimension. Also, in order to obtain the description of an interesting strongly coupled theory, we require that the 4D gauge theory leads to non-trivial dynamics which triggers EWSB. This infra-red (IR) physics can be mimicked in the 5D theory by the appearance of an IR boundary. Thus, if we put the UV boundary at the origin of the extra dimension, $y = 0$, the statement of the AdS/CFT reads

$$\int [D\phi_0] e^{i\,S_{\rm UV}[\phi_0]} \int [D\phi_{\rm CFT}] e^{i\,S_{\rm CFT}[\phi_{\rm CFT}] + i\int d^4x \phi_0 \mathcal{O}} \\ = \int [D\phi_0] e^{i\,S_{\rm UV}[\phi_0]} \int_{\phi_0} [D\phi] e^{iS_{\rm bulk}[\phi]} \tag{4}$$

where $\mathcal{O}$ is an operator in the strongly coupled 4D theory, and $\phi_0 \equiv \phi(x, y = 0)$ is a UV boundary field which acts as a source for the 4D operator $\mathcal{O}$. The correspondence in Eq. (4) states the the 4D action is equivalent to the effective action for the source field ϕ_0 on the UV boundary, which is obtained by integrating over the bulk degrees of freedom of $\phi(x, y)$:

$$e^{i\,S_{\rm eff.}[\phi_0]} = \int_{\phi_0} [D\phi] e^{iS_{\rm bulk}[\phi]} \tag{5}$$

Then, n-point functions of the 4D theory can be obtained by using $S_{\rm eff.}[\phi_0]$ as a generating functional. It is in this sense that the bulk degrees of freedom are determining the dynamics of the 4D theory.

We then see that for us to build models of strongly coupled theories, for instance to explain EWSB, we must specify a weakly coupled 5D theory in AdS$_5$. The type of strongly coupled theories that we can build this way is not completely general. For instance, it requires that it be "large N", which should in principle translate in the presence of narrow resonances. In what follows we consider the steps to build such theories.

2.1 Solving the Hierarchy Problem in a slice of AdS$_5$

The starting point to build theories of EWSB using holography is the Randall-Sundrum setup as a solution of the hierarchy problem [9]. We consider an extra dimension compactified on an orbifold, i.e. S_1/Z_2, with the metric

$$ds^2 = e^{-2\,k\,y} \eta^{\mu\nu} dx_\mu dx_\nu - dy^2 \ , \tag{6}$$

where $k \sim M_P$ is the AdS curvature. The orbifold compactification S_1/Z_2 results in a slice of AdS in the interval $[0, \pi R]$, with R the compactification radius. This metric is a solution of Einstein's equations if we fine-tune the bulk cosmological constant to cancel the brane tensions. This choice of metric means that the graviton's wave-function is exponentially suppressed away from the origin. In general, this metric exponentially suppresses all energy scales away from the origin. Then, if the Higgs field is localized a distance $L = \pi R$ from the origin,

$$S_H = \int d^4x \int_0^{\pi R} dy \sqrt{g}\, \delta(y - \pi R) \left[g^{\mu\nu} \partial_\mu H^\dagger \partial_\nu H - \lambda \left(|H|^2 - v_0^2 \right)^2 \right] \tag{7}$$

where λ is the Higgs self-coupling and v_0 is its vacuum expectation value (VEV). The latter must satisfy $v_0 \sim k$ for the theory to be technically natural. Taking into account the exponential factors in $g^{\mu\nu}$ and $\sqrt{g}$, the renormalization of the Higgs field required to render its kinetic term canonical results in an effective four-dimensional VEV given by

$$v = e^{-k\pi R}\, v_0 \tag{8}$$

Thus, in order for the weak scale $v \simeq 246$ GeV to arise at the fixed point in $y = \pi R$, we need $kR \sim (10-12)$. Then, if the Higgs is for some reason localized at or nearly at this location, this setup constitutes a solution to the hierarchy problem.

In the original Randall-Sundrum (RS) proposal only gravity propagates in the extra dimension. However, this presents several problems, mostly associated with the fact that is not possible to sufficiently suppress higher-dimensional operators. For instance, operators mediating flavor violation might only be suppressed by the TeV scale, $k\, e^{-k\pi R}$. Grand Unified Theories (GUTs) might not be viable since we cannot effectively suppress proton decay. Many of these problems are solved when fermions and gauge bosons are allowed in the AdS_5 bulk. In fact, in order to solve the hierarchy problem, the only field that must remain localized near the πR or TeV brane is the Higgs. In addition, allowing the standard model fields in the bulk opens up a large number of model building possibilities including viable GUTs [10] and the modeling of the origin of flavor [11,12] just to mention two very prominent cases. But most importantly, it gives us a tool to build models of EWSB that address its dynamical origin. In building bulk models of EWSB we must dynamically explain why is the Higgs localized near the TeV brane. Building such models is like constructing strongly coupled theories of EWSB but from a different perspective.

2.2 Bulk RS Theories and the Origin of Flavor

Writing a theory in the bulk require several ingredients. First, we must decide what the gauge symmetry should be. It turns out that the SM electroweak symmetry, $SU(2)_L \times U(1)_Y$, is not suitable for this since it results in a large value of the parameter T. The reason is that there is large explicit isospin violation in the bulk: in addition to the SM-sanctioned isospin violation proportional to $g'/g = \tan\theta_W$, the bulk adds the isospin violation of the Kaluza-Klein (KK) modes of the SM gauge fields. As a consequence, it is necessary to implement a gauge symmetry that would exhibit isospin symmetry in the bulk. A minimal extension of the SM with this feature is $SU(2)_L \times SU(2)_R \times U(1)_X$. This bulk symmetry may be broken by boundary conditions to the SM gauge group or directly to $U(1)_{\mathrm{EM}}$. Additional discrete symmetries may be imposed to protect the $Z \to \bar{b}b$ coupling from large deviations [15].

One important consequence of writing a bulk theory, is that the KK states would start from masses of the order of $M_{\mathrm{KK}} \sim O(1)$ TeV, independently of whether they correspond to fermions, gauge bosons or even scalars. This also means that the wave-function of the KK excitations in the extra dimension also peaks at $y = \pi R$, i.e. at the TeV brane. This is related to the fact that position in the bulk can be thought of as an energy scale, and is a generic feature independent of the model considered.

Another important issue is the localization of zero modes in the bulk, i.e. their effective 5D wave-function. The strength of couplings between zero-modes and KK modes and, since the Higgs is TeV-localized, of the zero-mode fermion Yukawas, are determined by this. Fermions propagating in the bulk can have a mass term (as long as we assume is an odd mass term). The natural order of magnitude of this fermion bulk mass is k, the only dimensionfull bulk parameter. We can then write the bulk fermion mass as

$$M_f = c_f\, k \tag{9}$$

where $c_f \simeq O(1)$. Expanding the 5D fermion $\Psi(x,y)$ in KK modes and solving the equation of motion for the zero mode we see that its bulk wave-function, for instance for a left-handed zero

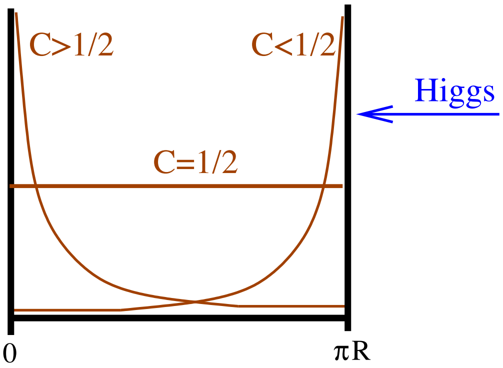

Figure 1: Localization of left-handed fermion zero-modes by variations of $O(1)$ in the bulk mass parameter.

mode, behaves like [11]

$$F^L_{\rm ZM}(y) \sim e^{(\frac{1}{2}-c_L)\,ky} \tag{10}$$

Then, if $c_L > 1/2$ the zero-mode fermion is localized towards the Planck brane, whereas if $c_L < 1/2$ it would be localized near the TeV brane. For a right-handed zero mode, localization near the Planck bran occurs if $c_R < -1/2$, and near the TeV brane if $c_R > -1/2$. If a zero mode fermion has a large wave-function near the TeV brane it has also a large overlap with the Higgs, which has to be localized there. Thus, heavier fermions must have a wave-function towards the TeV brane, whereas light fermions must be essentially Plank-brane localized in order to explain their small Yukawa couplings. We see then that fermion localization in the AdS$_5$ bulk provides a potential explanation for the hierarchy of fermion masses in the SM. This emerging picture of flavor requires that the top quark be highly localized towards the TeV brane. Furthermore, the left-handed third-generation doublet contains the left-handed b quark, which then also has to have a substantial TeV localization. The rest of the zero-mode fermions must be localized mostly near the Plank brane. Since the zero-mode gauge bosons are flat in the extra dimension, this does not affect the universality of the zero-mode gauge couplings. However, the KK modes of gauge bosons are TeV-brane localized, and then couple stronger to the TeV-brane localized fermions, i.e. the third generation. The couplings of light fermions to KK gauge bosons are nearly universal, making low energy flavor phenomenology viable, even in the presence of tree-level flavor violation. Also since light fermions are localized near the Plank brane, the scale suppressing higher dimensional operators responsible for proton decay is again M_P.

Then any sign of the characteristic tree-level flavor violation would have to appear in the interactions of the third generation quarks with the KK gauge bosons. Although these would have potentially important effects in flavor physics [16,17], a direct observation of the KK gluon decay into a single top and a jet, coming most likely from $G^{(1)} \to t\bar{c}$, would be an unambiguous signal of this theory of flavor [18].

Finally, a word about electroweak precision constraints. Since the bulk gauge theory has an isospin symmetry built in, we need not worry about the theory generating a large T parameter. However, this class of models all share the same problem with the S parameter. They have an S parameter which is approximately [13,19,20]

$$S_{\rm tree} \simeq 12\pi \frac{v^2}{M^2_{\rm KK}}, \tag{11}$$

which results in a bound of about $M_{\rm KK} > 2.5$ TeV. This is a feature we have to live with in most bulk RS constructions. We can interpret this in the dual 4D picture, as the fact that in the 4D theory we have a large N, which enter in $S_{\rm tree} \sim \frac{N}{\pi}$, where N is typically the size of the 4D gauge group. This can in principle be made considerably smaller if the light fermions

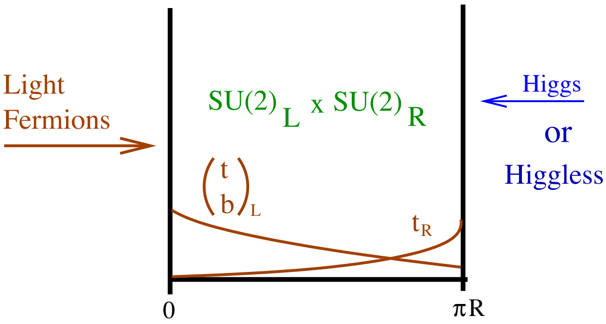

Figure 2: Cartoon representation of bulk RS models.

are allowed out of the Plank brane region and have almost flat profiles in the extra dimensions. Essentially this decouples them from the KK modes and avoids S_{tree} [13]. But this picture would lack a solution to the fermion mass hierarchy.

3 Electroweak Symmetry Breaking from AdS$_5$

We have arrived at a general picture of these kind of models in AdS$_5$:

- The Higgs is TeV-brane localized in order to solve the gauge hierarchy problem
- Fermion localization explains the fermion mass hierarchy: light fermions are Plank-brane localized resulting in small Yukawa couplings. Heavier fermions are TeV-brane localized (t_R, t_L and b_L).
- The bulk gauge symmetry must be enlarged to protect isospin, to be at least $SU(2)_L \times SU(2)_R \times U(1)_X$.

This is already quite a rich structure with a very interesting phenomenology and lots of model building possibilities beyond EWSB and fermion masses. However, if these models are dual to a strongly coupled theory in four dimensions, as the presence of the resonances (i.e. the KK modes) appears to suggest, then we must be a bit disappointed with the Higgs sector. What keeps the Higgs localized to the TeV brane ? Do we have to have a Higgs at all ? In what follows we briefly discuss three possibilities for the Higgs sector in these theories.

3.1 Higgsless EWSB in AdS$_5$

In the absence of a Higgs, the bulk gauge symmetry must be broken directly to $U(1)_{\text{EM}}$ by boundary conditions (BC) for the bulk gauge fields at the fixed point of the extra dimension. On the Plank brane the BC are such that the bulk gauge symmetry breaks as [14]

$$SU(2)_R \times U(1)_X \longrightarrow U(1)_Y, \quad \text{at } y = 0 \tag{12}$$

On the other hand, on the TeV brane

$$SU(2)_L \times SU(2)_R \longrightarrow SU(2)_V, \quad \text{at } y = \pi R \tag{13}$$

in such a way that it it preserves custodial symmetry. Then the gauge symmetry in the bulk has a gauged version of the SM custodial symmetry. This remains as a remnant global symmetry, resulting in the correct masses for the W and the Z.

More problematic in these models is how to give fermions their masses. Zero-mode fermions can obtain isospin conserving masses through a TeV-brane localized mass term. Since $SU(2)_V$

is not broken there, isospin splitting is not generated by these terms. In order to achieve the freedom to have the correct mass spectrum one must introduce the following bulk spectrum (schematically and only for the third generation case):

$$\begin{aligned} \Psi_L &= (t_L, b_L) \quad (\mathbf{2},\mathbf{1})_{1/6} \\ \Psi_R &= (t_R, b'_R) \quad (\mathbf{1},\mathbf{2})_{1/6} \\ \Psi'_R &= (t'_R, b_R) \quad (\mathbf{1},\mathbf{2})_{1/6} \end{aligned} \tag{14}$$

Each of these bulk fermions contains both left and right handed components. We can choose the BCs so that the zero-modes of Ψ_L correspond to the third generation left-handed quark doublet, the zero mode of Ψ_R is the right-handed top t_R, and the one corresponding to Ψ'_R is b_R. Mass terms localized in the TeV brane gives rise to fermion masses. It is still true that the larger the zero-mode wave-function is at the TeV brane, the larger its mass would be. But the top mass cannot be so easily adjusted. The reason is that there is a tension between the TeV localization of the top, which if too extreme produces noticeable deviation in the $Z\bar{b}_L b_L$ coupling, and the size of the isospin conserving TeV localized mass. The latter cannot be too large or it would induce a large mixing between b'_R and the b-quark's zero mode through the mass term responsible for the top quark mass. This would again result in a deviation of $Z\bar{b}_L b_L$. A way to circumvent this problem is to extend the custodial symmetry by a discrete symmetry [15], $P_{\rm LR}$ that relates the two $SU(2)$'s. In order to protect the b_L coupling, it must be included in a bi-doublet of $SU(2)_L \times SU(2)_R$. Then the right-handed fermions could be in singlets or triplets of the $SU(2)$'s. For instance, if $t_R \sim (\mathbf{1},\mathbf{1})_{2/3}$, then it does not contain any fermion that could mix with the left-handed b. On the other hand, the field resulting in the right-handed zero mode would have to be a full $O(4)$ triplet $\Psi_R \sim (\mathbf{3},\mathbf{1})_{2/3} \oplus (\mathbf{1},\mathbf{3})_{2/3}$ resulting in a distinct spectrum of KK fermions [22].

But the most important signal of this scenario stems from the absence of the Higgs as a unitarizing field in VV scattering [21], with $V = W^\pm, Z$. The unitarization of these amplitudes, unlike in other strongly coupled theories such as (4D) Techni-color, is the result of the presence of the narrow resonances that are the KK modes of the gauge bosons. The constraint of unitarization imposes sum rules on the couplings. For instance,

$$\begin{aligned} g_{WWWW} &= g^2_{WWZ} + g^2_{WW\gamma} + \sum_n (g_{WWV^{(n)}})^2 \\ &= \frac{3}{4M_W^2}\left[{g_{WWZ}}^2 M_Z^2 + \sum_n (g_{WWV^{(n)}})^2 M_n^2 \right] \end{aligned}$$

The requirement of unitarity of gauge boson scattering amplitudes means that the KK modes of gauge bosons cannot be too heavy. For example, if one wants to preserve perturbative unitarity, they must be below the TeV scale. Higgsless models in AdS$_5$ are then characterized by relatively low mass KK excitations.

3.2 Gauge-Higgs Unification

A remarkable mechanism to obtain a Higgs field naturally localized near the TeV, naturally light and suitable for EWSB is that in which the Higgs comes from a gauge field in 5D. In general, a 5D gauge field $A_M(x,y)$, $M = 0,1,2,3,5$, can be decomposed in a vector $A_\mu(x,y)$ and a scalar component $A_5(x,y)$. If we want to extract the Higgs $SU(2)_L$ doublet from a gauge field in 5D, then the gauge symmetry in 5D has to be enlarged beyond the SM gauge symmetry. In order to illustrate how this works let us take a simple example, an $SU(3)$ bulk gauge theory [23]. We can use BCs to break this gauge symmetry as $SU(3) \to SU(2)_L \times U(1)_Y$. By choosing the BCs appropriately, the gauge fields are

$$t^a A^a_\mu : \left(\begin{array}{cc|c} (+,+) & (+,+) & (-,-) \\ (+,+) & (+,+) & (-,-) \\ \hline (-,-) & (-,-) & (+,+) \end{array}\right)$$

$$t^a A^a_5 : \left(\begin{array}{cc|c} (-,-) & (-,-) & (+,+) \\ (-,-) & (-,-) & (+,+) \\ \hline (+,+) & (+,+) & (-,-) \end{array}\right)$$

where $a = 1, 2, 3$ is the $SU(3)$ adjoint index and t^a are the $SU(3)$ generators, and we use the fact that the BCs for the $A^a_5(x, y)$ are always opposite from those for $A^a_\mu(x, y)$. The signs correspond to the BCs in the Plank and TeV branes respectively. Thus, we see that the spectrum of zero-mode gauge bosons corresponds to $SU(2) \times U(1)$ as the gauge symmetry. The symmetry has been reduced or broken by this choice of BCs. Furthermore, we see that the $A^a_5(x, y)$'s corresponding to the "broken" generators, i.e. the generators for which $A^a_\mu(x, y)$ does not have a zero mode, have zero modes (i.e. $(+, +)$ BCs). In fact, these constitute four real degrees of freedom that can be seen to be a doublet of $SU(2)$ and its adjoint. Then, we can identify this $SU(2)$ doublet with the Higgs. In the case of an AdS$_5$ metric, if we impose the unitary gauge, this results in

$$\partial_y (k e^{-ky} A_5(x, y)) = 0, \tag{15}$$

which results in a scalar doublet with a profile localized towards the TeV brane. Thus, we achieved Higgs TeV-brane localization and extracted the Higgs from a gauge field in the bulk. These models are clearly related to Little Higgs theories, where the Higgs is a (pseudo-)Nambu-Goldstone boson (pNGB): the Higgs is associated to the broken generators of a symmetry, which from the 4D interpretation would be a global one. It cannot have a potential since shift symmetry (the remnant gauge symmetry for the A^a_5 zero-modes) forbids it. Thus, these models should be dual to 4D theories of a composite Higgs, where the Higgs is a pNGB.

This simple $SU(3)$ model of Gauge-Higgs unification has a lot of the features that we want. However, it does not have custodial symmetry in the bulk. The way to cure this is to simply enlarge the bulk gauge symmetry. The minimal realistic model of Gauge-Higgs unification in AdS$_5$ requires that we start with $SO(5) \times U(1)_X$ broken down to $SO(4) \times U(1)_X$ on the TeV brane, whereas it is reduced to $SU(2)_L \times U(1)_Y$ on the Plank brane [24]. Just as in the previous case, in the unitary gauge only the $A^a_5(x, y)$'s associated with the broken generators, i.e. transforming in the coset space $SO(5)/SO(4)$, have zero modes. These are arranged in a $\mathbf{4}$ of $SO(4)$, or a bi-doublet of $SU(2)_L \times SU(2)_R$.

Fermion masses are not very problematic and can be obtained by localization just as in the generic models with a TeV-brane localized Higgs. Regarding electroweak precision constraints, these models can evade them more efficiently. In particular, the S parameter can be made in agreement with experiment for gauge KK masses above 2 TeV. On the other hand, KK fermions could be quite a bit lighter, especially once the additional discrete custodial symmetry is introduced in order to keep the $Z \to \bar{b}_L b_L$ in check. For instance, possible embeddings are [25]

$$\mathbf{5_{2/3}} = (\mathbf{2}, \mathbf{2}) \oplus (\mathbf{1}, \mathbf{1}) \tag{16}$$

or in a

$$\mathbf{10_{2/3}} = (\mathbf{2}, \mathbf{2}) \oplus (\mathbf{1}, \mathbf{3}) \oplus (\mathbf{3}, \mathbf{1}) \tag{17}$$

With it, KK fermions can be as light as 500 GeV, and in some cases would have exotic charge assignments. The main reason for some KK fermions to be this light has to do with the need to get the top mass correctly. There are striking signals at the LHC, for instance from the pair production of charge 5/3 KK fermions, a distinct signature for the presence of the extended custodial symmetry [25,26].

3.3 Higgs from Fermion Condensation

Another alternative to dynamically generate the Higgs sector of the bulk Randall-Sundrum scenario is the condensation of zero-mode fermions. Since the localization of fermions near the TeV brane implies they must have strong couplings to the KK excitations of gauge bosons, it is possible that the induced four-fermion interaction is strong enough to result in fermion condensation, thus triggering EWSB. Among the SM fermions, the candidate would be the top quark: it has the strongest localization toward the TeV brane, therefore the largest coupling to KK gauge bosons, particularly the first excitation of the KK gluon. The four-fermion interaction would result in a top-condensation scenario. But we already know that this does not work if the scale of the underlying interaction is $O(1)$ TeV, as we expect the KK gluon mass to be. The problem is that the mass of the condensing fermion should be about 600 GeV in order for the condensation to result in the correct weak scale, $v \simeq 246$ GeV. We can then consider the possibility of a fourth generation, one that is highly localized near the TeV brane, more than the top quark. This results in a effective four-fermion interaction -mostly mediated by KK gluons- that is attractive enough to trigger the condensation of at least one of the fourth-generation quarks. For instance, the up-type fourth-generation quark U has a four-fermion interaction given by

$$-\frac{g^L_{01}\, g^R_{01}}{M^2_{KK}} \left(\bar{U}_L \gamma_\mu t^A U_L\right) \left(\bar{U}_R \gamma^x \mu t^A U_R\right) \;, \tag{18}$$

where $g^{L,R}_{01}$ are the couplings of the left and right-handed U quarks to the first KK mode of the gluon of mass M_{KK}, and t^A are the QCD generators.After Fierz rearrangement, we can re-write this interaction as

$$\frac{g^2_U}{M^2_{KK}} \left\{ \bar{U}^a_L U^a_R \; \bar{U}^b_L U^b_R - \frac{1}{N_c}\, \bar{U}^a_L U^b_R \; \bar{U}^b_L U^a_R \right\} \;, \tag{19}$$

where a, b are $SU(3)_c$ indices, and we have defined

$$g^2_U \equiv g^L_{01}\, g^R_{01} \;. \tag{20}$$

The color singlet term in (19) is attractive, whereas the color octet is repulsive, as well as suppressed by $1/N_c$. There is a critical value of g^2_U above which there forms a condensate $\langle \bar{U}_L\, U_R \rangle$ leading to electroweak symmetry breaking and dynamical masses for the condensing fermions. This is

$$g^2_U > \frac{8\pi^2}{N_c} \;. \tag{21}$$

One can also write an effective theory in terms of a scalar doublet which becomes dynamical at low energies. So this theory gets a composite Higgs that is heavy and made of the already mostly-composite fourth-generation up quarks. The U quark gets a large dynamical mass. All other zero-mode fermions, including the SM fermions and the other fourth-generation zero-modes, get masses through four-fermion interactions with the U quark. These operators come from bulk higher dimensional operators such as

$$\int dy\, \sqrt{g}\, \frac{C^{ijk\ell}}{M^3_P}\, \bar{\Psi}^i_L(x,y) \Psi^j_R(x,y) \bar{\Psi}^k_R(x,y) \Psi^\ell_L(x,y) \;, \tag{22}$$

where $C^{ijk\ell}$ are generic coefficients, with i, j, k, ℓ standing for generation indices as well as other indices such as isospin, and the $\Psi(x, y)$'s can be bulk quarks or leptons. Upon condensation of the U quarks these result in fermion masses that have the desired pattern as long as we choose the localization parameters appropriately.

These models have roughly the same S parameter problem as the generic ones. But to the tree-level S, now we must add also the loop contributions coming from a heavy Higgs as well as from the fourth-generation. These are, however, not as large as $S_{\rm tree}$.

The masses of the fourth-generation zero modes could be as small as 300 GeV due to mixing with KK modes, and as large as ~ 600 GeV. The Higgs is typically rather heavy, in the $(700-900)$ GeV range.

The phenomenology of these models is quite different from the three-generation RS models due to the fact that the fourth generation is the one that couples strongest to the KK gauge bosons, i.e. to the new physics in the s channel [28]. For instance the branching ratio of a KK gauge boson to $U^{(1)}\bar{U}^{(1)}$ is likely to be $5-10$ times larger than that for the $t\bar{t}$ channel, which is the one always dominating in three-generation RS models. Also the KK gluon tends to be very broad and can only be seen as an excess in the production of the fourth-generation, which is dominated by QCD. In general, all KK gauge bosons will be considerably broader, although electroweak KK gauge bosons might have more manageable widths.

4 Conclusions

Model building in a slice of AdS$_5$ extends the Randall-Sundrum solution to the hierarchy problem, and opens up the possibility of addressing dynamically the origin of EWSB and fermion masses, among other things. Through the AdS/CFT correspondence we can see that these weakly coupled 5D theories are dual to strongly coupled 4D gauge theories. Thus, building bulk RS theories of EWSB corresponds, through holography, to certain strongly coupled electroweak sectors. Although the type of strongly coupled theory is not completely generic, this procedure gives us access to a large variety of strongly coupled theories of the electroweak sector.

In addition to solving the hierarchy problem, RS bulk models provide a framework to understand the hierarchy of fermion masses. This implies the presence of tree-level flavor violation with KK gauge bosons. Rigorous compatibility with low energy data may require some level of flavor symmetry in the bulk. However, this is not surprising since fermion localization already signaled some amount of flavor breaking in the UV. The central point is that the metric in AdS$_5$ provides the necessary large scale separation between the light and the heavy fermions.

Finally, there are several alternatives for the Higgs sector. Higgsless models are viable, although require some measure of fine-tuning to cancel contributions to $Z \to b_L\bar{b}_L$. Gauge-Higgs unification models are very promising and in best agreement with electroweak precision constraints. They provide a dynamical origin for the localization of the Higgs near the TeV brane, and in the Holographic dual correspond to a composite pNGB Higgs. Finally, another alternative to localize a composite Higgs near the TeV brane, is the condensation of fourth-generation quarks via the attractive four-fermion interaction mediated mostly by the KK gluon. This is a distinct possibility, a realization of the fourth-generation condensation proposed long ago by Bardeen, Hill and Lindner [29]. These three Higgs sector possibilities have very different phenomenology and should be distinguishable at the LHC.

References

1. S. P. Martin, arXiv:hep-ph/9709356.
2. C. T. Hill and E. H. Simmons, *Phys. Rept.* **381**, 235 (2003), [Erratum-ibid. **390**, 553 (2004)].
3. E. Farhi and L. Susskind, *Phys. Rev.* D **20**, 3404 (1979).
4. E. Eichten and K. D. Lane, *Phys. Lett.* B **90**, 125 (1980).
5. Y. Kikukawa and N. Kitazawa, *Phys. Rev.* D **46**, 3117 (1992).
6. B. Holdom, *Phys. Rev.* D **24**, 1441 (1981).
7. C. T. Hill, *Phys. Lett.* B **345**, 483 (1995).
8. J. M. Maldacena, *Adv. Theor. Math. Phys.* **2**, 231 (1998) [Int. J. Theor. Phys. **38**, 1113 (1999)].

9. L. Randall and R. Sundrum, *Phys. Rev. Lett.* **83**, 3370 (1999)
10. A. Pomarol, *Phys. Rev. Lett.* **85**, 4004 (2000) [arXiv:hep-ph/0005293].
11. T. Gherghetta and A. Pomarol, *Nucl. Phys.* B **586**, 141 (2000).
12. Y. Grossman and M. Neubert, *Phys. Lett.* B **474**, 361 (2000).
13. K. Agashe, A. Delgado, M. J. May and R. Sundrum, *JHEP* **0308**, 050 (2003).
14. C. Csaki, C. Grojean, L. Pilo and J. Terning, *Phys. Rev. Lett.* **92**, 101802 (2004).
15. K. Agashe, R. Contino, L. Da Rold and A. Pomarol, *Phys. Lett.* B **641**, 62 (2006).
16. G. Burdman, *Phys. Rev.* D **66**, 076003 (2002).
17. G. Burdman, *Phys. Lett.* B **590**, 86 (2004).
18. P. M. Aquino, G. Burdman and O. J. P. Eboli, *Phys. Rev. Lett.* **98**, 131601 (2007).
19. G. Burdman and Y. Nomura, *Phys. Rev.* D **69**, 115013 (2004).
20. G. Cacciapaglia, C. Csaki, C. Grojean and J. Terning, *Phys. Rev.* D **70**, 075014 (2004).
21. A. Birkedal, K. Matchev and M. Perelstein, *Phys. Rev. Lett.* **94**, 191803 (2005).
22. G. Cacciapaglia, C. Csaki, G. Marandella and J. Terning, *Phys. Rev.* D **75**, 015003 (2007).
23. R. Contino, Y. Nomura and A. Pomarol, *Nucl. Phys.* B **671**, 148 (2003).
24. K. Agashe, R. Contino and A. Pomarol, *Nucl. Phys.* B **719**, 165 (2005).
25. R. Contino, L. Da Rold and A. Pomarol, *Phys. Rev.* D **75**, 055014 (2007).
26. M. Carena, A. D. Medina, B. Panes, N. R. Shah and C. E. M. Wagner, arXiv:0712.0095 [hep-ph].
27. G. Burdman and L. Da Rold, *JHEP* **0712**, 086 (2007).
28. G. Burdman,L. Da Rold, O. J. P. Eboli and R. Matheus, in preparation.
29. W. A. Bardeen, C. T. Hill and M. Lindner, *Phys. Rev.* D **41**, 1647 (1990).

ELECTROWEAK CONSTRAINTS ON SEE-SAW MESSENGERS AND THEIR IMPLICATIONS FOR LHC

F. DEL ÁGUILA, J.A. AGUILAR-SAAVEDRA, J. DE BLAS and M. PÉREZ-VICTORIA
Departmento de Física Teórica y del Cosmos and CAFPE,
Universidad de Granada, E-18071 Granada, Spain

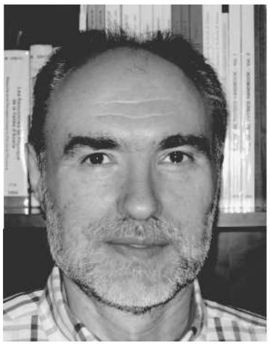

We review the present electroweak precision data constraints on the mediators of the three types of see-saw mechanisms. Except in the see-saw mechanism of type I, with the heavy neutrino singlets being mainly produced through their mixing with the Standard Model leptons, LHC will be able to discover or put limits on new scalar (see-saw of type II) and lepton (see-saw of type III) triplets near the TeV. If discovered, it may be possible in the simplest models to measure the light neutrino mass and mixing properties that neutrino oscillation experiments are insensitive to.

1 Introduction

As it is well known, the original see-saw mechanism [1], nowadays called of type I, explains the smallness of the light neutrino masses $|m_\nu| \sim 1$ eV invoking a very heavy Majorana neutrino $M_N \sim 10^{14}$ GeV:

$$|m_\nu| \simeq \frac{v^2|\lambda|^2}{M_N} \simeq |V^*|^2 M_N, \tag{1}$$

where $|\lambda| \sim 1$ is the corresponding Yukawa coupling and $v \simeq 246$ GeV the electroweak vacuum expectation value. For reviews see [2,3]. Alternatively, if the heavy scale is at the LHC reach $M_N \sim 1$ TeV, it requires a very small heavy–light mixing angle $|V| \sim 10^{-6}$. In its simplest form the model cannot be tested at large colliders, because the heavy neutrino N is a Standard Model (SM) singlet and only couples to SM gauge bosons through its mixing V. Hence it is produced through the vertex $-g/\sqrt{2}\ \overline{\ell}\gamma^\mu V_{\ell N} P_L N W_\mu^-$, with ℓ a charged lepton, with a cross section proportional to $|V_{\ell N}|^2$, which is strongly suppressed. See Fig. 1-(I). There are two other types of see-saw mechanism giving tree level Majorana masses to the light neutrinos ν, as shown

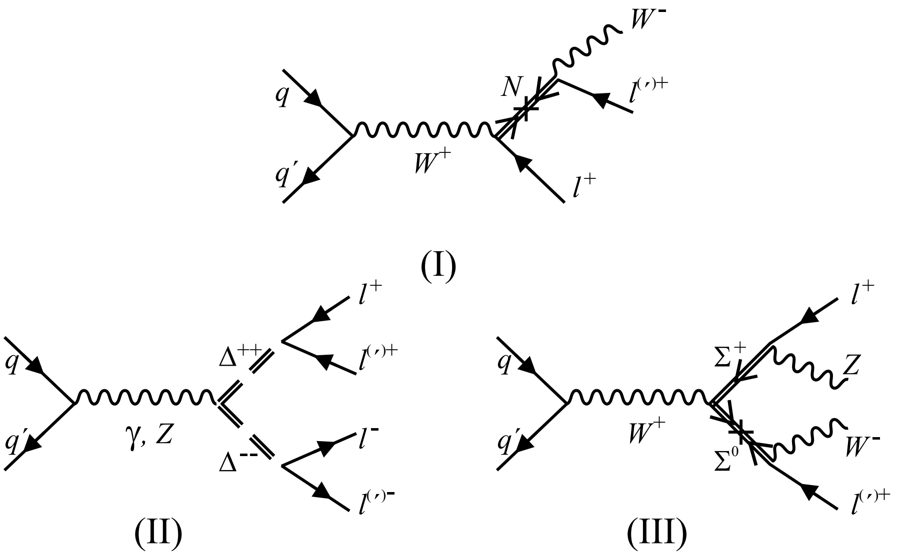

Figure 1: Examples of production diagrams for same-sign dilepton signals, $l^+l^{(\prime)+}X$, mediated by the three types of see-saw messengers.

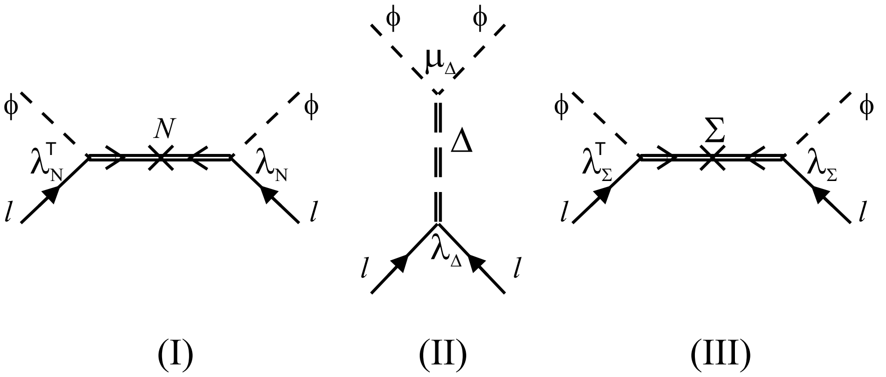

Figure 2: See-saw mechanisms of type I, II and III. λ_N, λ_Δ and λ_Σ are the Yukawa coupling matrices in the Lagrangian terms $-\overline{l_L}\tilde{\phi}\lambda_N^\dagger N_R$, $\overline{\tilde{l}_L}\lambda_\Delta(\vec{\sigma}\cdot\vec{\Delta})l_L$ and $-\overline{\vec{\Sigma}_R}\lambda_\Sigma(\tilde{\phi}^\dagger\frac{\vec{\sigma}}{2}l_L)$, respectively, with $\overline{\tilde{l}_L} = -l_L^T C i\sigma_2$ and C the spinor charge conjugation matrix. Whereas μ_Δ is the coefficient of the scalar potential term $\tilde{\phi}^\dagger(\vec{\sigma}\cdot\vec{\Delta})^\dagger\phi$.

in Fig. 2. In all cases the extra particles contribute at low energies to the dimension 5 lepton number (LN) violating operator [4]

$$(\mathcal{O}_5)_{ij} = \overline{(l_L^i)^c}\tilde{\phi}^*\tilde{\phi}^\dagger l_L^j \to \frac{v^2}{2}\overline{(\nu^i)^c}\nu^j \qquad (\text{with } l = \begin{pmatrix}\nu\\ \ell\end{pmatrix} \text{ and } \tilde{\phi} = i\sigma_2\phi^*)\ , \tag{2}$$

which gives Majorana masses to light neutrinos after spontaneous symmetry breaking. The see-saw of type II [5] in Fig. 2 is mediated by an $SU(2)_L$ scalar triplet Δ of hypercharge $Y = 1$, implying three new complex scalars of charges $Q = T_3 + Y$: $\Delta^{++}, \Delta^+, \Delta^0$. The see-saw of type III [6] exchanges an $SU(2)_L$ fermion triplet Σ of hypercharge $Y = 0$, assumed to be Majorana and containing charged leptons $\Sigma^\pm$ and a Majorana neutrino Σ^0. The main difference for LHC detection is that the see-saw messengers for these last two mechanisms can be produced by unsuppressed processes of electroweak size (Fig. 1). Their decay, even if suppressed by small couplings, can take place within the detector due to the large mass of the new particle. All three types of see-saw messengers produce LN conserving as well as LN violating signals, but the former have much larger backgrounds. On the other hand, same-sign dilepton signals, $l^\pm l^{(\prime)\pm}X$, do not have to be necessarily LN violating. Thus, in the example in Fig. 1–(II), the decay coupling λ_Δ needs not be very small because it is only one of the factors entering in the LN violating expression for ν masses (see Table 1). In fact, this process is LN conserving as we can conventionally assign LN equal to 2 to Δ^{--}. There are other processes that do violate LN, e.g. when one of the doubly-charged Δ in Fig. 2–(II) decays into WW. Then, what does violate LN is the corresponding ΔWW vertex, which is proportional to the coupling of the only LN violating term in the fundamental Lagrangian $\tilde{\phi}^\dagger(\vec{\sigma}\cdot\vec{\Delta})^\dagger\phi$, with total LN equal to 2. In the examples in Fig. 1–(I, III) LN is violated in the decay (mass) of the heavy neutral fermion.

Table 1: Coefficients of the operators up to dimension 6 arising from the integration of the heavy fields involved in each see-saw model. The parameters λ_3 and λ_5 are the coefficients of the scalar potential terms $-(\phi^\dagger\phi)(\vec{\Delta}^\dagger\vec{\Delta})$ and $-(\vec{\Delta}^\dagger T_i\vec{\Delta})(\phi^\dagger\sigma_i\phi)$, respectively, and $(\lambda_e)_{jj}$ the diagonalised SM charged-lepton Yukawa couplings. The remaining parameters are defined in the caption of Fig. 2.

Coefficient	Type I	Type II	Type III
α_4	–	$2\frac{\lvert\mu_\Delta\rvert^2}{M_\Delta^2}$	–
$\frac{(\alpha_5)_{ij}}{\Lambda}$	$\frac{1}{2}\frac{(\lambda_N^T)_{ia}(\lambda_N)_{aj}}{M_{Na}}$	$-2\frac{\mu_\Delta(\lambda_\Delta)_{ij}}{M_\Delta^2}$	$\frac{1}{8}\frac{(\lambda_\Sigma^T)_{ia}(\lambda_\Sigma)_{aj}}{M_{\Sigma a}}$
$\frac{(\alpha_{\phi l}^{(1)})_{ij}}{\Lambda^2}$	$\frac{1}{4}\frac{(\lambda_N^\dagger)_{ia}(\lambda_N)_{aj}}{M_{Na}^2}$	–	$\frac{3}{16}\frac{(\lambda_\Sigma^\dagger)_{ia}(\lambda_\Sigma)_{aj}}{M_{\Sigma a}^2}$
$\frac{(\alpha_{\phi l}^{(3)})_{ij}}{\Lambda^2}$	$-\frac{(\alpha_{\phi l}^{(1)})_{ij}}{\Lambda^2}$	–	$\frac{1}{3}\frac{(\alpha_{\phi l}^{(1)})_{ij}}{\Lambda^2}$
$\frac{(\alpha_{ll}^{(1)})_{ijkl}}{\Lambda^2}$	–	$2\frac{(\lambda_\Delta)_{jl}(\lambda_\Delta^\dagger)_{ki}}{M_\Delta^2}$	–
$\frac{\alpha_\phi}{\Lambda^2}$	–	$-6(\lambda_3+\lambda_5)\frac{\lvert\mu_\Delta\rvert^2}{M_\Delta^4}$	–
$\frac{\alpha_\phi^{(1)}}{\Lambda^2}$	–	$4\frac{\lvert\mu_\Delta\rvert^2}{M_\Delta^4}$	–
$\frac{\alpha_\phi^{(3)}}{\Lambda^2}$	–	$4\frac{\lvert\mu_\Delta\rvert^2}{M_\Delta^4}$	–
$\frac{(\alpha_{e\phi})_{ij}}{\Lambda^2}$		–	$\frac{4}{3}\frac{(\alpha_{\phi l}^{(1)})_{ij}}{\Lambda^2}(\lambda_e)_{jj}$

In conclusion, all the three mechanisms produce same-sign dilepton signals, but only the last two are observable at LHC [7,8,9,10,11,12,13] in minimal models. Heavy neutrino singlets in particular non-minimal scenarios could also be observed, as described in Section 3.

In the following we first review the experimental constraints on the parameters entering the three see-saw mechanisms, and then the LHC reach for the corresponding see-saw messengers. Complementary reviews on this subject have been presented by other speakers at this Conference (see F. Bonnet, T. Hambye and J. Kersten in these Proceedings).

2 Electroweak precision data limits on see-saw messengers

The low energy effects of the see-saw messengers can be described by the effective Lagrangian

$$\mathcal{L}_{\text{eff}} = \mathcal{L}_4 + \frac{1}{\Lambda}\mathcal{L}_5 + \frac{1}{\Lambda^2}\mathcal{L}_6 + \ldots, \tag{3}$$

where Λ is the cut-off scale, in our case of the order of the see-saw messenger masses M, and the different terms contain gauge-invariant operators of the corresponding dimension. The non-zero terms up to dimension 6 are [14,15]

$$\mathcal{L}_4 = \mathcal{L}_{SM} + \alpha_4\left(\phi^\dagger\phi\right)^2, \tag{4}$$

$$\mathcal{L}_5 = (\alpha_5)_{ij}\overline{(l^i_L)^c}\tilde{\phi}^*\tilde{\phi}^\dagger l^j_L + \text{h.c.}, \tag{5}$$

$$\begin{aligned}\mathcal{L}_6 = &\Big[(\alpha^{(1)}_{\phi l})_{ij}\left(\phi^\dagger iD_\mu\phi\right)\left(\overline{l^i_L}\gamma^\mu l^j_L\right) + (\alpha^{(3)}_{\phi l})_{ij}\left(\phi^\dagger i\sigma_a D_\mu\phi\right)\left(\overline{l^i_L}\sigma_a\gamma^\mu l^j_L\right)\\ &+ \left(\alpha_{e\phi}\right)_{ij}\left(\phi^\dagger\phi\right)\left(\overline{l^i_L}\phi e^j_R\right) + (\alpha^{(1)}_{ll})_{ijkl}\frac{1}{2}\left(\overline{l^i_L}\gamma^\mu l^j_L\right)\left(\overline{l^k_L}\gamma_\mu l^l_L\right) + \text{h.c.}\Big]\\ &+ \alpha^{(1)}_\phi\left(\phi^\dagger\phi\right)\left(\left(D_\mu\phi\right)^\dagger D^\mu\phi\right) + \alpha^{(3)}_\phi\left(\phi^\dagger D_\mu\phi\right)\left((D^\mu\phi)^\dagger\phi\right) + \alpha_\phi\frac{1}{3}\left(\phi^\dagger\phi\right)^3,\end{aligned} \tag{6}$$

where we choose the basis of Büchmuller and Wyler to express the result [16]. l_L stands for any lepton doublet, e_R for any lepton singlet, and ϕ is the SM Higgs doublet. In Table 1 we collect the explicit expressions of the coefficients in terms of the original parameters for each type of see-saw (see Fig. 2 and the table caption for definitions).

Only the dimension 6 operators can give deviations from the SM predictions for the electroweak precision data (EWPD). The operators of dimension 4 only redefine SM parameters. The one of dimension 5 gives tiny masses to the light neutrinos, and contributes to neutrinoless double β decay. An important difference is that the coefficient α_5 involves LN-violating products of two λ's or of μ and λ, while the other coefficients depend on $\lambda^*\lambda$ or $|\mu|^2$. Therefore, it is possible to have large cancellations in α_5 together with sizeable coefficients of dimension six [14,15]. Type I and III fermions generate the operators $\mathcal{O}^{(1,3)}_{\phi l}$, which correct the gauge fermion couplings. Type II scalars, on the other hand, generate 4-lepton operators and the operator $\mathcal{O}^{(3)}_\phi$, which breaks custodial symmetry and modifies the SM relation between the gauge boson masses. EWPD are sensitive to all these effects and put limits on the see-saw parameters.

There are two classes of processes, depending on whether they involve neutral currents violating lepton flavour (LF) or not. The first class puts more stringent limits [17,18], but only on the combinations of coefficients entering off-diagonal elements. The second class is measured mainly at LEP [19] and constrains the combinations in the diagonal entries [20]. The LF violating limits are satisfied in types I and III if N and Σ mainly mix with only one charged lepton family. In Table 2 we collect the bounds from EWPD on the N and Σ mixings with the SM leptons $V_{\ell N,\ell\Sigma}$ [20], and in Table 3 their product including the LF violating bounds [17,18]. These values update and extend previous bounds on diagonal entries for N [21,22] (see also [23].) Their dependence on the model parameters entering in the operator coefficients in Table 1 is explicit in the first column of Table 2. All low energy effects are proportional to this mixing, and the same holds for the gauge and Higgs couplings between the new and the SM leptons, responsible of the heavy lepton decay (and N production if there is no extra NP). An interesting by-product of a non-negligible mixing of the electron or muon with a heavy N is that the fit to EWPD prefers a Higgs mass M_H higher than in the SM, in better agreement with the present direct limit. This is so because their contributions to the most significative observables partially cancel [24], so that

Table 2: Upper limit at 90 % confidence level (CL) on the absolute value of the mixings. The first three columns are obtained by coupling each new lepton with only one SM family. The last one corresponds to the case of lepton universality: three new lepton multiplets mixing with only one charged-lepton family each, all of them with the same mixing angle. All numbers are computed assuming $M_H \geq 114.4$ GeV.

Coupling	Only with e	Only with μ	Only with τ	Universal
$\left\lvert V_{\ell N} = \frac{v(\lambda^\dagger_N)_{lN}}{\sqrt{2}M_N}\right\rvert <$	0.055	0.057	0.079	0.038
$\left\lvert V_{\ell\Sigma} = -\frac{v(\lambda^\dagger_\Sigma)_{l\Sigma}}{2\sqrt{2}M_\Sigma}\right\rvert <$	0.019	0.017	0.027	0.016

Table 3: Upper limit at 90 % CL on the absolute value of the products of the mixings between heavy singlets N and triplets Σ with the SM leptons, VV^*, entering in low energy processes. Row and column ordering corresponds to e, μ, τ.

$\lvert V_{\ell N} V^*_{\ell' N}\rvert <$			$\lvert V_{\ell \Sigma} V^*_{\ell' \Sigma}\rvert <$		
0.0030	0.0001	0.01	0.0004	1.1×10^{-6}	0.0005
0.0001	0.0032	0.01	1.1×10^{-6}	0.0003	0.0005
0.01	0.01	0.0062	0.0005	0.0005	0.0007

both the mixing and M_H can be relatively large without spoiling the agreement with EWPD. The new 90 % CL on M_H increases in this case [20] up to ~ 260 GeV (see also [25,26]). In all other cases the limit stays at ~ 165 GeV.

In type II see-saw a crucial phenomenological issue is the relative size of $(\lambda_\Delta)_{ij}$ and μ_Δ for $M_\Delta \sim 1$ TeV. The ν masses are proportional to their product, $(m_\nu)_{ij} = 2v^2 \frac{\mu_\Delta (\lambda_\Delta)_{ij}}{M^2_\Delta}$, which gives the strength of the LN violation. If μ_Δ is small enough, $(\lambda_\Delta)_{ij}$ can be relatively large and saturate present limits on LF violating processes, eventually showing at the next generation of experiments. If instead $(\lambda_\Delta)_{ij}$ are very small, the flavour structure appears only in the ν mass matrix. The present limits are reviewed in [15]. Neglecting LF violating bounds (i.e., assuming that $(\lambda_\Delta)_{ee}$ is small enough not to give a too large $\mu \to e\bar{e}e$ decay rate), μ_Δ and λ_Δ are constrained by the T oblique parameter and four-fermion processes, respectively. From a global fit to EWPD (see [20] for details on the data set used) we obtain the following limits at 90 % CL:

$$\frac{|\mu_\Delta|}{M^2_\Delta} < 0.048 \mathrm{TeV}^{-1}, \quad \frac{|(\lambda_\Delta)_{e\mu}|}{M_\Delta} < 0.100 \mathrm{TeV}^{-1}. \tag{7}$$

3 Dilepton signals of see-saw messengers

The previous limits apply to any particle transforming as the corresponding see-saw messenger, independently of whether it contributes or not to light neutrino masses. As indicated above, in minimal models the tight restriction imposed by ν masses (Eq. 1) gives much more stringent limits for the mixings of TeV-scale see-saw messengers. However, these limits can be avoided if additional particles give additional contributions to neutrino masses that cancel the previous ones, for instance if the fermionic messengers are quasi-Dirac, i.e. a nearly degenerate Majorana pair with appropriate couplings [27]. The EWPD limits are in this case relevant for production and detection of type I messengers N, but the signals are different because they conserve LN to a very large extent [14,28]. On the other hand, type II and III messengers with masses near the TeV can be produced and detected at LHC even in minimal models. Let us discuss the three types of see-saw mechanism in turn.

3.1 Type I: Fermion singlets N

As already explained, a type I heavy neutrino N with a mixing saturating the EWPD limit cannot be Majorana, unless extra fields with a very precise fine tuning keep the ν masses small enough [29]. Unnatural cancellations allowing for LN-violating signals are also possible in principle. In this case a fast simulation shows that LHC can discover a Majorana neutrino singlet with $M_N \simeq 150$ GeV for $|V_{\mu N}| \geq 0.054$ (near the EWPD limit) [8], assuming an integrated luminosity $\mathsf{L} = 30\ fb^{-1}$.

Such a signal can be also observed for much smaller mixings and larger masses if there is some extra NP [30], especially if the extra particles can be copiously produced at LHC [31]. This is the case, for instance, if the gauge group is left-right symmetric and the new W'_R has a few TeV mass. Then $pp \to W'_R \to \ell N \to \ell\ell' W$ is observable, even with negligible mixing $V_{\ell N}$, for M_N and $M_{W'_R}$ up to 2.3 TeV and 3.5 TeV, respectively,[32] for an integrated luminosity $\mathsf{L} = 30\ fb^{-1}$. Similarly, if the SM is extended with a leptophobic Z', the process $pp \to Z' \to NN \to \ell\ell' WW$ can probe Z' masses[33] up to 2.5 TeV, and M_N up to 800 GeV.

3.2 Type II: Scalar triplets Δ

$SU(2)_L$ scalar triplets can be produced through the exchange of electroweak gauge bosons with SM couplings, and then they may be observable for masses near the TeV scale (see for reviews [3,31]). Although suppressed, their decays can occur within the detector for these large masses. In Fig. 1-(II) we display one of the possible processes. The search strategy and LHC potential depend on the dominant decay modes. These are proportional to the Δ vacuum expectation value $| < \Delta^0 > | \equiv v_\Delta$, as for example[9] $\Delta^{\pm\pm} \to W^\pm W^\pm$, or to $(\lambda_\Delta)_{ij}$, as[11] $\Delta^{\pm\pm} \to l^\pm l^{(')\pm}$. $\Delta^{\pm\pm}$ can also decay into $\Delta^\pm W^{\pm *}$ if kinematically allowed (see[10]). All these different decay channels make the phenomenological analysis of single and pair $\Delta^{\pm\pm}$ production quite rich[12]. The EWPD limit in Eq. 7 translates into the bound $v_\Delta = \frac{v^2|\mu_\Delta|}{\sqrt{2}M_\Delta^2} < 2$ GeV. This is to be compared with $|m_\nu| = 2\sqrt{2} v_\Delta |\lambda_\Delta| \sim 10^{-9}$ GeV, which gives a much more stringent constraint for non-negligible λ_Δ. Dilepton (diboson) decays are dominant for $v_\Delta < (>)\ v^c_\Delta \sim 10^{-4}$ GeV. If for instance λ_Δ is of the same size as the charged lepton Yukawa couplings $\sim 10^{-2} - 5 \times 10^{-6}$, v_Δ varies from 5×10^{-8} to 10^{-4} GeV, below the critical value v^c_Δ, and Δ decays mainly into leptons. In this case the LHC reach for $M_{\Delta^{\pm\pm}}$ has been estimated, based on statistics, to be ~ 1 TeV for an integrated luminosity $\mathsf{L} = 300\ fb^{-1}$. In Fig. 3 we plot the invariant mass distribution $m_{\ell\ell}$ of same-sign dilepton pairs containing the lepton of largest transverse momentum for $M_\Delta = 600$ GeV. As this fast simulation analysis shows, the SM background is well separated from the signal, and the LHC discovey potential strongly depends on the light neutrino mass hierarchy. For the simulated sample we find 4 (44) signal events for the normal ν mass hierarchy NH (inverted IH), well separated from the main backgrounds: $t\bar{t}nj$ (1007 events), $Zb\bar{b}nj$ (91 events), tW (68 events), and $Zt\bar{t}nj$ (51 events). We get rid of other possible backgrounds like $ZZnj$ requiring no opposite-sign dilepton pairs with an invariant mass in the range $M_Z \pm 5$ GeV. For larger v_Δ values, with dominant non-leptonic decays, the corresponding reach estimate based on statistics is ~ 600 GeV. Note that only in the leptonic case LHC is sensitive to the see-saw flavour structure. Near the critical value, one could in principle extract information on the structure and on the global scale of the see-saw.

Tevatron Collaborations have already established limits on the scalar triplet mass assuming that $\Delta^{\pm\pm} \to l^\pm l^\pm$ 100 % of the time: At the 95 % CL $M_{\Delta^{\pm\pm}} > 150$ GeV for $\Delta^{\pm\pm}$ only decaying to muons[34], and an integrated luminosity $\mathsf{L} = 1.1\ fb^{-1}$.

3.3 Type III: Fermion triplets Σ

Not so much attention has been payed to the study of the LHC reach for $SU(2)_L$ fermion triplets Σ. Up to very recently a similar electroweak process, the production of a heavy vector-like lepton doublet[35], had to be used to guess that LHC could be sensitive to $M_\Sigma \sim 500$ GeV. A dedicated study[13] estimates that an integrated luminosity $\mathsf{L} = 10\ fb^{-1}$ should allow to observe LN violating signals (see Fig. 1-(III) for a relevant process) for $M_\Sigma < 800$ GeV. Vector-like fermion triplets couple to SM leptons proportionally to its mixing $V_{l\Sigma}$, which is $\leq 10^{-6}$ according to Eq. 1 if Σ is at the LHC reach ~ 1 TeV. So, one can eventually improve the analysis using the displaced vertex signatures of their decays.

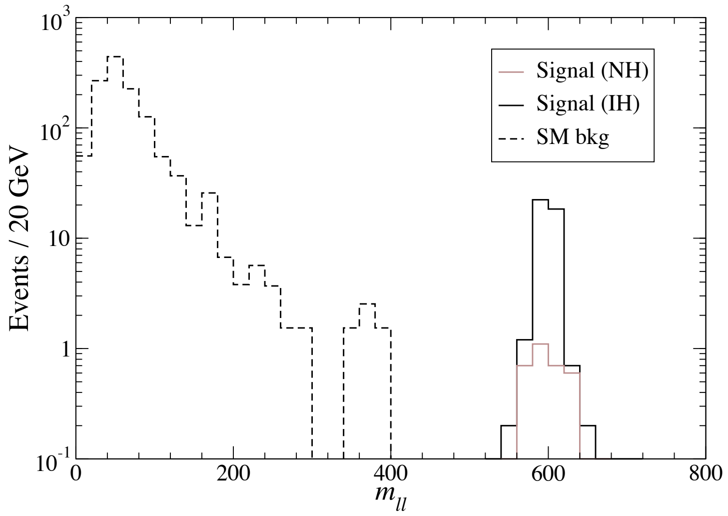

Figure 3: Same-sign dilepton invariant mass distributions for $M_\Delta = 600$ GeV and normal (NH) and inverted (IH) ν mass hierarchies, assuming an integrated luminosity $\mathsf{L} = 300\ fb^{-1}$.

4 Conclusions

Same-sign dilepton signals $l^\pm l(')^\pm X$ will allow to set significative limits on see-saw messengers at LHC, as illustrated in Table 4. The estimates for M_Δ and M_Σ are mainly based on statistics, and a more detailed analysis is needed to confirm them.

Table 4: LHC discovery limit estimates for see-saw messengers, assuming an integrated luminosity $\mathsf{L} = 30, 300$ and 10 fb^{-1} for N, Δ and Σ, respectively. See Section 3 for a detailed explanation.

	M_N	M_Δ	M_Σ
LHC reach (in GeV)	150	$600 - 1000$	800

Acknowledgments

We thank Ll. Ametller, S. Bar-Shalom, C. Biggio, T. Hambye, A. Soni and J. Wudka for discussions. F.A. thanks the organizers of the Rencontres de Moriond EW 2008 meeting for the excellent organization and the warm hospitality. This work has been supported by MEC project FPA2006-05294 and Junta de Andalucía projects FQM 101, FQM 437 and FQM03048. J.A.A.S. and J.B. also thank MEC for a Ramón y Cajal and an FPU grant, respectively.

References

1. P. Minkowski, *Phys. Lett.* B **67**, 421 (1977); T. Yanagida, Proceedings of the *Workshop on Unified Theories and Baryon Number in the Universe*, eds. A. Sawada and A. Sugamoto (Tsukuba, 1979); M. Gell-Mann, P. Ramond and R. Slansky, Proceedings of the *Supergravity Stony Brook Workshop*, eds. P. Van Niewenhuizen and D. Freedman (New York, 1979); S. L. Glashow, *NATO Adv. Study Inst. Ser.* B Phys. **59**, 687 (1979); R. Mohapatra and G. Senjanović, *Phys. Rev. Lett.* **44**, 912 (1980).
2. R. N. Mohapatra *et al*, *Rept. Prog. Phys.* **70**, 1757 (2007).
3. M. Raidal *et al*, arXiv:0801.1826 [hep-ph].

4. S. Weinberg, *Phys. Rev. Lett.* **43**, 1566 (1979).
5. W. Konetschny and W. Kummer, *Phys. Lett.* B **70**, 433 (1977); T. P. Cheng and L. F. Li, *Phys. Rev.* D **22**, 2860 (1980); J. Schechter and J. W. F. Valle, *Phys. Rev.* D **22**, 2227 (1980); see also E. Ma and U. Sarkar, *Phys. Rev. Lett.* **80**, 5716 (1998).
6. R. Foot, H. Lew, X. G. He and G. C. Joshi, *Z. Phys.* C **44**, 441 (1989).
7. T. Han and B. Zhang, *Phys. Rev. Lett.* **97**, 171804 (2006).
8. F. del Aguila, J. A. Aguilar-Saavedra and R. Pittau, *JHEP* **0710**, 047 (2007).
9. J. F. Gunion, R. Vega and J. Wudka, *Phys. Rev.* D **42**, 1673 (1990).
10. A. G. Akeroyd and M. Aoki, *Phys. Rev.* D **72**, 035011 (2005); see also S. Chakrabarti, D. Choudhury, R. M. Godbole and B. Mukhopadhyaya, *Phys. Lett.* B **434**, 347 (1998).
11. A. Hektor, M. Kadastik, M. Muntel, M. Raidal and L. Rebane, *Nucl. Phys.* B **787**, 198 (2007); M. Kadastik, M. Raidal and L. Rebane, arXiv:0712.3912 [hep-ph].
12. P. Fileviez Perez, T. Han, G. Y. Huang, T. Li and K. Wang, arXiv:0803.3450 [hep-ph]; arXiv:0805.3536 [hep-ph].
13. R. Franceschini, T. Hambye and A. Strumia, arXiv:0805.1613 [hep-ph].
14. F. del Aguila, J. A. Aguilar-Saavedra, J. de Blas and M. Zralek, *Acta Phys. Polon.* B **38**, 3339 (2007).
15. A. Abada, C. Biggio, F. Bonnet, M. B. Gavela and T. Hambye, *JHEP* **0712**, 061 (2007).
16. W. Buchmuller and D. Wyler, *Nucl. Phys.* B **268**, 621 (1986); C. Arzt, M. B. Einhorn and J. Wudka, *Nucl. Phys.* B **433**, 41 (1995).
17. S. Antusch, C. Biggio, E. Fernandez-Martinez, M. B. Gavela and J. Lopez-Pavon, *JHEP* **0610**, 084 (2006).
18. A. Abada, C. Biggio, F. Bonnet, M. B. Gavela and T. Hambye, arXiv:0803.0481 [hep-ph].
19. W. M. Yao *et al.* [Particle Data Group], *J. Phys.* G **33**, 1 (2006), and 2007 partial update for the 2008 edition available on the PDG WWW pages `http://pdg.lbl.gov/`.
20. F. del Aguila, J. de Blas and M. Perez-Victoria, arXiv:0803.4008 [hep-ph].
21. S. Bergmann and A. Kagan, *Nucl. Phys.* B **538**, 368 (1999).
22. D. Tommasini, G. Barenboim, J. Bernabeu and C. Jarlskog, *Nucl. Phys.* B **444**, 451 (1995).
23. P. Langacker and D. London, *Phys. Rev.* D **38**, 886 (1988).
24. W. Loinaz, N. Okamura, T. Takeuchi and L. C. R. Wijewardhana, *Phys. Rev.* D **67**, 073012 (2003).
25. G. Cynolter and E. Lendvai, arXiv:0804.4080 [hep-ph].
26. I. Gogoladze, N. Okada and Q. Shafi, arXiv:0805.2129 [hep-ph].
27. D. Wyler and L. Wolfenstein, *Nucl. Phys.* B **218**, 205 (1983); see also S. Bray, J. S. Lee and A. Pilaftsis, *Nucl. Phys.* B **786**, 95 (2007).
28. J. Kersten and A. Y. Smirnov, *Phys. Rev.* D **76**, 073005 (2007).
29. G. Ingelman and J. Rathsman, *Z. Phys.* C **60**, 243 (1993); F. del Aguila, J. A. Aguilar-Saavedra, A. Martinez de la Ossa and D. Meloni, *Phys. Lett.* B **613**, 170 (2005).
30. F. del Aguila, S. Bar-Shalom, A. Soni and J. Wudka, arXiv:0806.0876 [hep-ph]; see also S. Bar-Shalom, G. Eilam, T. Han and A. Soni, arXiv:0803.2835 [hep-ph].
31. F. del Aguila *et al*, arXiv:0801.1800 [hep-ph].
32. S. N. Gninenko, M. M. Kirsanov, N. V. Krasnikov and V. A. Matveev, *Phys. Atom. Nucl.* **70**, 441 (2007); see also J. M. Frere, T. Hambye and G. Vertongen, arXiv:0806.0841 [hep-ph].
33. F. del Aguila and J. A. Aguilar-Saavedra, *JHEP* **0711**, 072 (2007).
34. V. M. Abazov *et al.* [D0 Collaboration], arXiv:0803.1534 [hep-ex]; see also V. M. Abazov *et al.* [D0 Collaboration], *Phys. Rev. Lett.* **93**, 141801 (2004); D. E. Acosta *et al.* [CDF Collaboration], *Phys. Rev. Lett.* **93**, 221802 (2004).
35. F. del Aguila, L. Ametller, G. L. Kane and J. Vidal, *Nucl. Phys.* B **334**, 1 (1990).

The Standard model Higgs as the inflaton

F. L. Bezrukov
Institut de Théorie des Phénomènes Physiques, École Polytechnique Fédérale de Lausanne, CH-1015 Lausanne, Switzerland

We describe how non-minimal coupling term between the Higgs boson and gravity can lead to the chaotic inflation in the Standard Model without introduction of any additional degrees of freedom. Produced cosmological perturbations are predicted to be in accordance with observations. The tensor modes of perturbations are practically vanishing in the model.

1 Introduction

This talk is based on the recent work [1], and closely follows it. Note, that the expression for the inflationary potential presented here differs from the one presented in the original work—both expressions coincide in the region relevant for inflation, while the expression given here has a wider range of validity (down to the Standard Model regime).

The fact that our universe is almost flat, homogeneous and isotropic is often considered as a strong indication that the Standard Model (SM) of elementary particles is not complete. Indeed, these puzzles, together with the problem of generation of (almost) scale invariant spectrum of perturbations, necessary for structure formation, are most elegantly solved by inflation [2,3,4,5,6,7]. The majority of present models of inflation require an introduction of an additional scalar—the “inflaton”. Inflaton properties are constrained by the observations of fluctuations of the Cosmic Microwave Background (CMB) and the matter distribution in the universe. Though the mass and the interaction of the inflaton with matter fields are not fixed, the well known considerations prefer a heavy scalar field with a mass $\sim 10^{13}$ GeV and extremely small self-interacting quartic coupling constant $\lambda \sim 10^{-13}$ for realization of the chaotic inflationary scenario [8]. This value of the mass is close to the GUT scale, which is often considered as an argument in favour of existence of new physics between the electroweak and Planck scales.

It was recently demonstrated in [1] that the SM itself can give rise to inflation, provided non-minimal copling of the Higgs field with gravity. The spectral index and the amplitude of tensor perturbations can be predicted and be used to distinguish this possibility from other models for inflation; these parameters for the SM fall within the 1σ confidence contours of the WMAP-5 observations [9].

To explain our main idea, let us consider the Lagrangian of the SM non-minimally coupled to gravity,

$$L_{\rm tot} = L_{\rm SM} - \frac{M^2}{2}R - \xi H^\dagger H R \; , \tag{1}$$

where $L_{\rm SM}$ is the SM part, M is some mass parameter, R is the scalar curvature, H is the Higgs field, and ξ is an unknown constant to be fixed later. The third term in (1) is in fact required by the renormalization properties of the scalar field in a curved space-time background [10], so, in principle, it should be added to the usual SM Lagrangian with some constant. Here, we will analyse the situation with large non-minimal coupling parameter $\xi \gg 1$, but still not too large for the non-minimal term to contribute significantly to the Plank mass in the SM regime $(H \sim v)$, i.e. $\sqrt{\xi} \lll 10^{17}$. Thus, we have $M \simeq M_P = (8\pi G_N)^{-1/2} = 2.4 \times 10^{18}\,$GeV.

It is well known that inflation has interesting properties in models of this type[11,12,13,14,15,16,17]. However, in these works the scalar was not identified with the Higgs field of the SM. Basically, most attempts were made to identify the inflaton field with the GUT Higgs field. In this case one naturally gets into the regime of induced gravity (where, unlike this paper, $M = 0$ and M_P is generated from the non-minimal coupling term by the Higgs vacuum expectation value). In this case the Higgs field decouples from the other fields of the model [18,19,20], which is generally undesirable. Here we demonstrate, that when the SM Higgs boson is coupled non-minimally to gravity, the scales for the electroweak physics and inflation are separate, the electroweak properties are unchanged, while for much larger field values the inflation is possible.

The paper is organised as follows. We start from discussion of inflation in the model, and use the slow-roll approximation to find the perturbation spectra parameters. Then we will argue in Section 3 that quantum corrections are unlikely to spoil the classical analysis we used in Section 2. We conclude in Section 4.

2 Inflation and CMB fluctuations

Let us consider the scalar sector of the Standard Model, coupled to gravity in a non-minimal way. We will use the unitary gauge $H = h/\sqrt{2}$ and neglect all gauge interactions for the time being, they will be discussed later in Section 3. Then the Lagrangian has the form:

$$S_J = \int d^4x \sqrt{-g} \left\{ -\frac{M^2 + \xi h^2}{2} R + \frac{\partial_\mu h \partial^\mu h}{2} - \frac{\lambda}{4}\left(h^2 - v^2\right)^2 \right\} . \tag{2}$$

This Lagrangian has been studied in detail in many papers on inflation [13,14,16,17], we will reproduce here the main results of [13,16]. Compared to [1] we present a better approximation for the inflationary potential here. To simplify the formulae, we will consider only ξ in the region $1 \ll \sqrt{\xi} \lll 10^{17}$, in which $M \simeq M_P$ with very good accuracy.

It is possible to get rid of the non-minimal coupling to gravity by making the conformal transformation from the Jordan frame to the Einstein frame

$$\hat{g}_{\mu\nu} = \Omega^2 g_{\mu\nu} \; , \quad \Omega(h)^2 = 1 + \frac{\xi h^2}{M_P^2} \; . \tag{3}$$

This transformation leads to a non-minimal kinetic term for the Higgs field. So, it is convenient to make the change to the new scalar field χ with

$$\frac{d\chi}{dh} = \frac{\sqrt{\Omega^2 + \frac{3}{2} M_P^2 \left(\frac{d(\Omega^2)}{dh}\right)^2}}{\Omega^2} = \frac{\sqrt{1 + (\xi + 6\xi^2)\frac{h^2}{M_P^2}}}{1 + \xi \frac{h^2}{M_P^2}} \; . \tag{4}$$

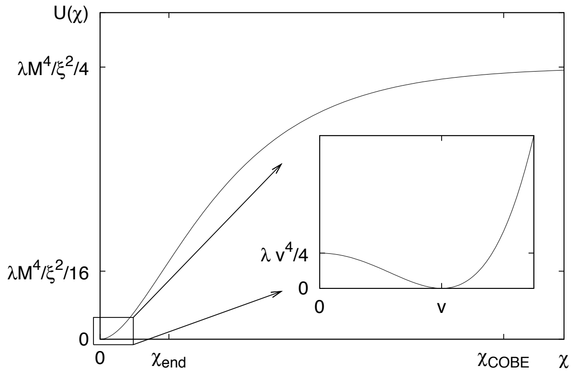

Figure 1: Effective potential in the Einstein frame.

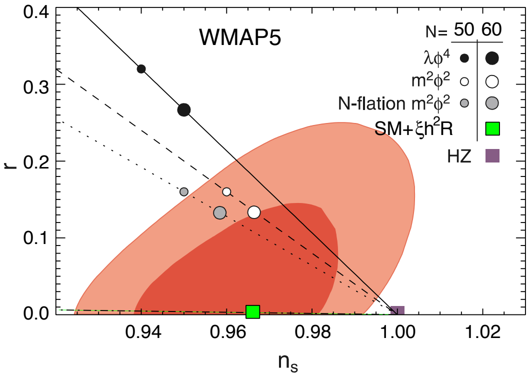

Figure 2: The allowed WMAP region for inflationary parameters $(r,\ n)$. The green boxes are our predictions supposing 50 and 60 e-foldings of inflation. Black and white dots are predictions of usual chaotic inflation with $\lambda\phi^4$ and $m^2\phi^2$ potentials, HZ is the Harrison-Zeldovich spectrum.

Finally, the action in the Einstein frame is

$$S_E = \int d^4x\sqrt{-\hat{g}}\Bigg\{-\frac{M_P^2}{2}\hat{R} + \frac{\partial_\mu\chi\partial^\mu\chi}{2} - U(\chi)\Bigg\}\ , \tag{5}$$

where $\hat{R}$ is calculated using the metric $\hat{g}_{\mu\nu}$ and the potential is

$$U(\chi) = \frac{1}{\Omega(h(\chi))^4}\frac{\lambda}{4}\left(h(\chi)^2 - v^2\right)^2\ . \tag{6}$$

For small field values $h, \chi < M_P/\xi$ the change of variables is trivial, $h \simeq \xi$ and $\Omega^2 \simeq 1$, so the potential for the field χ is the same as that for the initial Higgs field and we get into the SM regime. For $h, \chi \gg M_P/\xi$ the situation changes a lot. In this limit the variable change (4) is[a]

$$\Omega(h)^2 \simeq \exp\left(\frac{2\chi}{\sqrt{6}M_P}\right)\ . \tag{7}$$

The potential for the Higgs field is exponentially flat for large ξ and has the form

$$U(\chi) = \frac{\lambda M_P^4}{4\xi^2}\left(1 - \exp\left(-\frac{2\chi}{\sqrt{6}M_P}\right)\right)^2\ . \tag{8}$$

The full effective potential in the Einstein frame is presented in Fig. 1. It is the flatness of the potential at $\chi \gtrsim M_P$ which makes the successful (chaotic) inflation possible.

Basically, there are two distinct scales—for low field values $h, \chi \ll M_P/\xi$ we have the SM, for high field values $h \gg M_P/\sqrt{\xi}$ $(\chi > M_P)$ we have inflation with exponentially flat potential (8) and the Higgs field is decoupled from all other SM fields (because $\Omega \propto h$, see Section 3). In the intermediate region $M_P/\xi \ll h \ll M_P/\sqrt{\xi}$ $(M_P/\xi \ll \chi < M_P)$ the coupling with other particles is not suppressed $(\Omega \sim 1)$, while the potential and change of variables are still given by (8) and (7).

Analysis of the inflation in the Einstein frame[b] can be performed in the standard way using the slow-roll approximation. The slow roll parameters (in notations of [23]) can be expressed

---

[a] The following two formulae have wider validity range than those in [1], which are valid only for $h \gg M_P/\sqrt{\xi}$.

[b] The same results can be obtained in the Jordan frame [21,22].

analytically as functions of the field $h(\chi)$ using (4) and (6) (we give here the expressions for the case[c] $h^2 \gtrsim M_P^2/\xi \gg v^2$, $\xi \gg 1$, exact expressions can be found in[16]),

$$\begin{aligned} \epsilon &= \frac{M_P^2}{2}\left(\frac{dU/d\chi}{U}\right)^2 \simeq \frac{4M_P^4}{3\xi^2 h^4} , & (9)\\ \eta &= M_P^2 \frac{d^2U/d\chi^2}{U} \simeq \frac{4M_P^4}{3\xi^2 h^4}\left(1-\frac{\xi h^2}{M_P^2}\right) , & (10)\\ \zeta^2 &= M_P^4 \frac{(d^3U/d\chi^3)dU/d\chi}{U^2} \simeq \frac{16M_P^6}{9\xi^3 h^6}\left(\frac{\xi h^2}{M_P^2}-3\right) . & (11) \end{aligned}$$

Slow roll ends when $\epsilon \simeq 1$, so the field value at the end of inflation is $h_{\text{end}} \simeq (4/3)^{1/4} M_P/\sqrt{\xi} \simeq 1.07 M_P/\sqrt{\xi}$. The number of e-foldings for the change of the field h from h_0 to h_{end} is given by

$$N = \int_{h_{\text{end}}}^{h_0} \frac{1}{M_P^2}\frac{U}{dU/dh}\left(\frac{d\chi}{dh}\right)^2 dh \simeq \frac{3}{4}\frac{h_0^2 - h_{\text{end}}^2}{M_P^2/\xi} . \qquad (12)$$

We see that for all values of $\sqrt{\xi} \lll 10^{17}$ the scale of the Standard Model v does not enter in the formulae, so the inflationary physics is independent on it.

After end of the slow roll the χ field enters oscillatory stage with diminishing amplitude. After the oscillation amplitude falls below M_P/ξ, the situation returns to the SM one, so at this moment the reheating is imminent due to the SM interactions, which guarantees the minimum reheating temperature $T_{\text{reh}} \gtrsim (\frac{15\lambda}{8\pi^2 g^*})^{1/4}\frac{M_P}{\xi} \simeq 1.5 \times 10^{13}$ GeV, where $g^* = 106.75$ is the number of degrees of freedom of the SM. Careful analysis may give a larger temperature generated during the decay of the oscillating χ field, but definitely below the energy scale at the end of the inflation $T_{\text{reh}} < (\frac{2\lambda}{\pi^2 g^*})^{1/4}\frac{M_P}{\sqrt{\xi}} \simeq 2 \times 10^{15}$ GeV.

As far as the reheating mechanism and the universe evolution after the end of the inflation is fixed in the model, the number of e-foldings for the the COBE scale entering the horizon can be calculated (see[23]). Here we estimate it as $N_{\text{COBE}} \simeq 62$ (exact value depends on the detailed analysis of reheating, which will be done elsewhere). The corresponding field value is $h_{\text{COBE}} \simeq 9.4 M_P/\sqrt{\xi}$. Inserting (12) into the COBE normalization $U/\epsilon = (0.027 M_P)^4$ we find the required value for ξ

$$\xi \simeq \sqrt{\frac{\lambda}{3}}\frac{N_{\text{COBE}}}{0.027^2} \simeq 49000\sqrt{\lambda} = 49000\frac{m_H}{\sqrt{2}v} . \qquad (13)$$

Note, that if one could deduce ξ from some fundamental theory this relation would provide a connection between the Higgs mass and the amplitude of primordial perturbations.

The spectral index $n_s = 1 - 6\epsilon + 2\eta$ calculated for $N = 60$ (corresponding to the scale $k = 0.002/\text{Mpc}$) is $n_s \simeq 1 - 8(4N+9)/(4N+3)^2 \simeq 0.97$. The tensor to scalar perturbation ratio[9] is $r = 16\epsilon \simeq 192/(4N+3)^2 \simeq 0.0033$. The predicted values are well within one sigma of the current WMAP measurements[9], see Fig. 2.

3 Radiative corrections

An essential point for inflation is the flatness of the scalar potential in the region of the field values $h \sim 10 M_P/\sqrt{\xi}$ ($\chi \sim 6 M_P$). It is important that radiative corrections do not spoil this property. Of course, any discussion of quantum corrections is flawed by the non-renormalizable character of gravity, so the arguments we present below are not rigorous.

---

[c] These formulas are valid up to the end of the slow roll regime h_{end}, while the formulas (10) and (11) in[1] are applicable only for the earlier inflationary stages, $h^2 \gg M_P^2/\xi$, which is sufficient to calculate primordial spectrum parameters n_s and r.

There are two qualitatively different type of corrections one can think about. The first one is related to the quantum gravity contribution. It is conceivable to think [24] that these terms are proportional to the energy density of the field χ rather than its value and are of the order of magnitude $U(\chi)/M_P^4 \sim \lambda/\xi^2$. They are small at large ξ required by observations. Moreover, adding non-renormalizable operators h^{4+2n}/M_P^{2n} to the Lagrangian (2) also does not change the flatness of the potential in the inflationary region.[d]

Other type of corrections is induced by the fields of the Standard Model coupled to the Higgs field. In one loop approximation these contributions have the structure

$$\Delta U \sim \frac{m^4(\chi)}{64\pi^2}\log\frac{m^2(\chi)}{\mu^2}\ , \tag{14}$$

where $m(\chi)$ is the mass of the particle (vector boson, fermion, or the Higgs field itself) in the background of field χ, and μ is the normalization point. Note that the terms of the type $m^2(\chi)M_P^2$ (related to quadratic divergences) do not appear in scale-invariant subtraction schemes that are based, for example, on dimensional regularisation (see a relevant discussion in [25,26,27,28]). The masses of the SM fields can be readily computed [13] and have the form

$$m_{\psi,A}(\chi) = \frac{m(v)}{v}\frac{h(\chi)}{\Omega(\chi)}\ , \quad m_H^2(\chi) = \frac{d^2U}{d\chi^2} \tag{15}$$

for fermions, vector bosons and the Higgs (inflaton) field. It is crucial that for large χ these masses approach different constants (i.e. the one-loop contribution is as flat as the tree potential) and that (14) is suppressed by the gauge or Yukawa couplings in comparison with the tree term. In other words, one-loop radiative corrections do not spoil the flatness of the potential as well. This argument is identical to the one given in [13].

4 Conclusions

Non-minimal coupling of the Higgs field to gravity leads to the possibility of chaotic inflation in SM. Specific predictions for the primordial perturbation spectrum are obtained. Specifically, very small amount of tensor perturbations is expected, which means that future CMB experiments measuring the B-mode of the CMB polarization (PLANCK) can distinguish between the described scenario from other models (based, e.g. on inflaton with quadratic potential).

At the same time, we expect that the Higgs potential does not enter into the string coupling regime, nor generates another vacuum up to the scale of at least $M_P/\xi \sim 10^{14}$ GeV, so we expect the Higgs mass to be in the window $130\,\mathrm{GeV} < M_H < 190\,\mathrm{GeV}$ (see, eg. [29]), otherwise the inflation would be impossible.

The inflation mechanism we discussed has in fact a general character and can be used in many extensions of the SM. Thus, the νMSM of [30,31,32,33,25,34,35,36,37,38,39,40] (SM plus three light fermionic singlets) can explain simultaneously neutrino masses, dark matter, baryon asymmetry of the universe and inflation without introducing any additional particles (the νMSM with the inflaton was considered in [25]). This provides an extra argument in favour of absence of a new energy scale between the electroweak and Planck scales, advocated in [27].

Acknowledgements

The author thank M. Shaposhnikov, S. Sibiryakov, V. Rubakov, G. Dvali, I. Tkachev, O. Ruchayskiy, H.D. Kim, P. Tinyakov, and A. Boyarsky for valuable discussions. This work was supported by the Swiss National Science Foundation.

---

[d] Actually, in the Jordan frame, we expect that higher-dimensional operators are suppressed by the effective Planck scale $M_P^2 + \xi h^2$.

References

1. F.L. Bezrukov and M. Shaposhnikov, Phys. Lett. B659 (2008) 703.
2. A.A. Starobinsky, JETP Lett. 30 (1979) 682.
3. A.A. Starobinsky, Phys. Lett. B91 (1980) 99.
4. V.F. Mukhanov and G.V. Chibisov, JETP Lett. 33 (1981) 532.
5. A.H. Guth, Phys. Rev. D23 (1981) 347.
6. A.D. Linde, Phys. Lett. B108 (1982) 389.
7. A. Albrecht and P.J. Steinhardt, Phys. Rev. Lett. 48 (1982) 1220.
8. A.D. Linde, Phys. Lett. B129 (1983) 177.
9. WMAP, E. Komatsu et al., (2008), arXiv:0803.0547 [astro-ph].
10. N.D. Birrell and P.C.W. Davies, Quantum Fields in Curved Space (Cambridge, UK: Univ. Pr., 1982).
11. B.L. Spokoiny, Phys. Lett. B147 (1984) 39.
12. T. Futamase and K. Maeda, Phys. Rev. D39 (1989) 399.
13. D.S. Salopek, J.R. Bond and J.M. Bardeen, Phys. Rev. D40 (1989) 1753.
14. R. Fakir and W.G. Unruh, Phys. Rev. D41 (1990) 1783.
15. D.I. Kaiser, Phys. Lett. B340 (1994) 23.
16. D.I. Kaiser, Phys. Rev. D52 (1995) 4295.
17. E. Komatsu and T. Futamase, Phys. Rev. D59 (1999) 064029.
18. J.J. van der Bij, Acta Phys. Polon. B25 (1994) 827.
19. J.L. Cervantes-Cota and H. Dehnen, Nucl. Phys. B442 (1995) 391.
20. J.J. van der Bij, Int.J.Phys. 1 (1995) 63.
21. N. Makino and M. Sasaki, Prog. Theor. Phys. 86 (1991) 103.
22. R. Fakir, S. Habib and W. Unruh, Astrophys. J. 394 (1992) 396.
23. D.H. Lyth and A. Riotto, Phys. Rept. 314 (1999) 1.
24. A.D. Linde, Phys. Lett. B202 (1988) 194.
25. M. Shaposhnikov and I. Tkachev, Phys. Lett. B639 (2006) 414.
26. K.A. Meissner and H. Nicolai, Phys. Lett. B648 (2007) 312.
27. M. Shaposhnikov, (2007), arXiv:0708.3550 [hep-th].
28. K.A. Meissner and H. Nicolai, (2007), arXiv:0710.2840 [hep-th].
29. Y.F. Pirogov and O.V. Zenin, Eur. Phys. J. C10 (1999) 629.
30. T. Asaka, S. Blanchet and M. Shaposhnikov, Phys. Lett. B631 (2005) 151.
31. T. Asaka and M. Shaposhnikov, Phys. Lett. B620 (2005) 17.
32. F. Bezrukov, Phys. Rev. D72 (2005) 071303.
33. T. Asaka, M. Shaposhnikov and A. Kusenko, Phys. Lett. B638 (2006) 401.
34. M. Shaposhnikov, Nucl. Phys. B763 (2007) 49.
35. T. Asaka, M. Laine and M. Shaposhnikov, JHEP 06 (2006) 053.
36. T. Asaka, M. Laine and M. Shaposhnikov, JHEP 0701 (2007) 091.
37. F. Bezrukov and M. Shaposhnikov, Phys. Rev. D75 (2007) 053005.
38. D. Gorbunov and M. Shaposhnikov, (2007), arXiv:0705.1729 [hep-ph].
39. M. Shaposhnikov, (2008), arXiv:0804.4542 [hep-ph].
40. M. Laine and M. Shaposhnikov, (2008), arXiv:0804.4543 [hep-ph].

UNPARTICLES,
A VIEW FROM THE HIGGS WINDOW

J.R. ESPINOSA
IFT-UAM/CSIC, Fac. Ciencias UAM, 28049 Madrid, Spain

In this Moriond talk I give an introduction to what unparticles are supposed to be and then show how coupling unparticles to the Higgs opens a window to the exploration of unparticle sectors. The second part is based on work done in collaboration with Antonio Delgado, Mariano Quirós and José Miguel No in [1,2].

1 Introduction to Unparticles

We start by assuming (with Georgi [3]) that our theory contains a scale invariant sector. Such sector must look very different from the familiar Standard Model (SM). In the SM we have an explicit mass term in the Higgs potential, the origin of all mass scales. We cannot have such mass terms in the scale invariant sector so, one would naively think such sector is composed of massless fields. That is too naive as we will see later on.

In fact, not all SM masses come from the Higgs mass term: quantum running of couplings can generate mass scales as happens in QCD. So, another requirement of the scale invariant sector is that couplings there should not run at all, and this should happen in a non-trivial way, *i.e.* for non-zero coupling. In fact, there are examples in the literature of just that happening, like the Banks-Zaks (BZ) model [4]: a Yang-Mills theory with some particular choice of the number of colors and flavors. The gauge coupling reaches an IR fixed-point below some mass scale Λ_U. This requires cancellations between different orders of perturbation theory and normally occurs at strong coupling. Below Λ_U the theory becomes scale-invariant.

In order to explore the physics of such scale-invariant sector, Georgi considered the possibility of coupling it to the SM, *e.g.* assume there is a heavy sector, at the scale M_m, coupled both to the SM and the Banks-Zaks-like sector, see figure 1. The effective theory below this mass (M_m) will contain non-renormalizable interactions between SM operators and BZ operators:

$$\frac{1}{M_m^k}\mathcal{O}_{SM}\mathcal{O}_{BZ}\ . \tag{1}$$

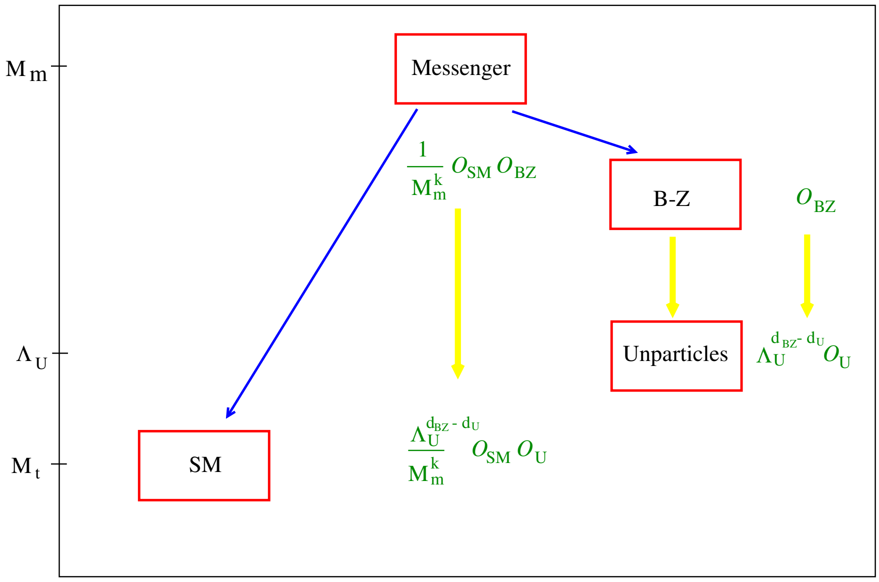

Figure 1: SM coupled to a Banks-Zaks-like sector through a messenger sector. The BZ-like sector becomes a conformal unparticle sector below the scale Λ_U.

In the BZ side interesting things happen when one reaches the scale-invariant fixed point below Λ_U. Operators with some scaling dimension d_{BZ} get transformed into operators with dimension d_U that can be very different from an integer value.

$$\mathcal{O}_{BZ} \to \Lambda_U^{d_{BZ}-d_U} \mathcal{O}_U \ . \tag{2}$$

For simplicity I only consider scalar operators, in which case unitarity demans $d_U > 1$ and I will take $d_U < 2$ because the most interesting effects take place in that range. The non-renormalizable term will now be a coupling between SM fields and unparticle operators:

$$\frac{\Lambda_U^{d_{BZ}-d_U}}{M_m^k} \mathcal{O}_{SM} \mathcal{O}_U \ . \tag{3}$$

One assumes that the parameter $\epsilon \equiv \Lambda_U^{d_{BZ}-d_U}/M_m^k$ is small enough so that unparticle effects haven't showed up so far (in fact, ϵ is not dimensionless so the appropriate power of the low-energy scale relevant for the process in question should be included). The important point is that, d_U being a non-integer, $\mathcal{O}_U$ cannot be interpreted in terms of particles in the usual way.

Once we have a coupling between SM fields and unparticles we can start discussing unparticle production, using this coupling as an insertion in some SM process. To first order in ϵ one simply gets missing energy and momentum. The probability for such a process goes like ϵ^2:

$$\epsilon^2 |\langle SM_{out}|\mathcal{O}_{SM}|SM_{in}\rangle|^2 |\langle U|\mathcal{O}_U|0\rangle|^2 \ , \tag{4}$$

and the unparticle matrix element will be determined, by scale-invariance, to go like the appropriate power of x:

$$\langle 0|\mathcal{O}_U(x)\mathcal{O}_U^\dagger(0)|0\rangle = \int e^{-ipx} |\langle U,p|\mathcal{O}_U(0)|0\rangle|^2 \rho(p^2) \frac{d^4p}{(2\pi)^4} \sim x^{-2d_U} \ . \tag{5}$$

Going to momentum space we find an unparticle two-point correlator (or propagator) that goes like this unusual power of momentum [3,5]

$$|\langle U,p|\mathcal{O}_U(0)|0\rangle|^2 = A_{d_U} \theta(p^0)\theta(p^2)(p^2)^{d_U-2} \ , \tag{6}$$

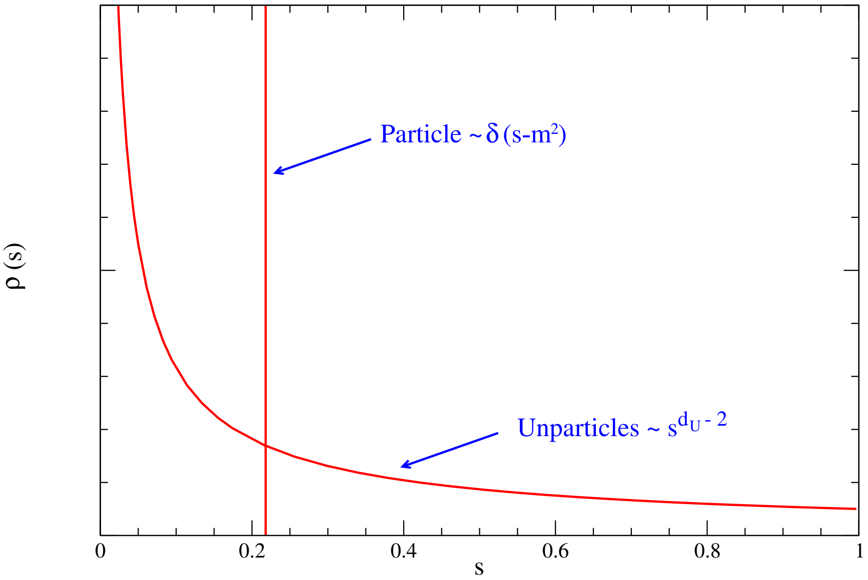

Figure 2: Spectral functions for a normal particle and for unparticles (with $d_U = 1.2$).

($d_U \to 1$ would correspond to a normal particle propagator). Georgi compared this to the phase space factor for production of n massless particles ($dLIPS_n = A_n s^{n-2}$) to conclude that unparticles could be interpreted as a non-integer number of massless particles but I think this does not help intuition much.

I find more useful to obtain the spectral function representation of the unparticle propagator: it gives a scan of what is being propagated. For a normal particle the spectral function is just a Dirac delta at the particle's mass, $\rho(s) = \delta(s - m^2)$. For unparticles we get a continuous function, $\rho(s) = s^{d_U - 2}$, see figure 2. This leads to the following picture: the operator $\mathcal{O}_U$ does not create particles out of the vacuum but rather a non-localized wave over the full range of p^2.

Another useful way of looking at unparticles was proposed by Stephanov [6]. He considered an infinite tower of scalars φ_n, $(n = 1, ..., \infty)$, with masses-squared separated by a constant splitting Δ^2, $M_n^2 = \Delta^2 n$. In the continuum limit, $\Delta^2 \to 0$, it is simple to show that one gets a scale-invariant spectrum. In fact, in the deconstructed action

$$S = \int d^4x \Sigma_{n=1}^{\infty} \left[\frac{1}{2} (\partial_\mu \varphi_n)^2 + \frac{1}{2} M_n^2 \varphi_n^2 \right] , \tag{7}$$

kinetic terms are scale invariant [under $\varphi_n(x) \to \lambda \varphi_n(\lambda x)$] while mass terms are not. However, when $\Delta^2 \to 0$, replacing the discrete sum by an integral and taking $\varphi_n/\Delta \to u(M^2)$, the continuum action including the mass term

$$S = \int d^4x \int_0^\infty dM^2 \left[\frac{1}{2} (\partial_\mu u)^2 + \frac{1}{2} M^2 u^2 \right] , \tag{8}$$

is indeed scale invariant [under $u(M^2, x) \to u(M^2/\lambda^2, \lambda x)$] thanks to the rescaling freedom in the integration variable. This is one example of scale invariant model not composed of massless fields. To make contact with unparticle operators one defines a linear combination O of the φ_n fields

$$O = \sum_n F_n \varphi_n , \tag{9}$$

with the appropriate mass-dependent coefficients

$$F_n^2 = \frac{A_{d_U}}{2\pi} \Delta^2 (M_n^2)^{d_U - 2} , \tag{10}$$

such that the two-point correlator of the deconstructed operator O has the correct unparticle continuum limit. In this way Stephanov could rederive many of the phenomenological unparticle implications working in the more familiar deconstructed version and taking the continuum limit at the end.

2 Looking at Unparticles through the Higgs

In the second part of the talk I want to discuss the possibility of having a direct coupling between the unparticle operator and the Higgs:

$$\kappa_U \mathcal{O}_{SM} \mathcal{O}_U = \kappa_U |H|^2 \mathcal{O}_U \ . \tag{11}$$

Notice that the Higgs is special in the sense that it offers the only possible renormalizable coupling with scalar unparticles[7]. One immediate difficulty one has to face is that, after electroweak symmetry breaking (EWSB), such coupling induces a tadpole for $\mathcal{O}_U$ and therefore a VEV for it. It is a simple matter to obtain this VEV: simply get the VEVs v_n for the deconstructed scalars and integrate over M^2 to obtain:

$$\langle \mathcal{O}_U \rangle = -\frac{\kappa_U v^2}{2} \int_0^\infty \frac{F^2(M^2)}{M^2} dM^2 \propto \int_0^\infty (M^2)^{d_U - 3} dM^2 \ , \tag{12}$$

where $F(M^2)$ is the continuum version of F_n. For $d_U < 2$ one sees that this integral has an IR divergence. Its origin is clear: the tadpole goes to ∞ when $M_n \to 0$ while the restoring term, which is M_n itself, goes to zero then.

However, this IR problem is easy to cure. For instance, if the Higgs also couples to quadratic terms for the φ_n's

$$\zeta |H|^2 \sum_n \varphi_n^2 \ , \tag{13}$$

this will give an extra mass squared ζv^2 to unparticles that will act as an IR cutoff in the previous integral:

$$\langle \mathcal{O}_U \rangle = -\frac{\kappa_U v^2}{2} \int_0^\infty \frac{F^2(M^2)}{M^2 + \zeta v^2} dM^2 \ . \tag{14}$$

Other more intriguing possibility uses quartic self-interactions of unparticles of the form

$$\delta V = \xi \left(\sum_n \varphi_n^2 \right)^2 \ , \tag{15}$$

but I do not have time to discuss it here, see[2]. The structure of the unparticle continuum after the IR problem is solved is therefore a continuum above a mass gap $m_g = \sqrt{\zeta} v$ (of EW size). Needless to say, the presence of such mass gap will affect dramatically the phenomenology of (and constraints on) unparticles.

Let me focus here on some implications for Higgs physics. After EWSB the Higgs scalar will mix with the unparticle continuum. The mixed mass matrix in the deconstructed picture looks like this:

$$\mathcal{M}^2 = \begin{bmatrix} m_{h^0}^2 & A_1 & .. & A_n & .. \\ A_1 & M_1^2 + m_g^2 & .. & 0 & .. \\ : & : & \ddots & 0 & .. \\ A_n & 0 & 0 & M_n^2 + m_g^2 & 0 \\ : & : & : & 0 & \ddots \end{bmatrix} \tag{16}$$

Here m_{h0}^2 is the SM Higgs mass squared. Along the diagonal we have the unparticle tower with a mass gap and the first row and column are non-zero with $A_n = v(\kappa_U F_n + 2\zeta v_n)$ and mix both

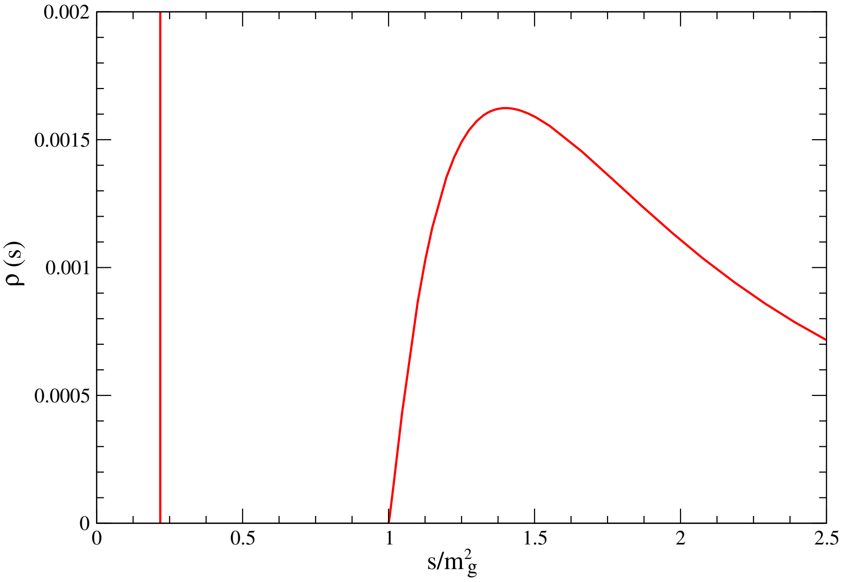

Figure 3: Spectral function ρ as a function of s for a case with $m_h < m_g$. The parameters are $\mu_U^2 = \mu_v^2$, $m^2 = 0$, $d_U = 1.2$ and $\zeta = 1$. All dimensions scaled by m_g^2.

sectors. To analyze what happens in the presence of such mixing we derive the propagator for h resumming U insertions to obtain the following:

$$iP(p^2)^{-1} = p^2 - m_{h^0}^2 + v^2(\mu_U^2)^{2-d_U}\int_0^\infty \frac{(M^2)^{d_U-2}}{M^2+m_g^2-p^2}\left[\frac{M^2}{M^2+m_g^2}\right]^2 dM^2 \ , \tag{17}$$

a propagator with a SM part and a more complicated term coming from unparticles. The same propagator can be obtained by diagonalizing the full propagator matrix. Here we have used

$$(\mu_U^2)^{2-d_U} \equiv \kappa_U^2 \frac{A_{d_U}}{2\pi} \ . \tag{18}$$

The first effect is a shift in the Higgs mass $m_{h^0}^2 \to m_h^2$, with $P(m_h^2)^{-1} = 0$. One can consider two qualitatively different cases depending on whether the shifted Higgs mass is below or above the mass gap. Let us start with a Higgs below the gap. Again it is quite useful to go to the spectral function representation of the modified propagator (17). It looks as shown in fig. 3: a Dirac delta at the pole Higgs mass and a continuum above m_g^2. In this plot we have chosen $m^2 = 0$, $\zeta = 1$, $d_U = 1.2$ and $\mu_U^2 = \mu_v^2 \equiv v^2[A_{d_U}/(2\pi)]^{2-d_U}$. Explicitly the spectral function is

$$\rho(s) = \frac{1}{K^2(m_h^2)}\delta(s-m_h^2) + \theta(s-m_g^2)\frac{Q_U^2(s)}{[iP(s)^{-1}]^2 + \pi^2 Q_U^4(s)} \ , \tag{19}$$

where the functions $K^2(m_h^2)$ and $Q_U^2(s)$ can be found in [1]. This spectral function has a very diret physical interpretation. For a given s it gives the projection of the state with mass-squared s onto the interaction eigenstate h:

$$\rho(s) \equiv \langle h|s\rangle\langle s|h\rangle = |\langle h|H\rangle|^2\delta(s-m_h^2) + \theta(s-m_g^2)|\langle h|U,s\rangle|^2 \ , \tag{20}$$

where $|h\rangle, |u,s\rangle$ are interaction eigenstates and $|H\rangle, |U,s\rangle$ are mass eigenstates. This is crucial for instance in studying the ZZ coupling as h is the state that couples to ZZ. In this way we learn that the prefactor $R_h^2 = |\langle h|H\rangle|^2 = 1/K^2(m_h^2)$ of the delta function gives how much of the isolated pole is a pure Higgs. On the other hand, the spectral function above the mass gap,

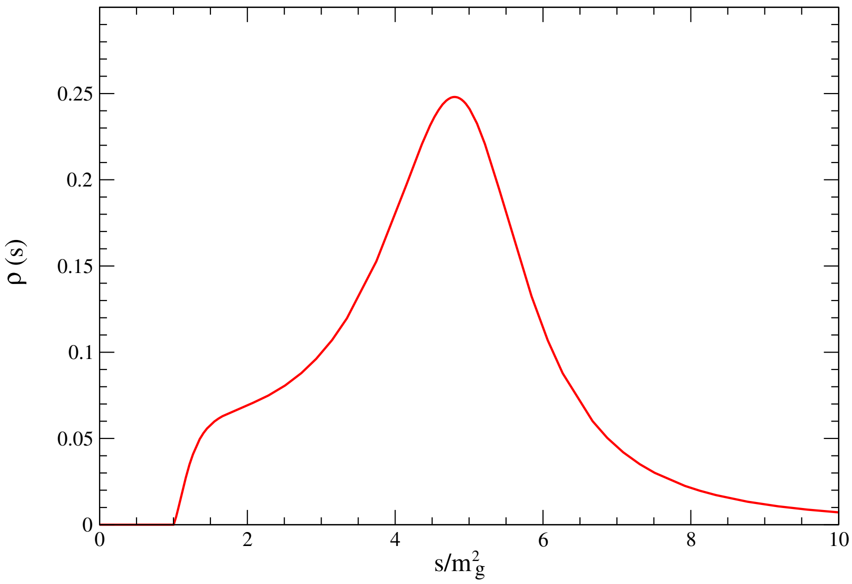

Figure 4: Spectral function ρ as a function of s for a case with $m_h > m_g$. The parameters are $\mu_U^2 = \mu_v^2$, $m^2 = 0$, $d_U = 1.2$ and $\zeta = 0.2$. All dimensions scaled by m_g^2.

$R_U^2(M^2) = |\langle h|U, s\rangle|^2$, gives information about how the unparticle continuum couples to the Z through Higgs mixing. Of course the following sum rule

$$R_h^2 + \int_0^\infty R_U^2(M^2)dM^2 = 1 \ , \tag{21}$$

that implies that no “Higgsness” is lost in the mixing, is satisfied.

The case with a Higgs mass above the mass gap is also interesting. From the spectral function we learn that there is no delta function associated with the Higgs pole but rather a broad resonance due to the mixing of the Higgs with unparticles:

$$\rho(s) = \theta(s - m_g^2)\frac{Q_U^2(s)}{[iP(s)^{-1}]^2 + \pi^2 Q_U^4(s)} \ . \tag{22}$$

In fact the Higgs is totally swallowed by this continuum, see fig. 4 (same parameters as in fig. 3 except for $\zeta = 0.2$). How big the width can be is shown by plot 5, where we show (as a function of d_U) the width, given by:

$$\Gamma_h = \frac{\pi Q_U^2(m_h^2)}{m_h K^2(m_h^2)} \ , \tag{23}$$

and also the Higgs mass. We see that in some cases the width can be as large as the mass itself. Such effects will totally modify the expected Higgs collider phenomenology.

3 Conclusions

While almost everybody agrees that the idea of unparticles is extremely speculative it remains an intriguing theoretical possibility and we should keep it in mind for LHC. In this talk I focussed on the effects that one would expect from a direct coupling between the Higgs and an unparticle scalar operator. After dealing with an IR problem easy to solve I discussed how a mass gap is generated from EWSB. This gap would have important implications for unparticle phenomenology. I also showed how Higgs-unparticle mixing can greatly modify Higgs properties and how it can also give us a very interesting handle to explore the unparticle sector.

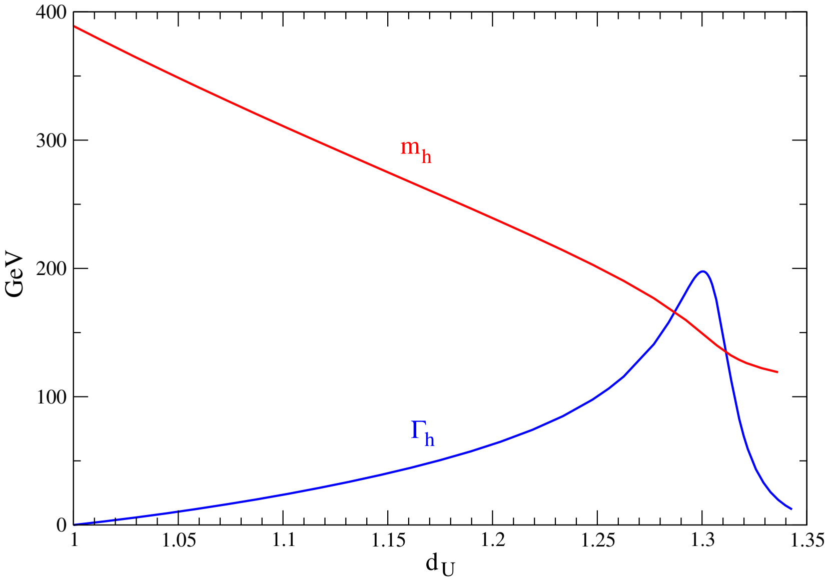

Figure 5: Width Γ_h (from unparticle merging) and mass m_h of the Higgs boson as a function of d_U for $\mu_U^2 = \mu_v^2$, $m^2 = 0$ and $\zeta = 0.2$.

Acknowledgments

I thank the Moriond organizers for their kind invitation and Antonio Delgado, José Miguel No and Mariano Quirós for the enjoyable collaboration that lead to the results presented here. In the preparation of this talk I have benefitted from several other unparticle talks by P. Ball, H. Georgi and J. Terning. I also thank CERN for partial financial support. Work supported in part by the European Commission under the European Union through the Marie Curie Research and Training Networks "Quest for Unification" (MRTN-CT-2004-503369) and "UniverseNet" (MRTN-CT-2006-035863); by the Spanish Consolider-Ingenio 2010 Programme CPAN (CSD2007-00042); by a Comunidad de Madrid project (P-ESP-00346) and by CICYT, Spain, under contract FPA 2007-60252.

References

1. A. Delgado, J. R. Espinosa and M. Quirós, JHEP **0710** (2007) 094 [hep-ph/0707.4309].
2. A. Delgado, J. R. Espinosa, J. M. No and M. Quirós, JHEP **0804** (2008) 028 [hep-ph/0802.2680].
3. H. Georgi, Phys. Rev. Lett. **98** (2007) 221601 [hep-ph/0703260]; Phys. Lett. B **650**, 275 (2007) [hep-ph/0704.2457].
4. T. Banks and A. Zaks, Nucl. Phys. B **196** (1982) 189.
5. K. Cheung, W. Y. Keung and T. C. Yuan, Phys. Rev. Lett. **99** (2007) 051803 [hep-ph/0704.2588].
6. M. A. Stephanov, Phys. Rev. D **76**, 035008 (2007) [hep-ph/0705.3049]; N. V. Krasnikov, Int. J. Mod. Phys. A **22**, 5117 (2007) [hep-ph/0707.1419].
7. P. J. Fox, A. Rajaraman and Y. Shirman, Phys. Rev. D **76** (2007) 075004 [hep-ph/0705.3092]; M. Bander, J. L. Feng, A. Rajaraman and Y. Shirman, Phys. Rev. D **76** (2007) 115002 [hep-ph/0706.2677].

Commissioning of CMS and early standard model measurements with jets, missing transverse energy and photons at the LHC

Tim Christiansen
for the ATLAS and CMS Collaborations
CERN, CH-1211 Geneva 23, Switzerland

We report on the status and history of the CMS commissioning, together with selected results from cosmic-muon data. The second part focuses on strategies for optimizing the reconstruction of jets, missing transverse energy and photons for early standard model measurements at ATLAS and CMS with the first collision data from the Large Hadron Collider at CERN.

1 CMS Commissioning

With the first collisions from the LHC expected soon, the CMS experiment [1] at CERN has entered the final stage of commissioning. Nearly all of the detectors have been installed in the experiment and the last heavy structure of CMS was lowered into the experimental hall in January 2008 (see photograph in Fig. 1). The CMS collaboration has launched over the past years a series of combined data-taking exercises, so-called Global Runs, with increasing scope and complexity. More and more components have been integrated with the trigger and DAQ systems, and data from cosmic muons as well as high-rate random triggers have been used to prove readiness for LHC collisions.

One of the first highlights in the commissioning of the CMS detector was the "Magnet Test and Cosmic Challenge" (MTCC) [2], which took place in 2006 when the CMS detector was operated in the assembly hall on the surface. The superconducting magnet of CMS required testing before lowering, providing a unique opportunity to operate all the subdetectors and subsystems together and to take data with cosmic-ray muons. The participating systems included a 60^o sector of the muon system, comprising gas detectors like the drift tubes (DTs), Cathode Strip Chambers (CSCs) and Resistive Plate Chambers (RPCs), both in the barrel part and endcaps of CMS. The tracking system comprised elements of the Silicon-Strip Tracker, and parts of the Electromagnetic (ECAL) and Hadron Calorimeter (HCAL) detected energy depositions of

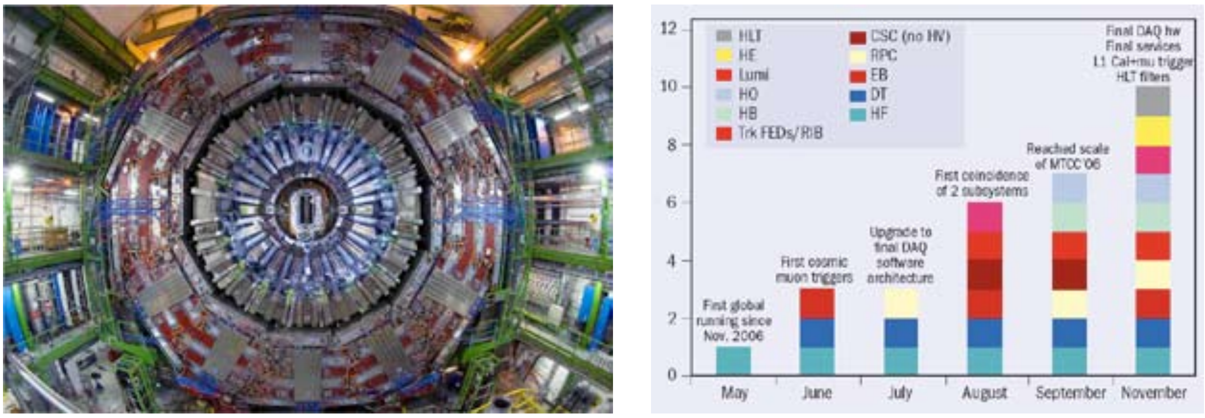

Figure 1: The CMS barrel detector in the experimental hall (left). The increasing number of subsystems integrated in global data taking over 2007 (right): HLT: High-Level Trigger, HE: Endcap Hadron Calorimeter, Lumi: Luminosity system, HO: Outer Hadron Calorimeter, HB: Barrel Hadron Calorimeter, Trk FEDs/RIB: Tracker frontend drivers/"rod-in-a-box", CSC: Cathode Strip Chambers, RPC: Resistive Plate Chambers, EB: Barrel Electromagnetic Calorimeter, DT: Drift Tubes, HF: Forward Hadron Calorimeter. The diagram is for illustration of the progress only, the scale is arbitrary and non-linear.

the traversing muons. In the second phase of the MTCC, the ECAL modules and the tracker elements were replaced by a specially designed mapping device to measure the three components of the magnetic field in the volume of the inner detectors with high precision, while HCAL and the muon systems continued to record cosmic-ray data.

Only six months after the conclusion of the MTCC, global data taking was resumed in the first of a series of Global Runs, this time in the underground experimental hall. With the end of 2007, CMS has recorded data from synchronized cosmic triggers from parts of all trigger detectors (CSCs, DTs, RPCs, ECAL and HCAL). The diagram on the right of Fig. 1 illustrates the progress made in the integration of subdetectors and subsystems in various Global Runs in 2007. One of the many results from these exercises is the confirmation of a single-hit resolution $\delta x < 280\,\mu$m along ϕ [a] of the Muon Drift Tubes. One of the next goals before the LHC startup is the integration of the central tracker in the Global Runs.

2 Early Standard Model Measurements with Jets, Missing Transverse Energy and Photons

Already the first 10 to 100 pb^{-1} of recorded data at the LHC experiments will allow QCD measurements with minimum-bias events and will open the window to the Z- and W-boson and top-quark production. However, it is natural to expect that the first $\sim 100\,\mathrm{pb}^{-1}$ of integrated luminosity will first be used to test and improve the understanding of the detector response and to calibrate and measure the performance of the physics objects used in the various searches and measurements to follow. Therefore, this article focuses on the strategies for the "commissioning" of the physics objects with the first data, using the standard model processes accessible with the recorded data set. Details about the longer term physics plans of ATLAS and CMS can be found in the references [1,3].

Physicists from ATLAS and CMS are taking care that the experiments will make the best use of the early data to align and calibrate the detectors. Analyses are prepared to study and optimize the performance of the triggers and of physics objects. The strategies range from transverse-momentum balancing to exploiting well-known SM signatures, such as *tag-and-probe*

---

[a] ϕ is the azimuth angle of the CMS coordinate system with the z axis pointing in the direction of the beam and the origin in the center of the detector. η denotes the pseudorapidity $\eta = -\ln[\tan\theta/2]$ where θ is the polar angle of the CMS coordinate system.

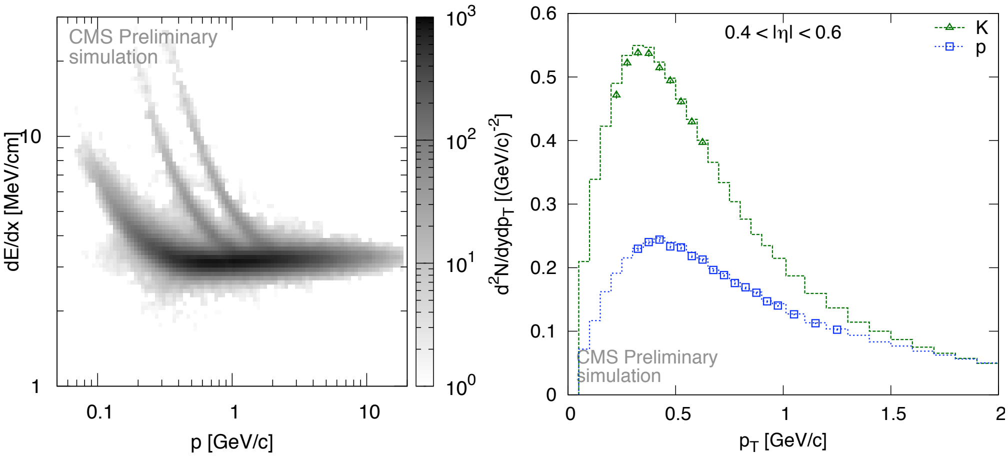

Figure 2: Left: Energy loss dE/dx spectra for charged pions, kaons (K) and protons (p) in the Silicon Tracker (Pixels and Strips combined) of CMS. The scatter plot clearly shows the three separate bands for charged pions, kaons and protons (from left to right). Right: Charged-hadron spectra $dN/dydp_T$ of protons and kaons as a function of transverse momentum. The "data" statistics correspond to approximately one month of data taking with 1 Hz allocated bandwidth from minimum- or zero-bias events.

with leptonic Z-boson decays. As the field is too large to cover in this article all the aspects of measurements with jets, electrons, photons and missing transverse energy, we report on a few selected recent studies from ATLAS and CMS with a focus on the reconstruction performance and strategies.

One of the first measurements to be performed at the LHC aims at the understanding of the spectrum of charged hadrons. These spectra have never been explored in hadron collisions at such high energies ($\sqrt{s} > 2\,\text{TeV}$) and they are an important tool for the calibration and understanding of the detector response. Recent studies at CMS show that it is feasible to distinguish charged pions, kaons and protons with momenta up to 2 GeV/c and individually measure their spectra (see Fig. 2) [4]. Cross-sections and differential yields of charged particles (unidentified or identified pions, kaons and protons), produced in inelastic proton-proton collisions at $\sqrt{s} = 14\,\text{TeV}$, can be measured with good precision with the CMS Pixel vertex detector and tracker system.

An important ingredient for the correct simulation of standard model processes at LHC is the understanding of the "underlying event", consisting of the beam-beam remnants (a soft component coming from the break-up of the two beam hadrons). Furthermore, it is sensitive to test multiple-parton interaction (MIP) tunes of QCD [5]. Technically, it is impossible to fully separate the underlying event from the hard scattering process, however, the observation of charged particles in the region "perpendicular" to the leading jet ($60^o < |\Delta\phi_j| < 120^o$ in the transverse projection) in QCD di-jet events can be used to distinguish between various MIP tunes that have been considered: DW [6], DWT [7], S0 [8] and Herwig [9] (see Fig. 3) [10].

Up to now, the analyses of the two experiments reconstruct jets mainly with variations of the iterative cone algorithm [11] that forms jets from energy depositions in calorimeter towers in a cone of fixed size $\Delta R = \sqrt{\Delta\phi^2 + \Delta\eta^2}$. Calorimeter towers are the energy sums measured in the various depths of the calorimeter along r at fixed η and ϕ. Even though iterative cone algorithms are well established and fast, which make them particularly useful for triggering, new algorithms have been studied to improve infrared- and collinear-safety. Among those alternative algorithms are the *Seedless Infrared-Safe Cone* [12] and *Fast-k_T* [13] algorithms.

Rather than relying on the Monte Carlo simulation, the jet energy corrections can be extracted from transverse-energy asymmetry measured in di-jet events, a technique developed at the Tevatron [14]. In $2 \rightarrow 2$ events, transverse momenta of two jets are equal. This property can be used to scale the jet transverse momentum (p_T) at a given η to a jet p_T in a reference η

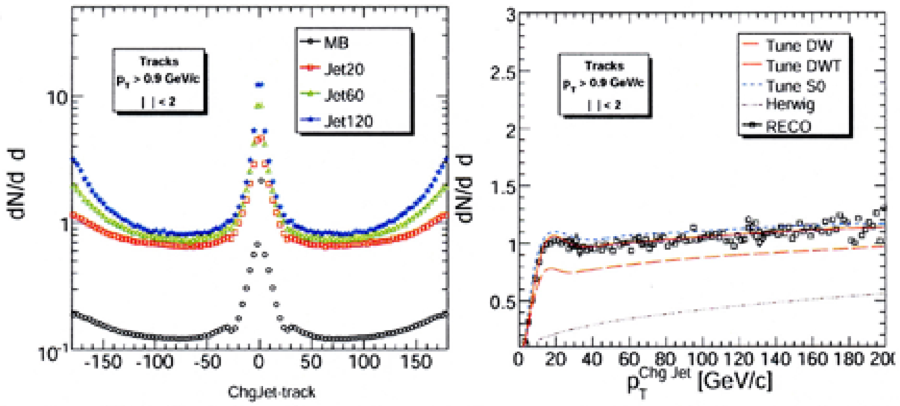

Figure 3: Densities $dN/d\eta d\phi$ of charged particle multiplicity as a function of the azimuthal distance to the leading charged jet direction $\Delta\phi$ (left). The "transverse" region used for the measurement of the underlying event is defined as $60^o < |\Delta\phi| < 120^o$. The data points are shown for different trigger conditions (minimum-bias (MB) or single-jet calorimetric p_T thresholds), sensitive to different ranges of jet momenta. Right: Densities $dN/d\eta d\phi$ for tracks in the transverse region with $p_T > 0.9\,\mathrm{GeV/c}$, as a function of the transverse momentum of the leading charged jet. The simulated "data" (open squares) correspond to an integrated luminosity of $100\,\mathrm{pb}^{-1}$.

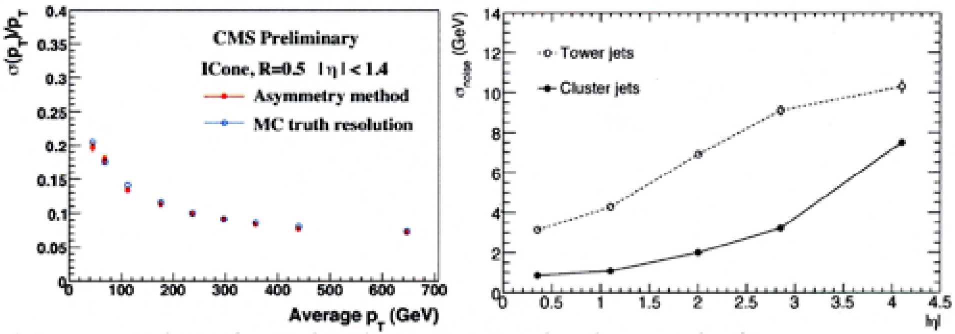

Figure 4: Jet energy resolution from a data-driven correction, based on a study of transverse-energy asymmetry in di-jet events in CMS (left). ATLAS study of the noise contribution to $R = 0.7$ cone jets made from 3D clusters compared to *standard* jets based on calorimeter towers in QCD di-jet events (right).

region, in order to correct for the variation of the jet energy response as a function of η based on data. However, as most events in the QCD di-jet samples have more than two reconstructed jets, which primarily originate from soft radiation and which degrade the momentum balance in the transverse plane between the two leading jets, the resolution obtained from the asymmetry is studied as a function of the maximum p_T of the third jet. The final resolution is then extracted from the extrapolation of the p_T of the third jet in the limit $p_T(3^{\mathrm{rd}}\,\mathrm{jet}) \to 0$. The left plot in Fig. 4 shows how well this data-driven method compares to Monte-Carlo *truth* as studied by CMS.

It has been shown for the ATLAS experiment, that the noise contribution in jets can be reduced when using topological cell clusters as inputs to the jet reconstruction rather than the total deposited energies in the calorimeter towers. The improvement from this attempt to reconstruct three-dimensional energy depositions is shown in Fig. 4 (right) [15]. As a result of the noise reduction shown in this figure, the angular and energy resolution and the jet efficiency is expected to improve for relatively low-momentum jets (below $p_T = 40\,\mathrm{GeV/c}$).

It has also been shown that a clear signal of top-quark pair events, where one W boson from the top-quark decay produces a lepton (electron or muon) and a neutrino, while the other W boson decays into two quarks ($t\bar{t} \to Wb + W\bar{b} \to l\nu bq\bar{q}\bar{b}$), can be extracted from the first $100\,\mathrm{pb}^{-1}$ without the use of missing transverse energy or b-quark flavor tagging [16]. With the help of the W-mass constraint, such a sample will be exploited to improve the jet-energy scale

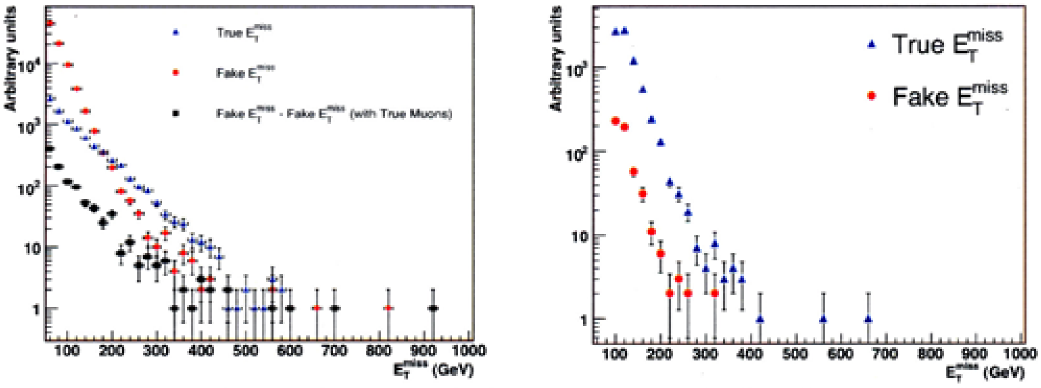

Figure 5: Distribution of $\not{E}_T$, fake $\not{E}_T$ and fake $\not{E}_T$ from escaped muons for QCD di-jet events with leading-jet transverse energies between 560 and 1120 GeV. Right: after applying an isolation cut on the azimuth of the reconstructed $\not{E}_T$ vector and the high-p_T jets: $\Delta\phi(\not{E}_T, E_T^{\rm jet}) > 17^\circ$.

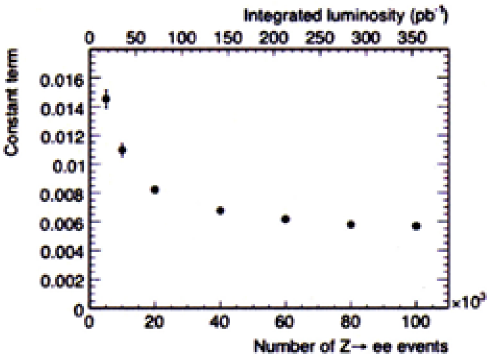

Figure 6: Anticipated improvement in the constant term of the energy resolution, which is related to the overall-uniformity of the electromagnetic calorimeter, as a function of integrated luminosity at ATLAS.

uncertainty and to study jet-flavor tagging.

The missing transverse energy ($\not{E}_T$) is one of the most complex physics objects at hadron collider experiments, because it combines information from all sub-detectors and requires homogeneous calorimeter coverage in the pseudorapidity region of $|\eta| < 5$. A good understanding of the measurement of $\not{E}_T$ is important, as it is present in signatures of physics beyond the standard model, but also required for the reconstruction of e.g. leptonically decaying W bosons. Various contributions of *fake* $\not{E}_T$ can degrade the performance: machine background from the accelerator and beam-gas interactions, noisy or dead calorimeter cells or regions, non-linearity in the hadronic response and finite energy resolution. Figure 5 illustrates an example on how to make analyses less sensitive to fake $\not{E}_T$: ATLAS has recently studied the reduction of the fake $\not{E}_T$ contribution from muons escaping the fiducial region of the detector by requiring angular separation of the direction of the missing transverse energy and high-momentum jets [15].

The first data recorded at the LHC experiments will be used to establish the calibration and uniformity of the response of the electromagnet calorimeters. At first, the calibration can be obtained from the analysis of neutral pions. With increasing luminosity, events with Z bosons decaying into an electron and a positron will become more important, as they open the probed range to higher energies and provide the kinematical constraint from the well known mass of the Z boson. Figure 6 shows the expected improvements in the ECAL uniformity as a function of recorded data for ATLAS. The figure shows that for a relatively small data set of $100\,\mathrm{pb}^{-1}$ integrated luminosity, the constant term in the energy resolution can be greatly improved and that the plateau can be reached for $> 300\,\mathrm{pb}^{-1}$.

3 Conclusions

The commissioning of the CMS detector is in its final phase. More and more subsystems are joining global data taking exercises that use muon signals from cosmic rays for coarse timing, calibration and alignment. Parallel to the commissioning of the detectors, the two multipurpose experiments ATLAS and CMS are preparing the commissioning of the basic physics objects, such as jets, photons and missing transverse energy, with first data. Various methods have been studied with more realistic simulations of the initial calibration and alignment and techniques are developed to establish the sound understanding of the detector response and calibration flows from the early data itself.

References

1. The CMS Collaboration, *CMS Physics TDR, Volume I*, CERN-LHCC-2006-001 (2006); The CMS Collaboration, *CMS Physics TDR, Volume II*, CERN-LHCC-2006-021, J. Phys. G: Nucl. Part. Phys. 34 995-1579 (2006).
2. T. Christiansen, *The CMS Magnet Test and Cosmic Challenge*, presented at the 2006 Nuclear Science Symposium and Medical Imaging Conference, San Diego, California, Oct. 29 - Nov. 4, 2006, CMS Conference Report CMS-CR-2006-091; CERN-CMS-CR-2006-091; The CMS Collaboration, *The CMS Magnet Test and Cosmic Challenge (MTCC Phase I and II) Operational Experience and Lessons Learnt*, CMS Note-2007/005.
3. The ATLAS Collaboration, *Detector and Physics Performance Technical Design Report*, LHCC 99-14/15 (1999).
4. The CMS Collaboration, *Measurement of charged hadron spectra in proton-proton collisions at* $\sqrt{s} = 14\,\mathrm{TeV}$, CMS-PAS-QCD-07-001.
5. T. Sjostrand and M. van Zijl, *Multiple Parton-Parton Interactions in an Impact Parameter Picture*, Phys. Lett. B188, 149 (1987).
6. The CDF Collaboration, F. Abe et al., *Measurement of the Z* p_T *distribution in pp collisions at* $\sqrt{s} = 1.8\,\mathrm{TeV}$, Phys. Rev. Lett. 67, 29372941 (1991).
7. The CMS Collaboration, D. Acosta et al., *The underlying event at the LHC*, CERN CMS-NOTE-2006-067 (2006).
8. P. Skands and D. Wicke, *Non-perturbative QCD effects and the top mass at the Tevatron*, Eur. Phys. J. C52, 133140 (2007), arXiv:hep-ph/0703081.
9. G. Corcella et al., *HERWIG 6: An event generator for hadron emission reactions with interfering gluons (including supersymmetric processes)*, JHEP 101, 010 (2001), arXiv:hep-ph/0011363.
10. The CMS Collaboration, *Measurement of the Underlying Event in Jet Topologies using Charged Particle and Momentum Densities*, CMS-PAS-QCD-07-003.
11. G. C. Blazey *et al.*, *Run II jet physics*, Proceedings of the Run II QCD and Weak Boson Physics Workshop, hep-ex 0005012 (2000).
12. G. P. Salam and G. Soyez, *A practical seedless infrared-safe cone jet algorithm*, JHEP05(2007)086 (2007).
13. M. Cacciari and G. P. Salam, *Dispelling the N3 myth for the Kt jet-finder* , Phys. Lett. B641 57-61 (2006).
14. The DØ Collaboration, B. Abbott *et al.*, *High-*p_T *Jets in pp Collisions at* $\sqrt{s} = 630$ *and* 1800 GeV, Phys. Rev. D64, 032003 (2001).
15. The ATLAS Collaboration, *The ATLAS Experiment at the CERN Large Hadron Collider*, submitted to JINST (2007).
16. The CMS Collaboration, *Measurement of jet energy scale corrections using top quark events*, CMS-PAS-TOP-07-004.

SEARCHES FOR NEW PHYSICS IN PHOTON AND JET FINAL STATES

M. Jaffré
on behalf of the CDF and D0 collaborations
LAL, Université Paris-Sud, CNRS/IN2P3,
91898 Orsay Cedex, France

Recent results from searches of physics beyond the standard model in $p\bar{p}$ collisions are reported, in particular, reactions involving high transverse momentum photons or jets in their final state. Data analyzed by the CDF and D0 experiments at the Run II of the Tevatron correspond to integrated luminosities between 1 and $2fb^{-1}$ depending of the analyses.

1 Introduction

At an energy frontier collider, the usual way to search for indices of physics beyond the standard model (SM) is to look for the collisions with the highest momentum-transfer particles. Typically, one chooses a particular model, and the event selection is optimized to enhance its contribution against the SM expectation. The absence of any deviation in data provides a limit on the production cross-section times the branching ratio for the channel under study, which is then translated into exclusion limits in the parameter space of this model. However, by nature, a new phenomena is unknown, and it exists a lot of models at disposal. This is the reason which motivates the "signature-based" search strategy which casts a wider look for deviations to the SM.

Both strategies will be reported here for final states with photons and jets.

2 Randall-Sundrum (RS) graviton

Many models with extra spatial dimensions have been proposed to solve the hierarchy problem. In the RS model [1], the SM brane and the Planck brane are separated by an extra dimension with a warped geometry. Only the graviton is allowed to propagate in this extra dimension. It appears as Kaluza-Klein (KK) towers in the SM brane. This model has only 2 parameters: M_1, the mass of the lowest KK excited mode, and k/M_{Pl}, a dimensionless coupling constant whose value should lie between 0.01 and 0.1.

KK towers couple to any boson or fermion pairs. CDF [2] looks separately at $\gamma\gamma$ and ee final states, whereas D0 [3] looks at both final states at once as they look similar in the electromagnetic calorimeter. Because of the spin 2 of the graviton, the ratio of the branching ratios to $\gamma\gamma$ and ee final states is 2. Both experiments have analyzed about the same amount of data ($\sim 1\ fb^{-1}$), and found no excess of events over the SM predictions (Drell-Yan and QCD where jets are misidentified as photons) excluding graviton masses below 900 GeV/c^2 for $k/M_{Pl} = 0.1$. Fig. 1 shows the excluded contour in the 2D parameter space as measured by D0.

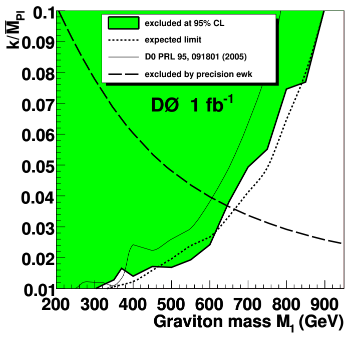

Figure 1: 95% C. L. upper limit on $k/\overline{M}_{Pl}$ versus graviton mass compared with the RS expected limit.

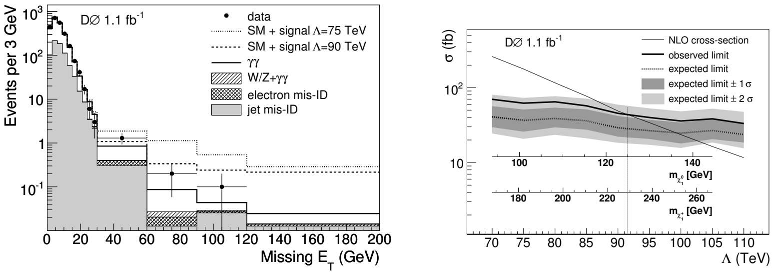

Figure 2: The $\not\!\!E_T$ distribution in $\gamma\gamma$ data with the various background contributions (left). Predicted cross section for the Snowmass Slope model versus Λ. The observed and expected 95% C.L. limits are also shown (right).

3 Gauge mediated SUSY breaking(GMSB)

SUSY [4] is a broken symmetry. Experimental signatures are determined through the manner and scale of the SUSY breaking. In the GMSB scenario, the lightest supersymmetric particle (LSP) is the gravitino, a very light and weakly interacting particle. The next to lightest supersymmetric particle (NLSP) is assumed in this analysis to be the neutralino which decays into the LSP and a photon. Assuming R-parity conservation [5], SUSY particles are pair produced and the experimental signature will be 2 photons and missing energy from the 2 gravitinos. To get a quantitative result, the "Snowmass Slope SPS 8" model [6] is considered. All the GMSB parameters[a] are fixed as a function of the effective energy scale Λ of SUSY breaking.

In this event topology, the SM background is the $Z\gamma\gamma$ production where the Z boson decays into neutrinos. There is also important instrumental background from events with real $\not\!\!E_T$ (W boson production) and fake $\not\!\!E_T$ (QCD where jets are misidentified as photons). Fig. 2 (left) shows the $\not\!\!E_T$ distribution. The observed distribution agrees well with the SM prediction; the entire spectrum is then used to set limits on the GMSB production cross section. Fig. 2 (right) shows the 95% C.L. cross section limit as a function of the effective scale Λ obtained by D0 [7]. The observed limit on the signal cross section is below the prediction of the Snow-mass Slope model for $\Lambda < 91.5\ TeV$, or for gaugino masses $m_{\tilde{\chi}_1^0} < 125\ GeV/c^2$ and $m_{\tilde{\chi}_1^\pm} < 229\ GeV/c^2$.

4 Large Extra Dimensions

The hierarchy problem can also be solved by postulating the existence of n new large extra dimensions as proposed first by Arkani-Hamed, Dimopoulos and Dvali[8] (ADD); the extra volume serves to dilute gravity so that it appears weak in our 3D world as the graviton is the only particle allowed to propagate in the extra space. If the extra dimensions are compactified in a torus of radius R, according to the Gauss law, one can relate the fundamental Planck mass scale M_D, R, the Planck mass and the number of extra dimensions by the relation $M_{Planck}^2 = 8\pi M_D^{n+2} R^n$, allowing M_D to be compatible with the electroweak scale.

In this model, the graviton can be produced directly in the reaction $q\bar{q} \to G\gamma$; G will remain undetected leaving a signature with a single photon and $\not\!\!E_T$.

The only SM background is the $Z\gamma$ production where the Z boson decays into a neutrino pair. In addition to the usual instrumental background coming from misidentification of electrons or jets into photons, the event topology is rather sensitive to a contribution from beam halos and

---

[a] The messenger mass $M_m = 2\Lambda$, the number of messengers $N_5 = 1$, $tan(\beta) = 15$, $\mu > 0$.

cosmics where muons produced photons by bremsstrahlung.

To fight the latter background, both experiments had to develop specific tools in addition to the usual ones based on the EM shower profile. Special hit finders in the tracker starting from the EM cluster increase the track veto efficiency. In addition, D0 uses a EM pointing tool thanks to its preshower detector, and CDF the timing system built within its EM calorimeter.

The results of CDF which has analysed about $2fb^{-1}$ of data, twice as much as D0 [9], are displayed in Fig. 3. The left plot shows a good agreement for the photon transverse between data and the sum of the various backgrounds. This allows to set limits on the fundamental scale M_D (right plot) as a function of the number of extra dimensions. For $n > 4$ the limits are comparable with the limits obtained in the monojet search, and better than the LEP combined result [10].

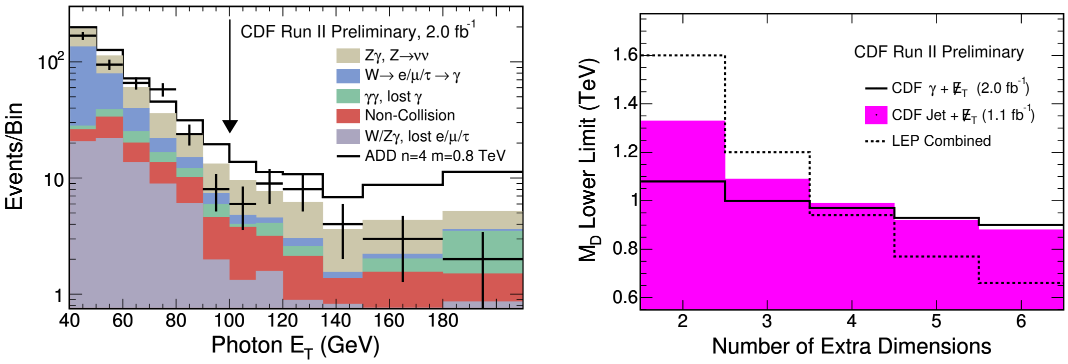

Figure 3: The left figure shows the $\not{E}_T$ distribution in the CDF monophoton search. The signal expected from the ADD model (n=4, m=0.8TeV) is added on top of the SM backgrounds. The right figure shows the exclusion limits for the ADD model obtained in this analysis, in comparison with the CDF jet and $\not{E}_T$ result and LEP combined result.

5 Squarks and gluinos, stops

5.1 Squarks and gluinos

Squarks and gluinos can be copiously produced at the Tevatron if they are sufficiently light. The analysis is performed within the mSUGRA model [11]. The final state is composed of jets with a large $\not{E}_T$ due to the two escaping neutralinos, assumed to be the LSP. According to the relative mass of squarks and gluinos different event topologies are to be expected. If squarks are lighter than gluinos, a "dijet" topology is favored. On the contrary if squarks are heavier than gluinos, the final state contains at least 4 jets. Finally, the jet multiplicity is at least 3 if squarks and gluinos have similar masses. After a common event preselection, the three topologies have been studied and optimised separately. The left plot on Fig. 4 shows the D0 $\not{E}_T$ distribution obtained in the "dijet" search, the right one is obtained by CDF in the "3-jet" search. D0 has analyzed 2.1 fb^{-1} of data without finding any excess over the SM predictions. It allows to extend the exclusion domain in the squark gluino plane (Fig. 5). Using the most conservative hypothesis, D0 [12](CDF [13]) excludes a gluino lighter than 308(290) GeV/c^2.

5.2 Stop

Due to the large Yukawa coupling, there could be a large mixing in the 3rd generation of squarks. The lighest of the 2 stops could be the lightest squark and even the NLSP. Furthermore if its

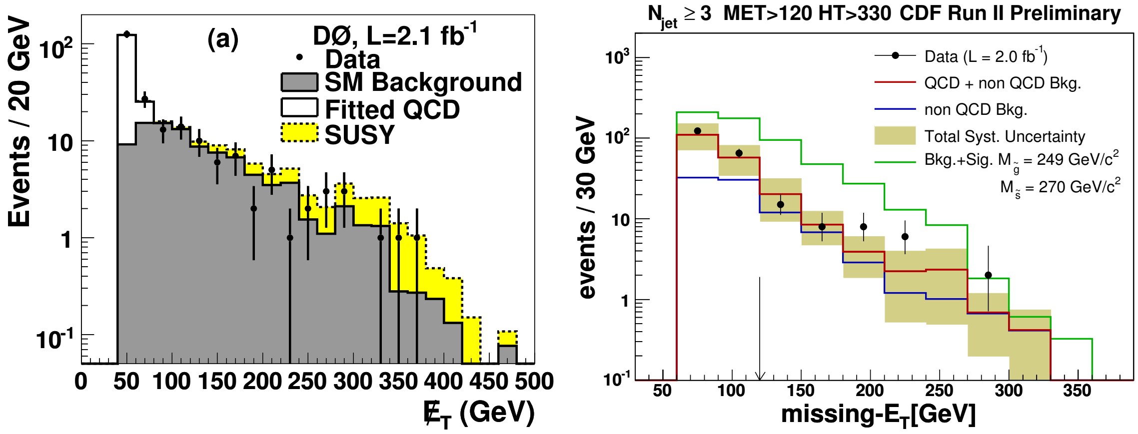

Figure 4: Distributions of $\not\!\!E_T$ after applying all analysis criteria except the one on $\not\!\!E_T$ for the "dijet" (D0 left) and "3-jets" (CDF right) squark-gluino analyses; data (points with error bars) and the cumulated contributions from SM background, QCD background and signal MC are shown.

mass is less than the sum of the masses of the b quark, the W boson, and the neutralino, the dominant decay mode is $\tilde{t} \to c\tilde{\chi}_1^0$, a flavor changing loop decay, assumed to be 100% in the analysis. The final state will then be 2 acoplanar charm jets and $\not\!\!E_T$. The analysis proceeds with 2 jets detected in the central part of the detector with a loose heavy quark tag for one of them. No excess of events has been observed[14] in about 1 fb^{-1} of data, which provides a lower limit for the stop mass at 149 GeV/c^2 for a neutralino mass of 63 GeV/c^2 (Fig. 6).

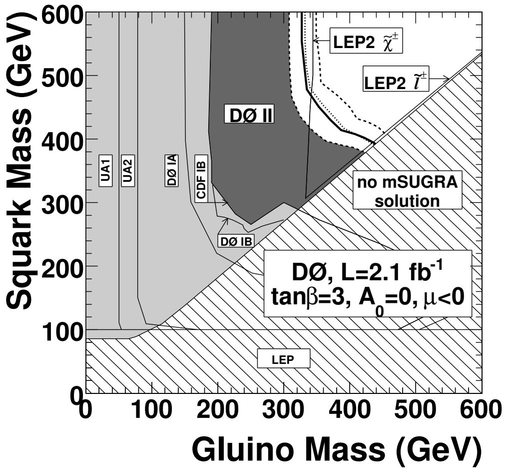

Figure 5: Excluded region in the squark and gluino mass plane; newly excluded domain by D0 is shown in dark shading. The region where no mSUGRA solution can be found is shown hatched.

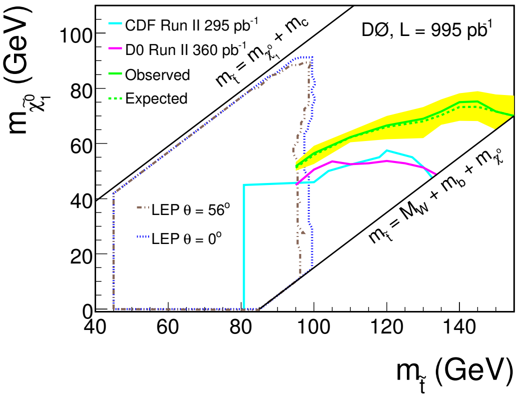

Figure 6: Region in the $\tilde{t}$–$\tilde{\chi}_1^0$ mass plane excluded at the 95% C.L. by the D0 search. The yellow band represents the theoretical uncertainty on the scalar top quark pair production cross section due to PDF and renormalization and factorization scale choice.

6 Signature-based searches

6.1 Search for anomalous production of di photon events

In its quest for "signature-based" excess, CDF has searched for anomalous production of events in the $\gamma\gamma + \not\!\!E_T$ topology. In this analysis, use is made of the $\not\!\!E_T$ resolution model. The aim of this model is to discriminate events with large mismeasured $\not\!\!E_T$ from events with real $\not\!\!E_T$. It has been shown to provide a better background rejection power than a simple $\not\!\!E_T$ cut. This model is based on the assumption that individual particle's energy resolution has Gaussian shape proportional to particle's $\sqrt{E_T}$. Only two sources of fake $\not\!\!E_T$ are considered : soft unclustered energy (from underlying event and multiple interactions), and jets. The latter is responsible for most of the $\not\!\!E_T$ as it is collimated energy in contrast to the former which is spread out all over the calorimeter. According to this model, each event is given a $\not\!\!E_T$ significance value. Most of the QCD background is eliminated by requiring a significance above 5, leaving only the expected number of SM events with real $\not\!\!E_T$ (Fig. 7), and not much room for an extra signal.

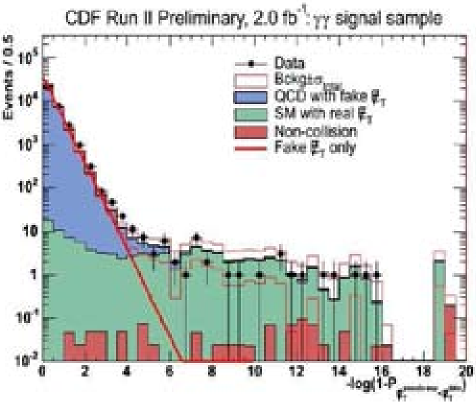

Figure 7: Distribution of missing transverse energy significance for diphoton candidates.

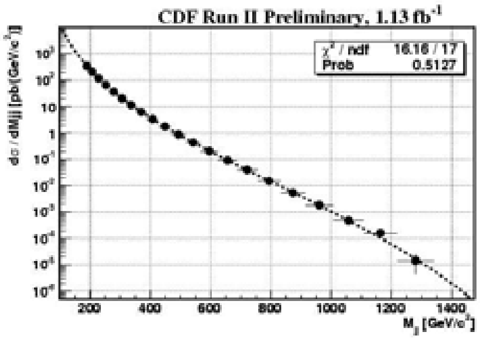

Figure 8: The measured dijetmass spectrum and results of the fit to the parametrization form 1.

6.2 Search for dijet mass resonances

Many classes of models beyond the SM predict the existence of new massive particles decaying into 2 partons which would appear as resonances in the dijet mass spectrum. Such classes include excited quarks, techniparticles, new W' or Z' bosons, RS graviton,... Jets are reconstructed by the cone-based midpoint jet algorithm [15] with a cone radius of 0.7 and have central rapidity ($|y| < 1$). CDF has analysed about 1.1 fb^{-1} of data and measured the dijet differential cross section (Fig. 8). The spectrum is fitted by the smooth parametrization :

$$\frac{d\sigma}{dm} = p_0(1-x)^{p_1}/x^{p_2+p_3\log(x)}, \qquad x = m/\sqrt{(s)}. \tag{1}$$

This parametrization is found to fit well the dijet spectra from PYTHIA and HERWIG MC events as well as from NLO pQCD. As no evidence for existence of a new massive particle is observed, limits on new particle production cross sections can be derived as a function of the dijet mass. These limits are then translated into mass exclusion limits, see Table 1.

7 Conclusions

No hints of physics beyond the SM have been found so far. As the Tevatron is continuing to provide experiments with more data to analyze, the quest for indices will be pursued by CDF

Table 1: Mass exclusion ranges for several models.

Model description	Observed mass exclusion range (GeV/c^2)
Excited quark ($f = f' = f_s = 1$)	260-870
Color octet technirho (top-color-assisted-technicolor couplings)	260-1110
Axigluon and flavor universal coloron (mixing of 2 SU(3)'s cot(theta)=1)	260-1250
E6 diquark	290-630
W' (SM couplings)	280-840
Z' (SM couplings)	320-740

and D0. Some analyses presented in this talk have already been published, for the others, further details can be found at:

CDF http://www-cdf.fnal.gov/physics/exotic/exotic.html

D0 http://www-d0.fnal.gov/Run2Physics/WWW/results/np.htm

Acknowledgments

The author would like to thank the CDF and D0 working groups for providing the material for this talk, and the organizers of the *Rencontres* for a very enjoyable conference and the excellent organization.

References

1. L. Randall and R. Sundrum, *Phys. Rev. Lett.* **83**, 3370 (1999); **83**, 4690 (1999).
2. T. Aaltonen *et al* (CDF Collaboration), *Phys. Rev. Lett.* **99**, 171801 (2007); **99**, 171802 (2007).
3. V.M. Abazov *et al* (D0 Collaboration), *Phys. Rev. Lett.* **100**, 091802 (2008).
4. H.E. Haber and G.L. Kane, Phys. Rep. **117**, 75 (1985).
5. G.R. Farrar and P. Fayet, *Phys. Lett.* B **79**, 442 (1978).
6. S.P. Martin, S. Moretti, J.M. Qian, and G.W. Wilson, "Direct Investigation of Supersymmetry: Subgroup summary report," in *Proceedings of the APS/DPF/DPB Summer Study on the Future of Particle Physics (Snowmass 2001),* edited by N. Graf, eConf **C010630**, p. 346 (2001); B.C. Allanach *et al.*, Eur. Phys. J. C **25**, 113 (2002).
7. V.M. Abazov *et al* (D0 Collaboration), *Phys. Lett.* B **659**, 856 (2008).
8. N. Arkani-Hamed, S. Dimopoulus, G. Dvali, *Phys. Lett.* B **429**, 263 (1998).
9. V.M. Abazov *et al* (D0 Collaboration), arXiv:hep-ex/0803.2137, submitted to Phys. Rev. Lett. B.
10. LEP Exotica Working Group, CERN Note LEP Exotica WG 2004-03.
11. H.P. Nilles, Phys. Rep. **110**, 1 (1984).
12. V.M. Abazov *et al* (D0 Collaboration), *Phys. Lett.* B **660**, 449 (2008).
13. CDF Collaboration, Public note CDF 9229 (unpublished).
14. V.M. Abazov *et al* (D0 Collaboration), arXiv:hep-ex/0803.2263, submitted to Phys. Lett. B.
15. G.C. Blazey *et al.*, in *Proceedings of the Workshop: "QCD and Weak Boson Physics in Run II"*, edited by U. Baur, R.K. Ellis, and D. Zeppenfeld, Batavia, Illinois (2000).

COMMISSIONING OF ATLAS AND EARLY MEASUREMENTS WITH LEPTONS IN ATLAS AND CMS

M. PLAMONDON
LAL, Univ Paris-Sud, IN2P3/CNRS, Orsay, France
on behalf of ATLAS and CMS collaborations

With only a few months until the LHC start-up, the commissioning of ATLAS is in its final stage as the last components of the detector are installed. The understanding of the detector response acquired during the preparation phase is presented as well as the expected performance at start-up. The strategies of both ATLAS and CMS regarding the use of early data involving leptons is then described. Assuming an integrated luminosity of $100\,\mathrm{pb}^{-1}$ in 2008, examples of calibration procedures and early measurements are given.

1 Commissioning of ATLAS

At the time of this paper, everything except the endwall muon chambers has been installed. In this section we summarize the acquired understanding of the detector performance before start-up.

1.1 Detector status at start-up

The endwall muon chambers are the last components to be installed in the cavern (June 2008). With the full magnet tests performed soon afterwards in order to check the endcap toroids at their nominal field, the entirety of the ATLAS detector will have been assembled ready for the first collisions. Data taking has already been tested with cosmic rays throughout the two preceeding years of commissioning as the different detectors have been installed. The complete acquisition and processing chain has been successfully exercised from the primary site at CERN and throughout worldwide distributed sites.

1.2 Inner detectors

The commissioning of the Inner Detector was initiated on the surface where cabling checks and debugging were performed. Once in the cavern, the noise levels were the same as those measured on the surface. The global alignment between the silicon strip (SCT) and transition radiation (TRT) trackers was measured with reconstructed cosmic ray tracks (as shown in Fig.1), where the results were consistent with precision survey measurements. Little time was available for cabling cross-checks of the innermost layer of pixels which was cabled just before ATLAS was closed. The number of non-working channels was measured to be small (0.3%).

1.3 Calorimeters

The calorimeters went down into the cavern beginning in 2006 and have been operating under stable conditions for a long period of time. For example, the liquid argon calorimeter was cold (88 K) with a measured temperature variation of 10 mK for over a year. The degree of understanding of the detector response is well illustrated by cosmic rays. Large signals as in Fig.1 are frequently observed, interpreted as muons emitting a bremsstrahlung photon in the calorimeters. These events have allowed timing studies (channel intercalibration at the level of 2 ns) as well as improving the description of the pulse shape. In general, muons are minimum ionising particles and deposit energy according to a Landau distribution. By analyzing these distributions, the uniformity of response across EM readout channels could be cross-checked to the 2% level[1]. Taking advantage of the several months of commissioning running, many problems were identified and corrected, leaving only a small fraction of defective channels ($\sim 0.1\%$ in the case of the LAr calorimeter).

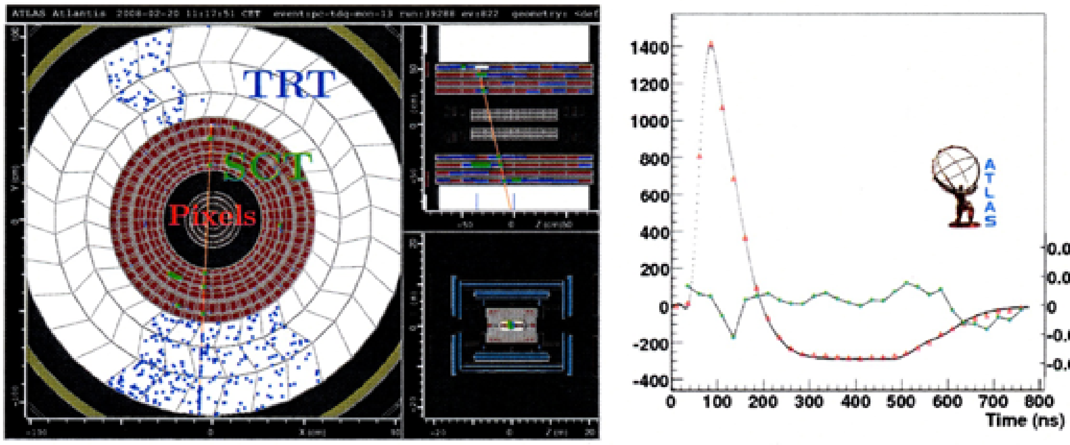

Figure 1: On the left is shown the trajectory of a cosmic muon reconstructed in the inner detectors. No zero suppression being performed, this display reveals that only a fraction of the TRT was recording data. The right plot shows a large amplitude signal ($\sim$ 13 GeV) in the LAr calorimeter which was also recorded during the commissioning. Compared to the predicted pulse, the residual in green is showing good agreement at the percent level.

1.4 Muon spectrometer

The commissioning of the muon spectrometer was aimed at testing its complex alignment system using optical sensors. The alignment is of crucial importance as a 1 TeV muon is bent only by 500 μm under the magnetic field produced by the toroids. In order to reach 10% accuracy on the momentum measurement, the chambers must be aligned with a precision of 50 μm. After a calibration of the system by moving and rotating modules, the reconstructed cosmic tracks have shown that the misalignments can be well monitored.

2 Early physics with leptons

With the first collisions, the main goal will be to calibrate the detectors *in situ* using well-known physics samples. Table 1 summarizes the expected performances at start-up and those expected to be ultimately reached. The rediscovery of standard model at $\sqrt{s} = 10$ TeV will be followed by an effort to validate and tune the MC generators. Leptons will play a crucial role in paving the way to new physics, taking half the trigger rate of the foreseen menu at $\mathcal{L} = 10^{31}\,\mathrm{cm}^{-2}\mathrm{s}^{-1}$. Assuming 3 months of operation in 2008 and an integrated luminosity around $100\,\mathrm{pb}^{-1}$, calibration procedures and possible early measurements are described in the following.

		Performance		Physics goals	Physics signals tools
		@ start-up	nominal		
EM energy uniformity	ATLAS	$\lesssim$1-2%	0.7%	$H \rightarrow \gamma\gamma$	isolated e, $Z \rightarrow ee$
	CMS	$\lesssim$2-4%	0.5%		ϕ-symmetry
EM energy scale		$\sim$ 2%	0.02%	W mass	$Z \rightarrow ee$
Inner detector alignment		50-100 μm	<10 μm	b-tagging	isolated μ, $Z \rightarrow \mu\mu$
Muon system alignment		<200 μm	30 μm	$Z' \rightarrow \mu\mu$	$Z \rightarrow \mu\mu$
Muon momentum scale		$\sim$1%	0.02%	W mass	$Z \rightarrow \mu\mu$

Table 1: This table summarizes the detector performance concerning leptons which are expected at start-up. The values, mostly given for the ATLAS case, are compared to those ultimately reached using the physics tools mentionned in the last column.

2.1 *First peaks:* $(J/\psi, \Upsilon, Z) \rightarrow \mu\mu$

Assuming a 30% overall detector and machine efficiency at $10^{31}\,\mathrm{cm}^{-2}\mathrm{s}^{-1}$, around 16000 J/ψ and 3000Υ in dimuons are accumulated per pb^{-1}, useful to perform checks, tracker alignment and momentum scale determination. After all cuts, $\sim$600 $Z \rightarrow \mu\mu$ events are also recorded. As shown in figure 2, the measured Z boson mass is sensitive to misalignments of the tracker or the muon system as well as uncertainties on the magnetic field (distorded B field): a misaligned tracker would affect noticeably the shape of the Z peak.

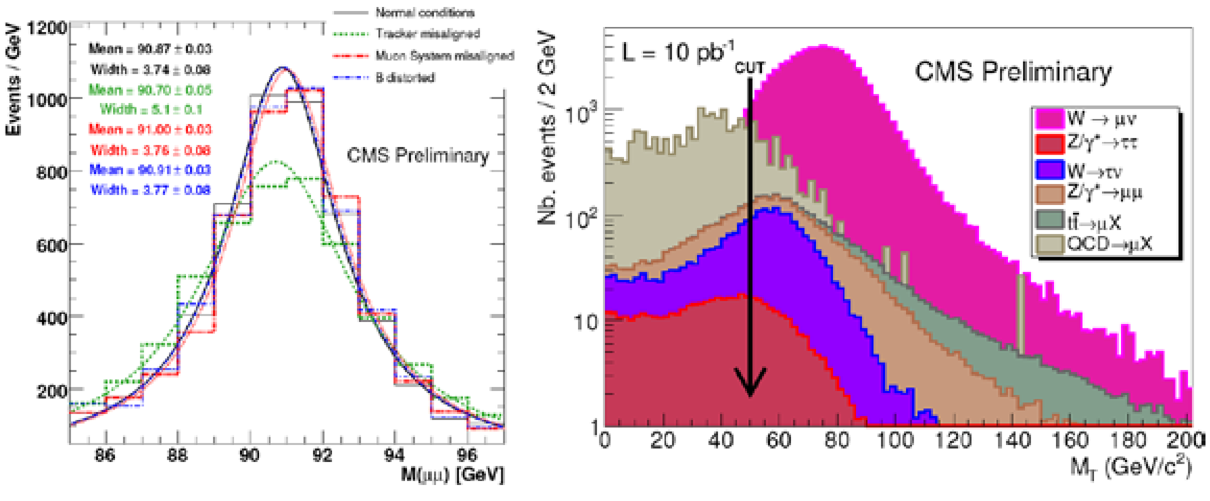

Figure 2: A peak of $\sim$6000 Z obtained with $10\,\mathrm{pb}^{-1}$ is the starting point of many studies of the muon system as shown on the left in the case of CMS (the same effects exist in ATLAS). A clear W peak is obtained as well (right). A cut at 50 GeV on the transverse mass (M_T) gives a clean W sample that can be used for $\not{E}_T$ studies.

2.2 $Z \rightarrow ee$ *calibration and energy scale*

Simple analysis cuts are used to obtain the first Z and W samples with low background levels as in figure 2 (right). For example, they can be done without the tracker or restricted to the barrel region if required. The Z-mass constraint is a key tool for the commissioning of electron reconstruction and will also be used to correct residual long-range non-uniformities. From the design of ATLAS LAr calorimeter, relatively large regions (0.2×0.4 in $\eta \times \phi$) are exected to be locally uniform and this was demonstrated from testbeam data[2]. In order to intercalibrate them, ~30000 $Z \to ee$ events will be sufficient to achieve the desired response uniformity of $\sim 0.7\%$ (see Fig.3). The situation in CMS [3] is different due to the crystal-to-crystal response which varies by $\gtrsim 2\%$. Higher statistics (~10 fb^{-1}) are required to perform a similar intercalibration.

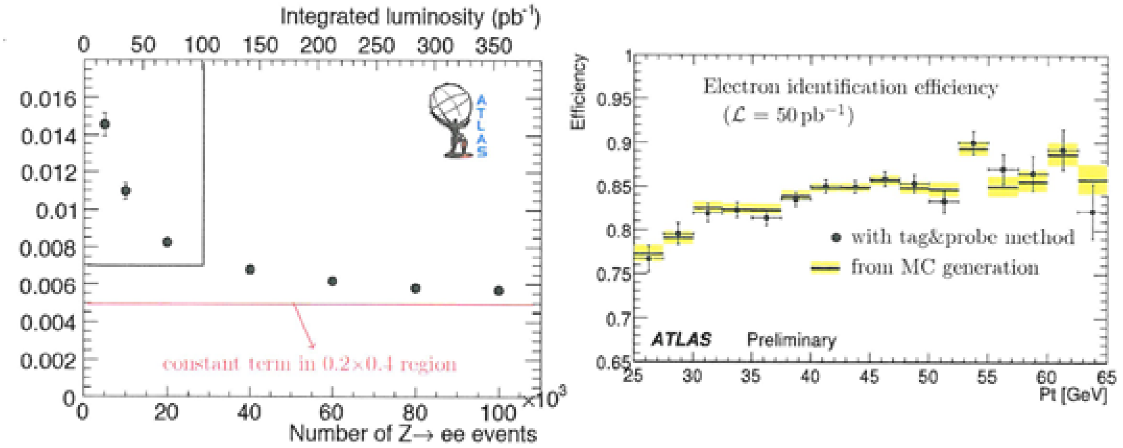

Figure 3: The ATLAS EM intercalibration as a function of the integrated luminosity (left) reaches 0.7% at about 100 pb^{-1}. In the right plot, the efficiency of selecting electrons in ATLAS is accurately evaluated using the tag&probe method described in the text (1% agreement w.r.t. MC generation).

2.3 *Z and W cross-sections*

The expected precision for ATLAS and CMS in the measurements of the Z and W cross-sections (table 2) are limited by statistical uncertainties. Theoretical uncertainties remain at 2%, mainly due to acceptance determination and PDFs. The luminosity uncertainty of 10% will dominate until the dedicated detectors [4,5] refine these measurements in 2009. Systematics are kept to the 1% level with efficiency precisely determined using data-driven methods (tag&probe) as illustrated in Fig.3 in the case of electron identification. In simulated Z events, an electron candidate is tagged by fulfilling stringent isolation and reconstruction requirements. A simple object is then looked for on the opposite side, either a track or an EM cluster. If the invariant mass of the pair falls in the mass window of the Z ($M_{ee}=M_Z\pm20$ GeV), the latter is known to be an electron and the efficiency can be computed in this way.

process		$\frac{\Delta\sigma}{\sigma}$	
$Z/\gamma^* + X \to \mu\mu$	ATLAS	0.004(stat)±0.008(sys)	±0.02(th)±0.1(lumi)
	CMS	0.004(stat)±0.011(sys)	
$W \to e\nu$	ATLAS	0.002(stat)±0.050(sys)	//

Table 2: The various contributions to the uncertainty of cross-section measurements are given for 50 pb^{-1} of integrated luminosity. Higher systematic uncertainties are expected in the case of σ_W, especially from the $\not{E}_T$ measurement.

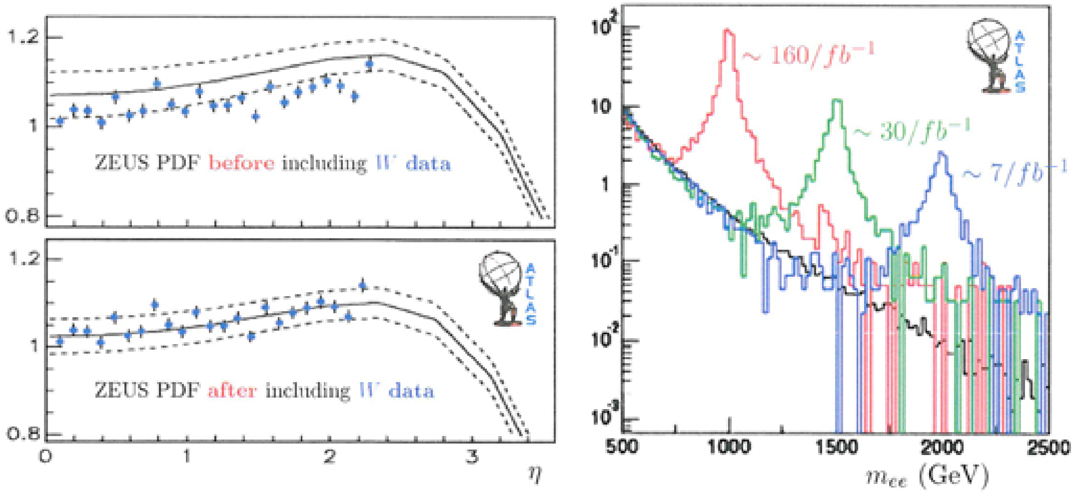

Figure 4: The electron rapidity distributions in W decays can be used to constrain PDF distributions (left). Dielectron resonances at the TeV scale could be seen with a fraction of the statistics shown here for 1 fb^{-1} (right).

2.4 Constrain PDFs with $W \to \ell\nu$

A region of the $x - Q^2$ plane becomes accessible at the LHC with a higher centre-of-mass energy ($x_{1,2} = \frac{M}{\sqrt{s}} e^{\pm y}$). For instance, the W production would involve 10^{-4}<$x_{1,2}$<0.1, a region dominated by sea-sea parton interactions. At these low x values, the current PDF uncertainties remain large (4-8% [6]). By adding LHC data into global fits, it would be possible to constrain further the PDFs. With a 5% experimental precision, $e^{\pm}$ angular distributions could be used to discriminate between different PDF parametrizations. The principle is demonstrated by generating 10^6 $W \to e\nu$, equivalent to 150 pb^{-1} of data. These simulated events are generated with the CTEQ6.1 PDF and full detector simulation. Statistical uncertainty being negligible, only a 4% systematic error is introduced by hand, a level already attained with the $Z \to ee$ sample. These pseudo-data are included in the global ZEUS PDF fit in order to asssess their impact. The uncertainty on the low-x gluon shape parameter λ [$xg(x) \sim x^{-\lambda}$] is reduced by 40%.

2.5 Leptons for early top

The easiest channel to consider at the beginning is one lepton plus jets ($t\bar{t} \to b\ell\nu bjj$) with $t\bar{t}$ combinatorics, W+jets and QCD as main backgrounds. The b-tagging will not be available at start-up and $\not{E}_T$ might be problematic as well. For these reasons, early top analyses are *lepton-triggered*. Nevertheless, a signal can be quickly seen with only ∼10 pb^{-1}, even with limited detector performance and a simple analysis. With 100 pb^{-1}, these early measurements of $\delta\sigma_{t\bar{t}}$ will reach ∼20% and δm_{top} at <10 GeV. It will be an excellent sample for light jet calibration and b-jet efficiency determination.

2.6 Early discoveries with leptons?

The discovery of a narrow resonance decaying to e^+e^- (Fig.4) is accessible with as few as 70 pb^{-1} if M≃1 TeV. At these energies, ultimate calorimeter performance is not needed. Early searches in the case of dimuons decays would be less straightforward since the resolution worsens as p_T increases. However, the generally lower instrumental background may make dimuons a discovery channel along with dielectrons.

3 Conclusions

ATLAS has been commissioning its detector with cosmic rays and is eagerly awaiting the first LHC collisions in 2008. The clean signatures involving leptons will have a major impact in the initial understanding of the detectors. Summarized in figure 5, the early physics program involves several activities with possible surprises along the way.

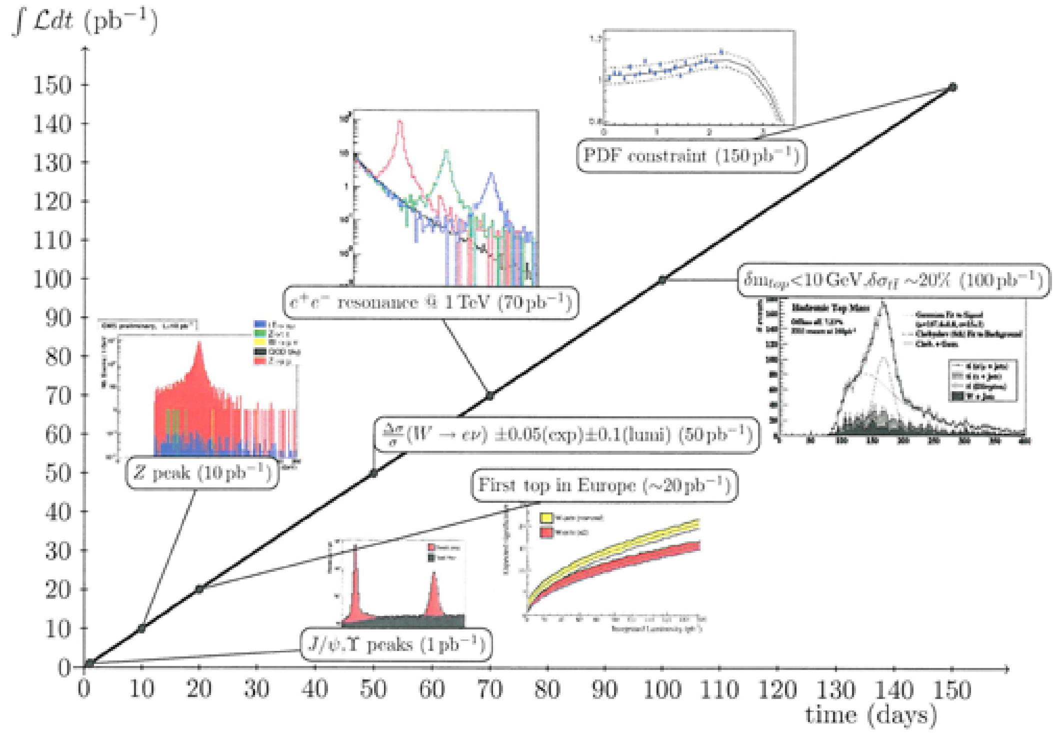

Figure 5: Summary of the physics program with the first year of LHC data taking.

References

1. M. Cooke et al. In situ commissioning of the atlas electromagnetic calorimeter with cosmic muons. Technical Report ATL-LARG-PUB-2007-013. ATL-COM-LARG-2007-012, CERN, Geneva, Nov 2007.
2. J. Colas et al. Response Uniformity of the ATLAS Liquid Argon Electromagnetic Calorimeter. *Nucl. Instrum. Meth.*, A582:429–455, 2007.
3. G. L. Bayatian et al. CMS physics: Technical design report. CERN-LHCC-2006-001.
4. V. Berardi et al. TOTEM: Technical design report - Addendum. Total cross section, elastic scattering and diffraction dissociation at the Large Hadron Collider at CERN. CERN-LHCC-2004-020.
5. Peter Jenni, Markus Nordberg, Marzio Nessi, Kerstin Jon-And, , and and. Atlas forward detectors for measurement of elastic scattering and luminosity. 2008. CERN-LHCC-2008-004.
6. Amanda Cooper-Sarkar and Claire Gwenlan. Comparison and combination of ZEUS and H1 PDF analyses. 2005. hep-ph/0508304.